The effects of nanoparticles on the physical properties of type I collagen

A thesis presented in partial fulfilment of the requirements for the degree of

Master of Science
in
Chemistry

At Massey University, Palmerston North, New Zealand.

Jiaxin Lian

2016

Acknowledgements

I would like to thank everyone who gave me guidance and support throughout my master project. I would like to thank in particular:

My primary supervisor Prof. Bill Williams for his supervision and encouragement. There were so many times when I was stuck and frustrated but a conversation with him made me relax and had a clear idea about what to do next.

My co-supervisor Dr. Sujay Prabakar for his time for discussions and encouragement, and giving me the opportunity to undertake this project for my master.

Dr. Bradley Mansel for his help and assistance in conducting some experiments, developing experimental protocols and data analysis.

Dr. Allan Raudsepp for his training on the rheometers.

Dr. Meekyung Ahn for her training on collagen extraction and characterization with SDS-PAGE, and her encouragements during my study.

Niki Murray for conducting the confocal microscopy imaging.

Dr. Bridget Ingham for the training and discussions on the synchrotron experiments and data analysis.

Pablo Hernandez-Cerdan, Lisa Kent and other biophysics group members for the interesting discussions on parts of the project.

Chris Hall for his assistance when using the rheometer in the Riddet Institute.

I would like to thank my parents, cousins and uncles for their support and encouragement.

Finally, I would like to acknowledge New Zealand Leather and Shoe Research Association and the MacDiarmid Institute for fundings. I would also like to

acknowledge the Ministry of Business, Innovation and Employment (MBIE) for funding through grant LSRX-1301.

The SAXS experiments for this project were undertaken on the SAXS/WAXS beamline at the Australian Synchrotron, Victoria, Australia.

Abstract

This thesis concerned with the interactions of surface functionalized TiO_2 and ZnO NPs with type I collagen. The collagen nanocomposites formed with TiO_2 and ZnO NPs may be potential candidates for some biomedical applications thanks to the synergetic effects between two materials. How the physical properties of collagen have been changed when interacting with TiO_2 and ZnO NPs has been investigated in this project. The general background and research objectives of this study are introduced in Chapter 1, followed by Chapter 2 which gives details about the preparation of the samples, in addition to the characterization techniques and protocols. The TiO_2 and ZnO NPs were synthesized by colloidal synthetic methods and their surfaces were functionalized with different functional groups. The physical properties of the TiO_2-collagen nanocomposites and ZnO-induced collagen gels were studied by rheology, DSC, swelling ratio assay, FTIR and confocal microscopy. The mechanical studies are the main focus of this thesis.

In Chapter 3, TiO_2 NPs coated with chitosan and PAA were introduced into collagen solutions before fibrillogenesis was carried out. They were found to affect the linear rheology of the collagen gels as a function of their concentration. There were no significant differences in the strain-stress response in the non-linear rheology. It was found that the PAA coated TiO_2 NPs promoted collagen fibrillogenesis, resulting in thin fibrils, and a dense and more crosslinked structure, while the chitosan coated TiO_2 NPs slowed down the collagen fibrillogenesis and created a heterogeneous network with thick fibrils and less crosslinks.

ZnO-PVP NPs were found to induce collagen gelation without the use of the conventional fibrillogenesis involving gelation buffer, as reported in Chapter 4. The

hydrogel formed with this method was found to be three times as strong as the gel formed with conventional gelation buffer at the same collagen concentration. Confocal images indicated those two gels have different molecular assembly states. A group of experiments showed ZnO acted as a neutralizing agent here to raise the pH of the collagen solution to the pH close to the isoelectric point of the collagen.

Both the TiO_2 and ZnO NP-collagen systems have demonstrated that different collagen networks can be created by the direct or indirect interactions between collagen monomer solution and the nanoparticles. By manipulating the assembly of collagen to design different networks, it is possible to achieve the physical properties required for different applications.

The results are followed by the conclusions and future perspectives of this study.

Table of Contents

List of Figures

List of Tables

Abbreviations

Col	Collagen
CS	Chitosan
DSC	Differential scanning calorimetry
FTIR	Fourier transform infrared spectroscopy
G’	Storage modulus
G_o’	Equilibrium storage modulus
G”	Loss modulus
γ_c	Critical strain
γ_y	Yield strain
HCl	hydrochloric acid
HOAc	Acetic acid
K	Differential shear modulus
min	Minute
NaOH	Sodium hydroxide
NaCl	Sodium chloride
NP	Nanoparticle
PAA	Poly (acrylic acid)
PBS	Phosphate buffered saline
PVP	Polyvinylpyrrolidone
s	Second
SAED	Selected area electron diffraction

σ	Stress
TEM	Transmission electron microscopy
TGA	Thermogravimetric analysis
THF	Tetrahydrofuran
TiO_2	Titanium dioxide
TiO_2-CS	Chitosan coated TiO_2
TiO_2-PAA	PAA capped TiO_2
TiO_2-UM	Surface un-modified TiO_2
$TiCl_4$	Titanium tetrachloride
ZnO	Zinc oxide

1. Introduction

Each year around 800, 000 metric tons of chrome-free solid waste is produced by the leather industry in the world, with a large percentage of it being 'limed split', which is the layer shaved off from the inner side of the cow hide.[1] The disposal of the waste may cause serious environmental issues.[1] However, because the major component of the limed split is collagen, researchers have successfully extracted native collagen from the limed split waste.[1-2] In this way, the value of limed split can be improved significantly due to the incredible value of collagen in the global market. This is the motivation of this research project conducted at the New Zealand Leather & Shoe Research Association.

1.1. Collagen

1.1.1. Importance and diversity of collagen in animal

Collagen is one of the most abundant proteins and accounts for more than 30 percent of the structural proteins in animals.[3] It widely exists in tissues including skin, bone, tendon, cartilage and cornea. The diverse properties and functions of collagen in these tissues are attributed to the different collagen types and structures. There are more than 27 types of collagen found in vertebrate species.[4] All of them have the unique triple helical molecular structure composed of three polypeptide α chains.[5] The parallel stacking of collagen microfibrils along the axial direction enriches the strong tensile strength of the tendon.[4] Collagen fibrils weaving into a two dimensional network gives skin flexibility.[4] The coexistence of inorganic material and collagen allows tissues like bone and teeth to achieve superior hardness.[4]

1.1.2. Collagen structure at molecular level

A collagen molecule is composed of three left handed polypeptide α chains right hand twisted into a triple helical structure.[5] The polypeptide has a characteristic repeating amino acid sequence Gly-Xaa-Yaa.[5] Glycine occupies every third position, while Xaa and Yaa can be any amino acid.[6] With the smallest side group in all amino acids, glycine is the only possible amino acid that can approach the centre of the triple helix.[4] Different types of collagen are distinguished by the α chains.[5] Fibrillar collagens, including collagen type I, II, III, V, etc, have continuous triple helical domains in the centre of the α chains.[6] While the non-fibrillar collagens or the fibril associated collagens have interrupted triple helical domains connected by one or more non-helical domains.[6] The α chains are held together mainly by inter-molecular H-bonding. Every three peptide unit forms one direct H-bond between the N-H of glycine and C=O of Xaa in the neighbouring peptide (Figure 1.1).[4] Water molecules assist in the formation of indirect H-bonds between peptides.[4] The three α chains can be the same or different in a collagen molecule, depending on the type of collagen.[6] A type I collagen molecule has two identical α1 chains and one α2 chain.[6] The Xaa and Yaa amino acid positions are predominantly occupied by proline and 4-hydroxyproline, respectively.[3]

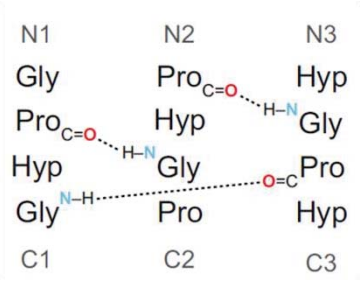

Figure 1.1 Illustration of direct inter H-bonding formed in a segment of collagen triple helix.[5]

1.1.3. Hierarchical structure of collagen

As type I collagen is a fibrillar collagen, a process called fibrillogenesis can occur. At the time when collagen molecules are formed *in vivo*, they are called 'procollagen' and contain long N- and C- terminal non-helical propeptides which prevent them from self-assembling (Figure 1.2).[5] *In vivo* fibrillogenesis is initiated by both N- and C- non-helical propeptides being truncated by their proteases, so that tropocollagen molecules with short N- and C- telopeptides are formed.[5] A tropocollagen molecule is less than 300 nm in length and less than 2 nm in diameter. It is not the thermodynamically favourable form at physiological temperature, so the tropocollagen molecules parallel stack one on the other, offset by 67 nm, forming microfibrils with a characteristic 'D-periodic' spacing close to 67 nm.[5] Subsequently, a lysyl oxidase modifies the lysine or hydroxylysine in the C- and N- telopeptides to allow crosslinking to form within or between the microfibrils to form larger fibres.[5]

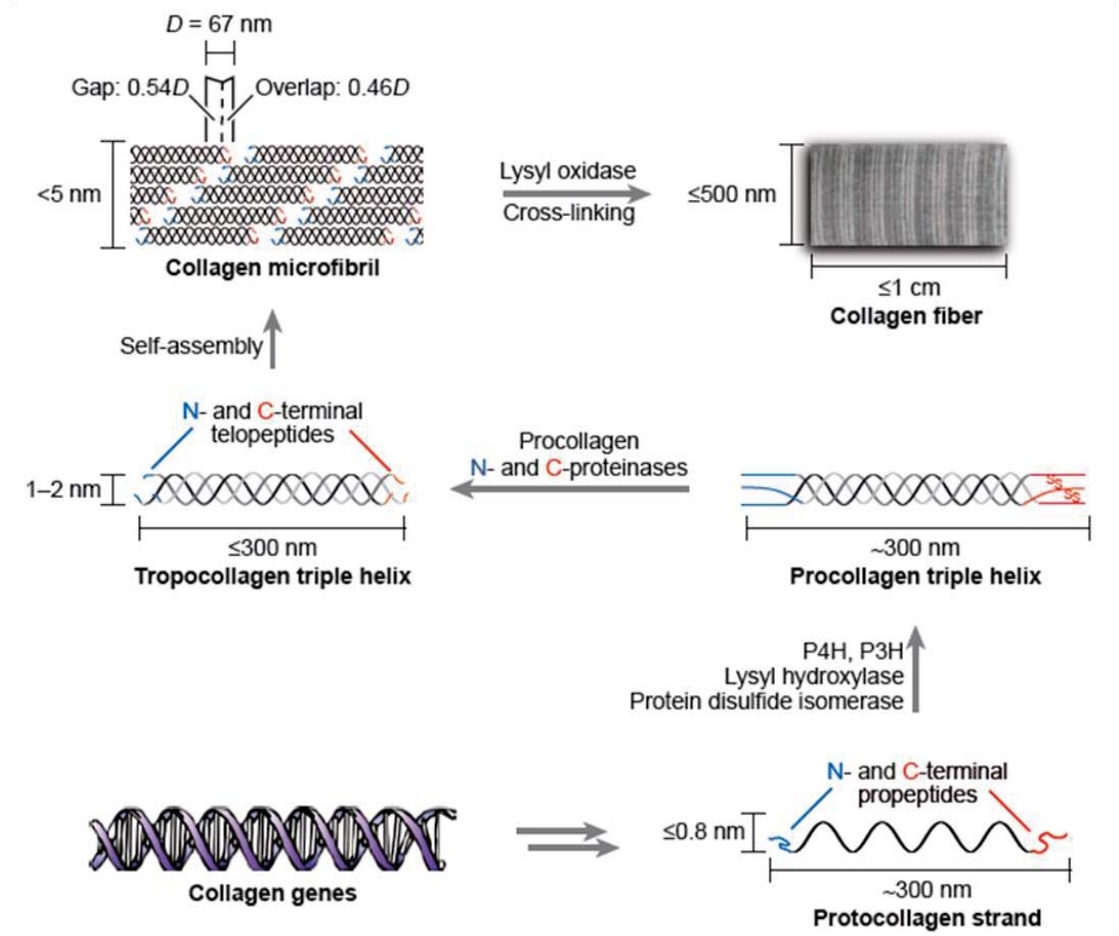

Figure 1.2 Scheme of collagen fibrillogenesis *in vivo*.[5]

The process of fibrillogenesis is driven by entropy, because it reduces the non-favourable interaction between hydrophobic amino acid residues and the hydrophilic solvent, and a fraction of the rigid orientated solvent molecules become free.[6]

Fibrillogenesis can also occur *in vitro* under physiological conditions for the extracted collagen monomers.[6] It happens faster in acid extracted collagen than pepsin extracted collagen, as the C- telopeptide, which has been digested by pepsin during the extraction process, plays a role in initiating the nucleation of the fibrillogenesis.[6] When the acidic collagen solution is neutralized, nuclei are formed by the association of few numbers of collagen molecules.[6] The system then enters a growth phase to form larger fibrils. The structure of the fibrils formed is affected by pH, temperature, buffer content, the

intactness of the telopeptides and the coexistence of other molecules.[6] The collagen fibrils reconstructed *in vitro* from pepsin extracted collagen do not however possess the same mechanical properties and thermal stability to the collagen in organism's tissues, as the telopeptides which correspond to *in vivo* covalent crosslinking are absent[6]

1.1.4. Applications of collagen

Collagen has been widely used in biomedical areas including tissue engineering and drug delivery.[7] The reasons why collagen is such a widely used material include: abundance of raw materials, simple extraction processes, biocompatibility and biodegradation.[8] The raw material for collagen extraction can be tendon, fish skin,[9] rat tail, chicken skin, bovine hide and limed split.[1-2] Most of them are the byproducts of food or leather industries and by themselves do not have a high value. Being the main component in these materials the yield of collagen extracted can be high. As a natural material, collagen is the main protein in human extracellular matrix, skin, muscle and bone. The use of collagen in humans for implants is less likely to cause immunogenic responses and so the implants are less often rejected by the body. In addition, collagen is biodegradable by enzymes and there are no concerns about side effects after application.[10]

The basic idea of tissue engineering is to provide a three dimensional supportive template with the combination of cells from the body to assist the damaged tissue re-growing process.[10] Collagen for skin replacement was initially prepared in the form of a sponge.[8] Fibroblasts encapsulated in a lyophilized collagen sponge used as artificial skin for transplantation was considered to be suitable for epithelialisation.[8] The osteoinductive effect of collagen itself enables it to be used for bone regeneration.[8] This application could be further enhanced by incorporating bone-inducing protein or

hydroxyapatite into collagen .[8] In addition, modified collagen biomaterials have also been fabricated into artificial blood vessels, heart valves, etc.[8] Artificial blood vessels of a very small diameter have been reconstructed which provide a large surface for cell adherence and promote the tissue healing process.[8]

Collagen biomaterials for drug or biomolecule (such as gene or protein) delivery can be prepared in the forms of sponge for wounds, film, or shield for ophthalmology.[8] Drug molecules can be entrapped in a collagen matrix via electrostatic interactions, covalent interactions or H-bonding.[8] Collagen films or shields for ophthalmology should be thin, in order to minimise visual blurring. After it is applied onto the surface of the cornea, it is hydrolysed naturally and the drug molecules dissolve into the tear fluid and release to the site.[8] Anti-biotic loaded collagen films have been used to treat corneal tissue infection.[8] Collagen shields physically protect the wound from mechanical harm, absorb the tissue exudate to leave a low moisture environment and deliver antibiotics to cure the infection, as well as acting as a scaffold to promote fibroblast proliferation.[8]

However, the low thermal stability, fast degradation by bacteria and weak mechanical property of the extracted collagen monomers limit the applications of collagen in some areas.[3] In order to achieve drug delivery at a more controllable rate, usually the structure of the collagen matrix needs to be modified.[8] Incorporating organic crosslinkers, polymers or inorganic materials are ways to enhance the properties of collagen.[8]

1.1.5. Crosslinking of collagen

Methods for crosslinking collagen can be classified into physical and chemical categories and are summarized in Table 1.1. The physical crosslinking methods are γ-irradiation, UV irradiation and dehydrothermal treatment (DHT).[3] The physical methods

do not require the addition of chemicals, so there are no concerns about the toxicity of the crosslinkers and byproducts. The mechanism of UV crosslinking is a free radical reaction being initiated from the aromatic amino acids (tyrosine and phenylalanine) under UV irradiation at 254 nm.[3] Collagen crosslinked by UV irradiation has shown an improvement in thermal stability and mechanical strength. However, the degree of crosslinking will not be high in this case because there are only limited amounts of aromatic amino acids in collagen.[3] Also, UV irradiation partially denatures collagen.[3]

Table 1.1 Summary of collagen crosslinking methods and the mechanisms of action.

	Crosslinking method	Mechanism of action
Physical crosslinking	γ-irradiation	
	UV irradiation	Radical reaction on aromatic amino acids
	Dehydrothermal treatment (DHT)	
Chemical crosslinking	Formaldehyde 	Forming an intermediate with free amino acid group to react with tyrosine, asparagine or glutamine.
	Glutaraldehyde (GTA) 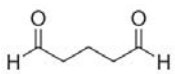	Be able to interact with free amino group, carboxylic group, amide bond and other amino acid side groups of collagen. A bridging crosslinker.

Chemical crosslinking	Hexamethylenediisocyanate (HDC) 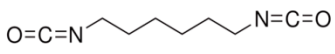	Forming crosslink with two amino groups.
	Polyepoxy compounds eg ethylene glycol diglycidyl ether 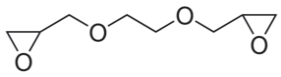	Forming crosslink with two amino groups.
	Carbodiimides eg 1-ethyl-3-(3-dimethylaminopropyl) carbodiimide 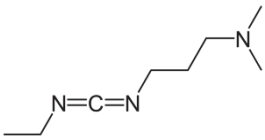	Forming active intermediate with a carboxylic group to react with an amine group to form a natural peptide bond. A ‘zero-length crosslinker’.

The commonly known crosslinkers for chemical crosslinking are glutaraldehyde (GTA), carbodiimides, hexamethylenediisocyanate (HDC), and polyepoxy compounds, etc.[3] All of these except carbodiimides contain two active functional groups that could react with the functional groups of the collagen molecules therefore bridging the collagen molecules together. Thus, these crosslinkers are called ‘bridging crosslinkers’.[11] Their mechanisms of action with collagen are listed in Table 1.1. Carbodiimides are regarded as ‘zero-length crosslinkers’, because they only form intermediates with the carboxylic groups to assist amide bond formation, and themselves do not get involved in the linkages.[11] Apart from these, there is another group of crosslinkers called ‘multi-way

crosslinkers'. They contain more than two functional groups and are able to form more than two bonds with collagen, leading to a special three dimensional arrangement. The existing examples of multi-way crosslinkers are dendrimers and surface functionalized nanoparticles.[11-12]

1.2. Nanoparticles

Nanoparticles are particles with at least one dimension having size between 1-100 nm. Compared with bulk particles, they have larger surface area and higher surface to volume ratio. In addition, they have higher surface energy due to exposing more atoms on the surface. As a result, nanoparticles have different physical, chemical and biological properties compared to their bulk size counterpart.[13]

1.2.1. Synthesis of nanoparticles

The methods for nanoparticle synthesis can be classified into two categories, which are physical and chemical methods.[13] Physical methods utilize physical energy or mechanical actions to break down bulk phase material into nano-sized particles. The common methods are milling, heating, laser ablation, combustion, etc. However, chemical reactions may occur simultaneously during physical actions. In chemical methods, nanoparticles are fabricated by the formation of chemical bonds from precursors at atomic or molecular level to larger clusters.[13] Solution synthesis, chemical vapour decomposition and microwave synthesis are examples of chemical synthetic methods.[13] Physical methods are more widely used in industry as they are easier to scale up. However, the nanoparticles produced by physical methods tend to agglomerate. On the other hand, the properties of nanoparticles can be controlled more precisely by chemical methods.[13] In all of these, solution phase synthesis is promising, for the

reasons that it is able to control the size, shape, and surface functionality as well as the dispersibility of the nanoparticles.[14]

The process of solution phase synthesis can be divided into two stages which are nucleation and growth. Nucleation is the formation of small clusters from monomers when the monomers in the precursor solution are supersaturated.[14] After the nuclei are formed, the system enters a growth phase where the size of the small cluster increases. The growth of the nuclei can be either due to the deposition of free monomers on the nuclei surface, or through disintegrating some of the nuclei back to monomers and re-depositing onto the existing nuclei.[14]

1.2.2. Surface functionalization of nanoparticles

Surface functionalization of nanoparticles with capping agents or surfactants plays a very important role in improving the stability of nanoparticles.[14] A large portion of surface atoms means nanoparticles having a high surface energy, and they tend to minimise the surface energy by agglomeration.[14] By attaching surface passivating agents on nanoparticles, their surface energy can be lowered and the capping shields the nanoparticle cores from directly interacting with each other, hence stabilizing the nanoparticles by steric hindrance. Similarly, nanoparticles can also be stabilized when their surfaces are functionalized with charged functional groups due to electrostatic interactions.[14] The participation of surfactants or capping agents in the nanoparticle growth stage can direct nanoparticles to grow anisotropically, because of preferential binding of the capping agents to some specific facets of the crystal structure.[14] More importantly, surface functionalization of nanoparticles introduces functional groups onto the nanoparticle surface, which is very important for the biological applications of the nanoparticles.[14] Site-specific drug release using nanoparticles as carriers can be

achieved by attaching a ligand which will specifically bind to a target therapy site.[15] Nanoparticles for biosensing or bioimaging have been developed to recognize proteins, cells, DNA, viruses and bacteria, etc.[16]

1.2.3. Properties and applications of TiO_2 and ZnO NPs

Both TiO_2 and ZnO NPs are inorganic metal oxide NPs and they have many properties in common. Both of these nanoparticles are widely employed as ingredients or additives in many different areas due to their diverse properties. They are used as pigments in the paint industry, thanks to their high refractive indices.[16-17] In the cosmetic industry, they are one of the active ingredients in sunscreen as they are broad range UV absorbers.[14, 17] Their wide band gap semi-conductive properties allow them to be used for optoelectronic devices.[14, 18] TiO_2 and ZnO NPs have also been grown on fabric or glass to create self-cleaning and anti-bacterial surfaces due to their photocatalytic properties.[18-19] In addition, they can be potentially applied in biomedical areas including phototherapy, biosensing and bioimaging as mentioned above, thanks to their photoluminescence.[16] Additionally, both TiO_2 and ZnO NPs are also found useful as additives in the polymer industry.

TiO_2 and ZnO have been used to enhance the mechanical property of polymeric materials via three different routes. The incorporation of TiO_2 NP can act as a filler to improve the viscosity of a polymer solution as demonstrated for polybutane solutions in decaline.[20] The increase in viscosity tunes the Newtonian property of the polymer solution to non-Newtonian.[21] The degree of viscosity enhancement is affected by how well the NPs are dispersed in the polymer matrix.[22] TiO_2 and ZnO NPs can also improve the mechanical properties of the polymer materials by acting as crosslinkers, with an example of ZnO NPs functionalized with rubber coupling agent crosslinking a

silicone rubber matrix.[18] Other than these, TiO_2 and ZnO NPs can act as photocrosslinkers because they are photo-active and can generate superoxide radicals.[18, 23] TiO_2 NPs have been used to photocrosslink dimethylacrylamide (DMMA) monomer under UV irradiation.[23] The same principle was applied to photocrosslink carboxylated nitril rubber with ZnO NPs.[18]

1.3. Collagen nanocomposite

Nanocomposites are a new class of materials which contain multi-phases with at least one phase having a size smaller than 100 nm in one or more dimensions.[24] In many cases, the nano-sized materials are inorganic, which are embedded in other phases such as polymers, and can tune the optical, mechanical, conductive and magnetic properties of the polymers, to achieve superior properties and functions that are not achievable by the use of organic polymers.[24] For example, adding ZnO NP to rubber raises the thermal conductivity of the rubber while its high electric resistance is retained.[18] Similarly, some inorganic materials have been used as fillers or crosslinkers in order to enhance the thermal and mechanical properties of collagen materials. These collagen nanocomposites can be fabricated by mechanically mixing the nanoparticle suspension with collagen solution or by in situ synthesis of nanoparticles from a precursor in the collagen matrix.[24]

A lot of research has been carried out on silica-collagen composites. Silica collagen hybrids formed by in-situ condensation of silica from sodium silicate on collagen fibrils have been demonstrated to be a superior biomaterial for wound dressing.[25] The deposit of silica disturbs the fibrillogenesis process, and as a result larger diameter fibrils and more open three dimensional networks are formed.[25] The mechanical strength has been improved significantly, thus the degree of collagen gel contraction is reduced, and this

promotes fibroblast viability when the composite is used for tissue engineering.[25] Some researchers introduced silica NPs in different sizes to collagen and realized they modified the mechanical properties of the composites in different manners. The viscoelasticity of a 12 nm silica impregnated collagen composite was increased, while there was no significant change on 80 nm silica collagen composite.[26] Alvarez et al. introduced larger size silica (greater than 100 nm) to collagen matrix, and found that for composites made with 500 nm silica, increasing silica concentration enhanced the elastic property of the composites, but an opposite trend was observed in composites with smaller size silica particles.[27] The reason behind this was that the high loading of 100 nm size silica particles was found to distort the fibrillar network organization, while the 500 nm particles do not alter the collagen fibrillar network so they can reinforce the mechanical property of collagen. However, in these cases the size of the nanoparticle does not exhibit a dramatic effect on the thermal stability of the collagen, because the surface of the nanoparticles is not functionalized and there are only very weak interactions present between the silica and collagen.[26]

Studies have also been conducted on collagen nanocomposite hydrogels containing Au, Fe_2O_3 and Cr_2O_3 NPs etc. Carboxylic acid functionalized Au NPs have been used to crosslink collagen to form hydrogels with improved thermal stability and viscoelasticity.[11, 28] Another study on Au NP collagen composites was conducted by Wilson *et al*., who compared the interactions between collagen and Au NPs that had been coated with different polyelectrolyte multilayers.[29] They found that the polyanionic terminated Au nanoparticles not only accelerated the process of fibrillogenesis, but also enhanced the stiffness and elasticity of the collagen composite.[29]

Nidhin *et al*. crosslinked collagen with starch coated Fe_2O_3. The starch layer coating on Fe_2O_3 was reported to reduce the toxicity of Fe_2O_3, and at the same time improved its supermagnetic and fluorescent properties.[30] This maked the composite an interesting material for magnetic resonance and fluorescent imaging.[30] Collagen fibrils generated by fibrillogenesis were crosslinked via H-bonding with OH groups of the starch molecule which enhanced the mechanical strength to a certain degree, so it became more suitable for tissue engineering than the collagen without the nanoparticles. However, there was only about a 3°C increase in thermal denaturation temperature, because only non-covalent forces hold the fibre bundles together.[30] Polystyrene-block-PAA encapsulated Cr_2O_3 also crosslink collagen but via electrostatic interactions to build 3D structures. The existence of the Cr_2O_3 NPs does not destroy the intact triple helical structure of single collagen molecule and fibrillogenesis still occurs.[31]

In this project, we focus on preparing collagen nanocomposite hydrogels with TiO_2 and ZnO NPs, and investigate how the mechanical properties of the collagen hydrogels are affected by the nanoparticles.

1.4. Rheology

1.4.1. Linear rheology

One simple and appropriate method to study the mechanical properties of a hydrogel is rheology. Rheology is the study of deformation and flow of a matter after it is subjected to a force.[32] Linear rheology studies the rheological properties of the material in its steady state. A solid material obeys Hooke's law, that the stress is proportional to the strain (Eq 1.1).[32] It is said that the solid displays elastic behaviour:

$$\sigma = G\gamma \qquad \text{(Eq 1.1)}$$

σ is the shear stress and γ is the shear strain.[32] G is the elastic constant.

In contrast, a liquid will flow when it is subjected to a force. Viscosity is the measure of a liquid's resistance to its flow after a force is applied. It is the result of friction between particles moving with varied velocities.[32] An ideal liquid has zero viscosity which means it has no resistance to shear stress, while a liquid with high viscosity only flows slowly even after the application of a large stress. Here, a one-dimensional parallel plate model is used for illustration (Figure 1.3).

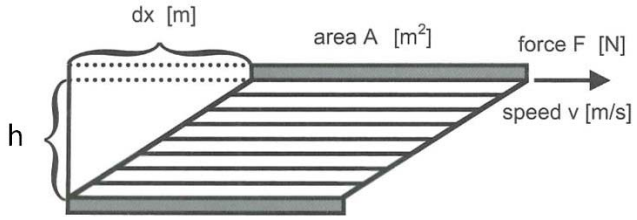

Figure 1.3 Illustration of shear flow using a one-dimensional parallel plate model.[33]

The shear stress (σ) is defined as the shear force (F) over the area which the force is applied (A),[33]

$$\sigma = F/A \qquad \text{(Eq 1.2)}$$

The shear rate $(\dot{\gamma})$ is the ratio of strain (dx/h) over time (Δt). It is also the ratio of the velocity ν to the thickness h.[33]

$$\dot{\gamma} = (dx/h)/\Delta t = (dx/\Delta t)/h = \nu/h \qquad \text{(Eq 1.3)}$$

A pure fluid has only viscosity and it satisfies the following relationship:

$$\sigma = \eta \cdot \dot{\gamma} \qquad \text{(Eq 1.4)}$$

where the proportionality factor, η, is the viscosity of the fluid. For Newtonian fluid, η is a constant and it is independent of the shear rate.[33]

However, most soft matter has mechanical properties which lie between an ideal solid and a pure liquid. They are defined to have viscoelastic behaviour.[32-33] The mechanical properties of the viscoelastic materials are usually measured by oscillatory rheology which gives both elasticity and viscosity information.[34] In a small oscillation measurement, a sinusoidal shear deformation is applied on the sample. While $\hat{\gamma}$ is the deformation amplitude and ω is the angular frequency, the strain with respect to the time scale of rotation is given by:[33]

$$\gamma = \hat{\gamma}\sin(\omega t) \qquad \text{(Eq 1.5)}$$

For an ideal solid material, stress σ is proportional to strain γ, so there is an in phase relationship for the stress and strain curves as illustrated in Figure 1.4.[33] On the other hand, shear stress σ is proportional to the shear rate $\dot{\gamma}$ for a pure viscous fluid.[33]

$$\dot{\gamma} = \frac{d\gamma}{dt} = d\,[\hat{\gamma}\sin(\omega t)]\,/dt = \omega\,\hat{\gamma}\cos(\omega t) = \hat{\dot{\gamma}}\sin\left[(\omega t) + \frac{\pi}{2}\right] \qquad \text{(Eq 1.6)}$$

So that the strain γ is 90° out of phase with the stress σ (Figure 1.4).[33]

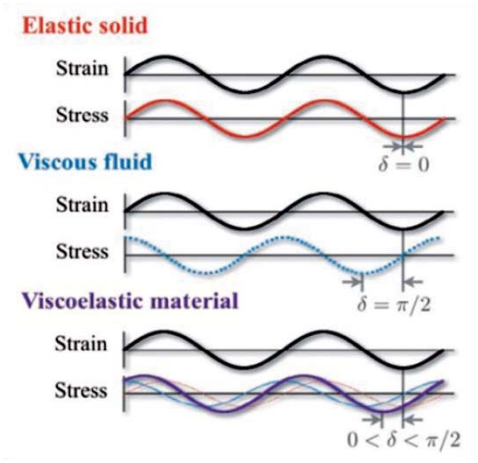

Figure 1.4 Strain and stress curves for solid, fluid and viscoelastic material.[34]

Therefore, viscoelastic materials obey the following equation:[33]

$$\sigma = G_E \hat{\gamma} \sin(\omega t) + \eta_V \omega \hat{\gamma} \cos(\omega t) = \hat{\gamma}[G_E \sin(\omega t) + \eta_V \omega \cos(\omega t)] \qquad \text{(Eq 1.7)}$$

Storage modulus G' and loss modulus G" are introduced and they describe elasticity and viscosity respectively. In another words, G' is the amount of energy being stored in the deformation process and G" measures the amount of energy being dissipated,[35] and they are frequency dependent. Eq 1.7 can be expressed as:[33]

$$\sigma = \hat{\gamma} [G'(\omega) \sin(\omega t) + G''(\omega) \cos(\omega t)]$$

$$= \hat{\gamma} \left| G^* \right| \sin [(\omega t) + \delta] \qquad \text{(Eq 1.8)}$$

where G* is the complex modulus and G* = G' + iG".[33] The phase angle δ will be between 0 and 90°.[33] All above only makes sense when the deformation is small and the material is not modified by the application of force.

1.4.2. Non-linear rheology—strain stiffening effect

Stress is only proportional to the strain in a linear rheological measurement when a small strain is applied to the material. When a large strain is applied, many biopolymers

including collagen have been shown to have strain stiffening behaviour, and ultimately fail irreversibly.[36] Strain stiffening means the stiffness of the material increases with the strain applied after the strain increases to a certain point.[37] In a polymer network, its persistence length (l_p) is the measurement of the rigidity of the polymer chain, while the contour length (l_c) is the distance between two crosslink points.[38] A filament in the network will be flexible if the filament has l_p much smaller than the l_c, whereas it will be rigid if the filament has l_p greater than l_c. A semi-flexible network with l_p and l_c of a comparable magnitude will exhibit strain stiffening.[36, 39] It is commonly agreed that how sensitive the network is to deformation is determined by the ratio of the l_p to the l_c of its constituent filaments or the mesh size.[36]

Figure 1.5(a) shows the strain stiffening response of some of the biomaterials which have been explored. The strain sweep curve of a strain stiffening polymer can be divided into three regimes. When a small strain is applied on the network, the constituent polymers are in a steady state and the material has constant equilibrium storage modulus (G_o'), until a point that G' starts to increase (critical strain γ_c). Then G' enters a non-linear regime where the stress is no longer proportional to the strain. It keeps increasing until the strain exceeds the tolerance of the network (yield strain γ_y), characterized by G' dropping suddenly (not shown in the figure).[40]

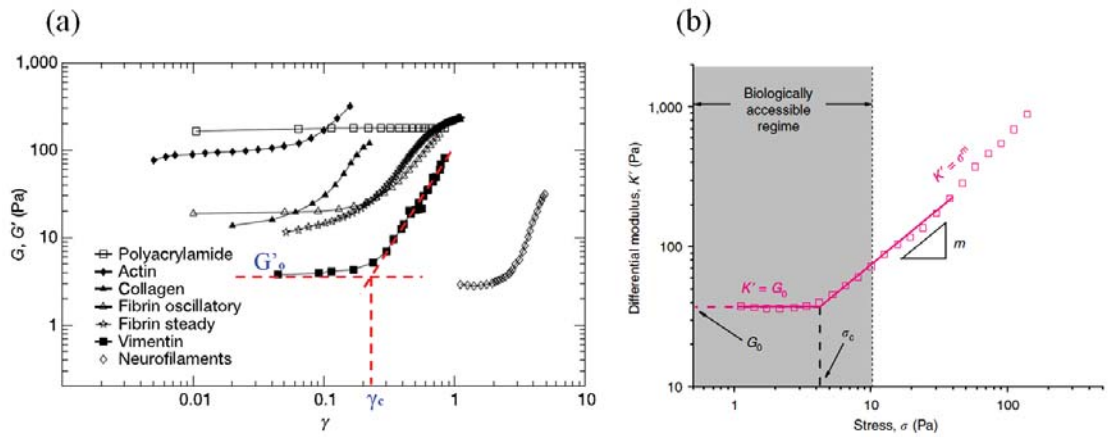

Figure 1.5 (a) Strain stiffening in some biopolymer networks, image obtained from Storm et al.[36] (b) A typical differential shear modulus versus stress curve of a strain stiffening biopolymer, image obtained from Jaspers *et al*.[41]

The mechanism of the strain stiffening behaviour is not fully understood and different theoretical models have been built to try to understand it. One model is built under the assumption that the polymer network is homogeneous, isotropic and deforms uniformly (affine).[36] Under stretching, its single filaments have independent non-linear force extension responses against entropy so the whole network shows a strain-stiffening response.[36] Another model explains the mechanism by postulating nonaffine (not uniform) reorientations of the network under strain. The semi-flexible filaments bend to align themselves along the direction of shearing under small strain, and the strain stiffening is accounted for this bending interaction followed by stretching the aligned filaments against enthalpy.[39, 42] It is considered that the first model is suitable to predict affine isotropic dense network deformations, while the second model is suitable to predict nonaffinely deformed heterogeneous networks. However, the strain stiffening behaviour of collagen has been described by both models.[39]

1.4.3. Rheometer

A mechanical rheometer is one of the instruments available to obtain the rheological behaviour of a sample. In a linear rheological measurement, a known small stress (or strain) is applied on the sample and the outcoming strain (or stress) is recorded.[33] Usually a rheometer is supplied with three different types of geometries which are cone-plate, plate-plate and cylindrical-Couette geometries. The following table compares the working principles and usages of cone-plate and plate-plate geometries.

Table 1.2 Comparing cone-plate geometry and plate-plate geometry.

Cone-plate geometry	Plate-plate geometry
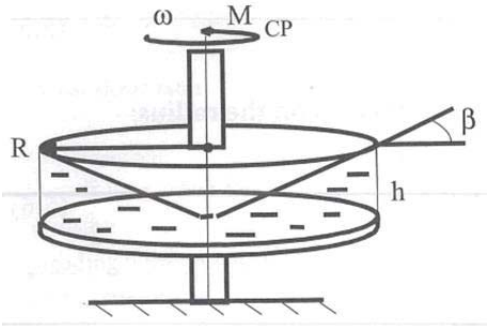	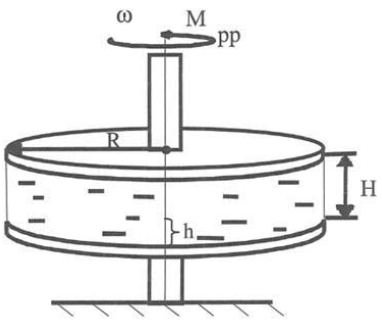
Shear rate $\dot{\gamma} = \omega/\tan\beta = \omega/\beta$ ($\tan\beta = \beta$ when β is small, $\tan\beta$ is constant for any point on the cone)[33]	Shear rate $\dot{\gamma} = r\Omega/H$ ($\dot{\gamma}$ depends on r)
Stress $\sigma = 3M_{cp}/2\pi R^3$	Stress $\sigma = 2M_{pp}/\pi R^3$
Measuring liquid samples[33]	Most suitable for semi-solid materials[33]

1.5. Objectives

Collagen nanocomposite hydrogels with SiO_2, Au and Fe_2O_3 NPs, etc, have shown improved properties thanks to the synergetic effects of collagen and the nanoparticles. However, very few works have been carried out on fabricating collagen nanocomposite hydrogels with TiO_2 and ZnO NPs. As introduced above, the roles of TiO_2 and ZnO NPs have been widely explored in different areas. Therefore, by introducing these two nanoparticles to collagen, it is expected to synthesize a novel class of collagen based nanocomposites which are potential candidates for biomedical applications. This project focuses on studying how surface functionalized TiO_2 and ZnO NPs affect the mechanical properties of type I collagen. The mechanical properties of these nanocomposites or hydrogels are studied by linear and non-linear rheology. Most of the previous work on collagen nanocomposites focuses only on the linear rheological properties of the nanocomposites and seldom considers the non-linear rheological response. Some other techniques including FTIR, confocal microscopy and DSC are also used in order to understand the nanoparticle collagen hydrogel systems.

The surfaces of the TiO_2 NPs are functionalized with chitosan or poly (acrylic acid) (PAA), with the aims of stabilizing the TiO_2 NPs as well as introducing the functional groups that are able to interact with the collagen. Chitosan is an amine functionalized polysaccharide. It is a natural polymer which is non-toxic, very biocompatible and biodegradable.[43] It has been employed in drug delivery and tissue engineering.[44] It is rich in functional groups including hydroxyl, amide, amine and ether, and so that it has a great affinity to many biological molecules such as collagen.[43a] Coating chitosan on TiO_2 NPs also allows the possibility of attachment of other molecules on the nanoparticles, so it is a useful candidate for a TiO_2 surface coating in order to broaden

the potential applications of the TiO_2-collagen composite. On the other hand, PAA is a synthetic polymer which is also non-toxic and biocompatible. The only functional group it carries is COOH which is a good chelating group for TiO_2, explaining why it has previously been used to improve the stability of TiO_2 NPs.[45] It is also miscible with collagen to form a bioartificial blend.[46] Therefore, it is expected that PAA can play a role in assisting TiO_2 to disperse in collagen solution. Chitosan and PAA have different functional groups, so how the surface functionalization of NPs affects the collagen nanocomposites can be studied.

ZnO NPs are capped with polyvinylpyrrolidone (PVP) which is a well known passivating agent. PVP strongly absorbs on ZnO surfaces during the growth phase to control the morphological growth and size distribution of the ZnO NPs.[47] It is a synthetic polymer, but has been found to improve the bioactivity of some bioartificial materials, and itself has been fabricated into an artificial blood plasma substitute.[48] It is also very compatible with collagen solutions.[48] PVP capped ZnO NPs induced collagen hydrogels are prepared with a different protocol to the TiO_2-collagen nanocomposites as described in detail in the relevant chapters. Their physical properties are compared with that of the collagen gel prepared with conventional fibrillogenesis protocol.

There are five chapters in this thesis. The general background information related to this project has been introduced in this chapter. Chapter 2 details the experimental methods used for fabricating the collagen nanocomposites and describes the characterization techniques. The properties of the TiO_2-collagen nanocomposites are discussed in Chapter 3. Chapter 4 discusses the properties of collagen hydrogels made by the introduction of ZnO NPs. Comparisons between TiO_2 and ZnO collagen hydrogel

systems, final conclusions and future perspective of this study are presented in Chapter 5.

2. Experimental methods

2.1. Materials

All of the materials were used as received without further purification. Titanium (IV) tetrachloride ($TiCl_4$, purity ≥ 99%) was purchased from Fluka. Benzyl alcohol (anhydrous, ≥ 99.8%), chitosan (low molecular weight, deacetylated), poly (acrylic acid) (PAA, Mw ~ 1, 800), zinc acetate dihydrate, polyvinylpyrrolidone (PVP, Mw ~ 55, 000) and porcine pepsin were purchased from Sigma-Aldrich. Glacial acetic acid (HOAc) was supplied by SDS. Ethanol, potassium chloride (KCl), di-sodium hydrogen phosphate anhydrous (Na_2HPO_4, buffer grade) and potassium dihydrogen phosphate (KH_2PO_4) were supplied by Pure Science, New Zealand. Sodium hydroxide (NaOH) and hydrochloric acid (HCl, 37%) were purchased from Pancreac. Potassium hydroxide (KOH) was purchased from Univar. Tetrahydrofuran (THF, HPLC grade) and ammonium chloride (NH_4Cl) were purchased from Fisher Scientific. Sodium chloride (NaCl, pharmaceutical grade) was supplied by Dominion Salt. Bovine limed split was supplied by Tasman Tanning, Wanganui, New Zealand.

2.2. Nanoparticle synthesis

2.2.1. TiO_2 NP synthesis

The method of making TiO_2 NPs was adapted from Niederberger et al.[49] The addition of $TiCl_4$ (1 mL) to benzyl alcohol (20 mL) at room temperature under vigorous stirring generated a yellowish-orange mixture. The mixture was heated up to 100°C and kept at that temperature for 24h. As the temperature increased, the yellowish-orange precipitate dissolved gradually, and the mixture turned to white. After the reaction, the TiO_2 NPs

were collected by centrifugation and washed with ethanol and THF, then re-dispersed in water.[49] They were dialysed against water to remove tetrahydrofuran (THF). The as-synthesized nanoparticle was denoted as 'TiO_2-UM NP'.

In order to investigate whether the surface capping of the TiO_2 NPs has an effect on its interaction with collagen, the surface of the as-synthesized TiO_2 NPs was subsequently modified by different capping agents.

PAA capped TiO_2 NP (TiO_2-PAA)

Poly (acrylic acid) (PAA) (40 mg) was dissolved in 5 mL water and added to 40 mL 1 mg/mL TiO_2 suspension while stirring. The reaction was continued for 5h at room temperature. In order to collect the PAA capped TiO_2 after the reaction, dilute HCl was added until a precipitate was formed. The precipitate was collected by centrifugation and easily re-dispersed in water.

Chitosan coated TiO_2 NP (TiO_2-CS)

Four mL of 1% chitosan (CS) in acetic acid (HOAc) solution was added to 40 mL of 1 mg/mL TiO_2 suspension and the mixture was stirred vigorously at room temperature for 5h. After that, dilute NaOH solution was added to neutralize the positive charges on CS until a precipitate formed. The CS coated TiO_2 NPs were collected by centrifugation. The precipitate was washed with distilled water and re-dispersed in 0.05 M HOAc solution.

2.2.2. ZnO NP synthesis

ZnO-plain and ZnO-PVP NP synthesis

PVP capped ZnO NPs were synthesized using a sol-gel method modified from Guo *et al*.[47] Zinc acetate dihydrate ($Zn(OAc)_2 \cdot 2H_2O$, 1.0975 g) was dissolved in ethanol (100

mL) to form a 0.05 M solution. Polyvinylpyrrolidone (PVP, MW 55,000, 0.3334 g) in the molar ratio of Zn^{2+}:PVP = 5:3 was added to the zinc acetate solution and the mixture was heated up to 60°C. Potassium hydroxide (KOH, 0.561 g) was dissolved in ethanol (50 mL), which was then added to the above mixture dropwise under vigorous stirring. The reaction was stopped after 2h at 60°C. ZnO NPs with no PVP (ZnO-plain) were synthesized by the same procedure except no PVP was added in the solution.

The purification process for the ZnO sols was carried out as follows. n-hexane (100 mL) was added to 50 mL ZnO-plain or ZnO-PVP sol to induce precipitation. After that, the nanoparticles were collected and dispersed in ethanol. Before the ZnO NPs were introduced to collagen, they were rotary evaporated to remove the ethanol completely and suspended in water.

2.2.3. Nanoparticle characterization

The NPs were characterized using transmission electron microscope (TEM) to monitor the size and morphology. The surface functionalization of the NPs was studied by Fourier transform infrared spectroscopy (FTIR), and the degree of surface capping was measured by thermogravimetric analysis (TGA).

Transmission electron microscope (TEM)

TEM is a technique which can be utilized to obtain structural and morphological information of a nanoparticle sample. After high energy primary electrons are generated from the electron gun, they are accelerated and then focused by a magnetic field condenser lens before reaching the sample.[13] The samples have to be thin, as the image is generated by transmitted electrons which pass through the sample. TEM coupled with selective area electron diffraction (SAED) is able to collect the crystallographic

information generated from the electrons scattered by the sample.[13] The TEM images of the nanoparticles were obtained from a JEOL 2100F Field Emission Electron Microscope operated at 200 keV.

Attenuated total reflectance-Fourier transform infrared spectroscopy (ATR-FTIR)

Infrared spectra of the samples were collected using Fourier transform infrared spectrometer (Model Nicolet iS5, Thermo Fisher Scientific, USA) equipped with a ZnSe attenuated total reflectance accessory detector (iD5, Thermo Fisher Scientific, USA). A background was collected with nothing on the accessory detector before the measurements of the samples. Dry samples were placed on the ZnSe crystal and compressed by the control knob to the maximum pressure before the spectra were collected. The spectra were collected in the range 600 to 4000 cm^{-1} (16 scans with a resolution of 4 cm^{-1}).

Thermogravimetric analysis (TGA)

Thermogravimetric analysis (TGA) of the nanoparticles was performed on TA Q50 at a heating rate of 5°Cmin^{-1} under N_2 flow. The nanoparticles were freeze dried overnight to remove solvent before the measurements. The residual weight of the sample was recorded as the temperature of the system was ramped from 20 to 600°C.

Monitoring nanoparticle stability by UV-Vis spectroscopy

The stability of the nanoparticles was evaluated by UV-Vis spectrophotometer (Cary 50 Probe, single beam mode). The measurements were conducted in range from 300 – 800 nm with a data interval of 1 nm. ZnO NPs have absorption peaks in UV-Visible region, and the intensity of the absorption spectrum is proportional to the concentration of the nanoparticle suspension. The absorption peak will decrease in intensity if the nanoparticles agglomerate and form sediments.

After the purified ZnO-plain and ZnO-PVP NPs were rotary evaporated to remove the solvent, they were re-suspended into water and diluted to concentrations which were suitable for the measurements by the UV-Vis spectrophotometer. The absorption spectra of the ZnO-plain and ZnO-PVP suspensions were recorded at 0, 1, 3, 5, 21, 28 and 47h without disturbing the suspensions between measurements.

2.3. Collagen extraction from limed split

2.3.1. Preparation of bovine limed split for collagen extraction

Bovine limed split is the layer shaved off from the inner side of the hide after it has been treated with lime during leather processing. The method of neutralizing limed split was adapted from Zhang *et al.*[2] Firstly, the limed split was de-limed with a solution containing 2% NH_4Cl and 0.5% HCl, based on the wet weight of the split. The pH of the split dropped to about 8 by the end of this process. It was then further neutralized with 0.5% HCl, followed by washing with distilled water and cutting into small pieces. The clean split pieces were freeze dried and stored at 4°C before they were used for collagen extraction.

2.3.2. Pepsin digested acid soluble collagen extraction

The procedure of extracting collagen from limed split was modified from Singh *et al.*[9] All the steps were carried out at 4°C. The dried limed split pieces were soaked in 0.5 M HOAc solution with volume 30:1 (v/w) to the dry weight of the limed split. Porcine pepsin (20 kU/g dry split) was added. The mixture was incubated for 48h with continuous stirring. A thick semi-transparent supernatant was collected by centrifugation. The solid residue was soaked in another 30 volumes 0.5 M HOAc solution for another 48h. The supernatant was collected again and combined with the

first extract. A saturated NaCl solution (with concentration 359 g/L) was poured into the supernatant until the collagen precipitated out. The precipitated collagen was collected and re-dispersed in a minimum volume of 0.5 M HOAc solution. It was then dialysed against 0.005 M HOAc for three days, with the dialysing solvent being changed every 24h. The pH of the collagen was about 4. The concentration of the collagen solution was calculated from the wet and lyophilized mass of an aliquot.

2.3.3. Characterization of the collagen

The limed split extracted collagen was characterized by FTIR. Its purity was examined by SDS-PAGE electrophoresis and its thermal stability was estimated by differential scanning calorimetry (DSC).

FTIR spectrum of the limed split extracted collagen

The FTIR spectrum of LSC is shown in Figure 2.1. It contains the classical collagen amide peaks which indicate the peptide linkage of the collagen molecules, as reported by Rabotyagova *et al.*[50] Amide A at 3305 cm^{-1} associates with the N-H stretching vibration of the peptide bond. It is at a lower frequency than the free N-H stretching mode, which can be explained by the formation of H-bonding between N-H and C=O group of the peptide backbone.[9] Amide B peak at 3078 cm^{-1} could also be assigned as N-H stretching. Amide I at 1633 cm^{-1} represents the stretching vibrational mode of C=O. It gives a good indication of the secondary structure of the polypeptide chain.[9] Amide II is at 1548 cm^{-1}, which is the combination of N-H bending vibration and C-N stretching vibration. The intensity ratio of amide III (1237 cm^{-1}) to the band at 1451 cm^{-1} is roughly 1, suggesting the helical structure of limed split extracted collagen molecules.[9, 51]

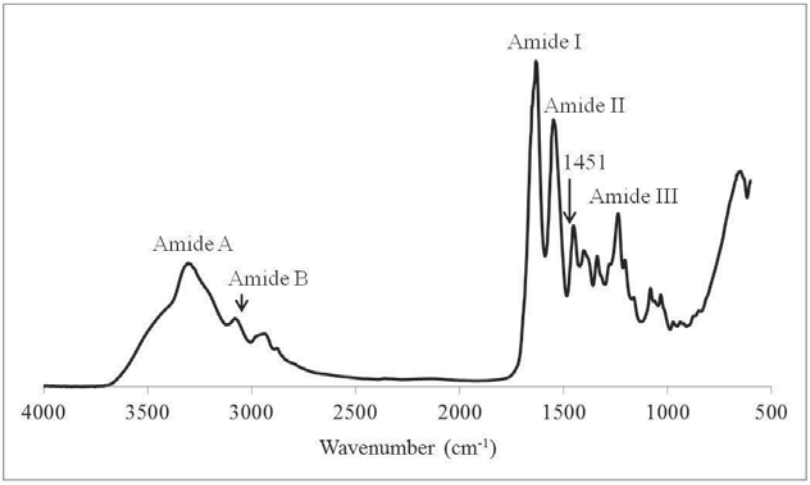

Figure 2.1 FTIR spectrum of limed split extracted collagen.

SDS-polyacrylamide gel electrophoresis (SDS-PAGE)

SDS-PAGE was performed based on the method described by Laemmli.[52] Samples were mixed with loading dye thoroughly and centrifuged at 14 000 rpm for 5 minutes to spin down the undissolved materials. They were loaded onto a polyacrylamide gel which is made of 7.5% separating gel and 4% stacking gel. The system was subjected to electrophoresis at a constant voltage of 200 V for 45min. After that, the gel was fixed with fixing solution (10% acetic acid, 40% ethanol) for 15min, then stained with Colloidal Coomassie Blue G-250 dye (8% $(NH_4)_2SO_4$, 0.8% phosphoric acid, 0.08% Coomassie Blue G-250, 20% methanol) overnight. It was de-stained with distilled water until bands became clear. For comparison, commercially available calf skin collagen, gelatin and denatured collagen were run on the SDS-PAGE gel together with the limed split extracted collagen. Each of them was loaded at two different concentrations. Markers were used to estimate the molecular weight of the constituent proteins.

The electrophoretic patterns of limed split extracted collagen (LSC), commercial calf skin collagen (CSC), gelatin (G) and partially denatured collagen (DC) are shown in Figure 2.2. A single collagen molecule contains two α1 peptide chains and one α2 chain

held together mainly by H-bonding.[50] The pattern of LSC contains four predominant bands, which are γ, β, α1 and α2 from high to low molecular weights, according to Singh *et al*.[9] The γ band has the highest molecular weight which indicates the presence of intact tri-peptide molecules in LSC sample. The β band is from the dimer of two α1 chains or an α1 and an α2 chains.[9] The intensity ratio of α1 to α2 is about 2:1, which suggests the major component of LSC is type I collagen.[9] No smaller molecular weight fragments presenting suggests the integrity and purity of the collagen molecules in LSC sample. In contrast, CSC sample has the same predominant bands, but it also has some other insignificant bands present, which may due to the presence of small amount of other types of collagen. The negative control gelatin (G) shows no bands on the lane. The partially denatured collagen (DC) does not show γ band, but instead, it has various lower molecular weight fragments.

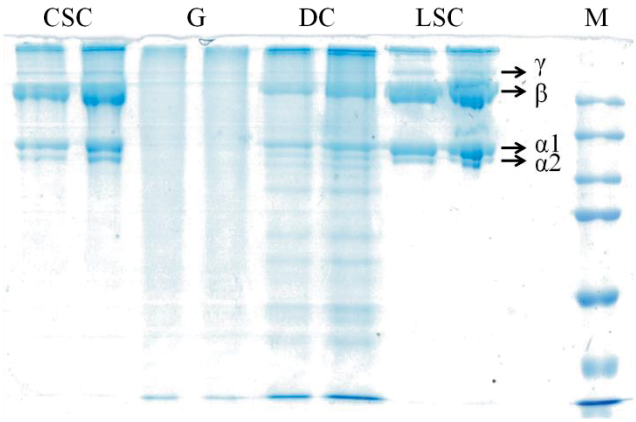

Figure 2.2 SDS-PAGE of commercial calf skin collagen (CSC), gelatin (G), partially denatured collagen (DC), limed split extracted collagen (LSC) and molecular weight marker (M).

2.4. Nanoparticle collagen hydrogels

2.4.1. TiO_2-collagen nanocomposite hydrogels

In an ice bath, 2 mL of 10 mg/mL collagen solution was mixed with 2 mL of 5 mg/mLTiO_2-UM or TiO_2-CS suspension in a petri dish, so that the mass ratio of

collagen:TiO_2 was 1:0.5. 10x PBS buffer (0.5 mL) was added, then the final pH of the mixture was adjusted to 7-7.5 with a NaOH solution. Extra water was added to make up the total volume of the mixture to 5 mL, so the final concentration of the collagen was 4 mg/mL. The mixture was then incubated at 30°C for 24h to induce gelation. For TiO_2-PAA samples, the pH of the collagen solution was raised with PBS before the addition of TiO_2-PAA, due to the fact that TiO_2-PAA NPs were not stable at low pH. As a control, a collagen gel (without nanoparticle) was also prepared with 2 mL water instead of TiO_2 suspension. Other control samples, collagen-chitosan and collagen-PAA hydrogels were also prepared. The amounts of chitosan and PAA present in the hydrogels were similar to that found in the coatings as bound on the nanoparticles based on the TGA measurements. About 32% weight loss was attributed to chitosan in TiO_2-CS NP and about 6% weight loss was attributed to PAA in TiO_2-PAA NP. After the gelation, the as-synthesized nanocomposite hydrogels were freeze dried for characterization.

In the study of the rheological behaviours of the collagen and TiO_2-collagen nanocomposites in different concentrations, collagen solutions were diluted to 5 mg/mL and 2.5 mg/mL, and they were mixed with TiO_2-CS or TiO_2-PAA suspensions in 2.5 mg/mL and 1.25 mg/mL respectively, so that the final collagen concentrations in the samples were 2 mg/mL and 1 mg/mL and the collagen to TiO_2 NP mass ratio was constant to be 1 to 0.5. The rest of the preparation steps were exactly the same as described for 4 mg/mL collagen gels. When studying the rheological behaviours of the TiO_2-collagen nanocomposites as functions of TiO_2 NP concentrations, the collagen concentration in the final gels were constant to be 4 mg/mL, while the concentrations of TiO_2 suspensions were varied to achieve different collagen to TiO_2 mass ratios.

Characterization of TiO_2-collagen nanocomposites

The rheological properties of the nanocomposite hydrogels were measured using a rheometer. The denaturation temperatures of the nanocomposites were measured by DSC. The morphologies of the hydrogel networks were visualized with confocal fluorescence microscope. The dry samples were also subjected to FTIR and swelling ratio assays.

Rheological measurements

The rheological measurements of the collagen and collagen nanocomposite hydrogels were conducted using a TA G2 or HR-2 rheometer coupled with a peltier temperature controlled lower plate. A 4°, 40 mm cone geometry was used for this group of experiments. The collagen and TiO_2 mixture was prepared and neutralized with the method as described above. It was quickly dispensed onto the lower plate of the rheometer which was pre-set to 4°C. A solvent trap was used to prevent solvent evaporating during the measurement. The collagen or TiO_2-collagen nanocomposite gelation was monitored as a function of time using small amplitude oscillatory measurements carried out at 1% strain and 1 Hz frequency for 30 min as the temperature of the lower plate was elevated to 30°C. The rate of gelation (K_{growth}) is the gradient of the linear increase part of G'. After that, the in-situ-formed gel was subjected to a frequency sweep test from 0.1 Hz to 10 Hz at 1% strain, and a strain sweep protocol was carried out from 1% to 100% at 1 Hz and 20°C to study the strain stiffening behaviour of the gel. The critical strain (γ_c), which is the point that G' starts to increase in a strain stiffening sample, can be characterized as the point when stress σ is at least 10% greater than $G_\circ'\gamma$.[40] The strain which gives the maximal G' before the network breaks is called the yield strain (γ_y).[40] The modulus ratio ($G'_{max}/G'_\circ$) reflects the degree of strain stiffening. All measurements were done in duplicate.

For consecutive strain sweep measurements, the collagen and collagen nanocomposite hydrogels were prepared and polymerized on the rheometer as other measurements. With critical strain γ_c and yield strain γ_y for each sample obtained from the last experiments, the sample was subjected to a strain ramp from 0.1% to a strain which was greater than the critical strain but lower than the yield strain of the sample, followed by the strain decreasing back to 0.1%. The loading and unloading cycle was repeated for four times. The collagen concentration in the hydrogels was 1 mg/mL and the mass ratio of collagen to TiO_2 was 1:0.5.

Swelling ratio

Lyophilized hydrogel samples were soaked in a phosphate buffered saline (PBS) at room temperature overnight. The samples were then removed and their surface was gently dried using a filter paper. The swelling ratio of the samples was calculated using the following formula:

$$\text{Swelling ratio (\%)} = (W_{wet} - W_{dry})/W_{dry} \times 100\%$$

where W_{dry} is the weight of the lyophilized sample and W_{wet} is the weight of the sample after soaking in PBS overnight.

Differential scanning calorimetry (DSC)

DSC was performed using a differential scanning calorimeter (TA DSC Q2000). The lyophilized collagen or collagen nanocomposite samples (3-6 mg) were weighted accurately in aluminium pans and re-hydrated with distilled water at a 1:1 (w/v) sample/water ratio. The pans were sealed and the dried samples were conditioned overnight. The samples were scanned at 5°C/min over the range from 20 to 110°C under

N_2 flow, with an empty aluminium pan as the reference. The denaturation temperature of the sample was the onset of the main endothermic peak.

Confocal microscopy

The morphologies of the collagen and nanoparticle-collagen hydrogels were examined through confocal fluorescence microscopy. A neutralized collagen solution (5 μL) prepared as described in 2.4.1 was added to a microscopic slide and warmed in a 30°C incubator for 1h. It was then stained in a Picro-Sirius red solution for 1h before it was covered with a coverslip and sealed with glycerol.

Imaging was carried out using the Leica DM6000B SP5 confocal laser scanning microscope system running LAS AF software (version 2.7.3.9723; Leica Microsystems CMS GmbH). Images were acquired with a HCX PL APO lambda blue 63x (N.A. 1.40) lens with an optical zoom of 3x. The fluorescent probe Picro-Sirius Red was imaged through excitation at 561 nm and emission collection at 571-653 nm. Z-series were collected with a step size of 0.08 μm.

2.4.2. ZnO induced collagen hydrogels

The ZnO NPs induced collagen hydrogels were prepared in a different way to the TiO_2-collagen hydrogels. Aqueous ZnO-PVP NP suspensions were obtained in the method described in 2.2.2. To a petri dish containing 5 mL 5 mg/mL collagen solution, 5 mL ZnO-PVP suspension with concentration from 0.1 mg/mL to 5 mg/mL was overlaid on the top of the collagen solution, so that the mass ratio of collagen to ZnO-PVP added was 1:1, 1:0.5, 1:0.1, or 1:0.05. Then it was incubated on a shaker at room temperature overnight to assist collagen gelation. After 24h, hydrogels were observed to form in some samples. The residual liquid on the surface of the hydrogel was drained off and

the gel was rinsed twice with distilled water. The samples with collagen to ZnO-PVP ratio of 1:0.05 did not gel so the washing step was not carried out. Another group of hydrogels with different collagen concentrations was prepared while the concentrations of ZnO NPs were 0.5:1 to the concentration of the collagen solutions. As an experimental control, a conventional collagen gel of the same concentration was prepared using the same protocol by adding a mixture of PBS buffer and NaOH solution to the top of the collagen solution without mixing the two phases. Hydrogels with ZnO-plain NPs or commercial bulk ZnO, and a conventional collagen gel containing PVP were also prepared in the exact same manner for comparative studies.

For rheological studies, since the hydrogels could not be formed directly on the rheometer as had been done with the TiO_2-collagen hydrogels, the samples were prepared on petri dishes then removed and loaded on the rheometer. Measurements were made using a hatched cross parallel plate geometry in attempt to limit slip. The gap was adjusted to about 1.6 mm which gave a slightly positive normal force again in an attempt to prevent slip. Dynamic frequency sweeps were performed from 0.1 to 10 Hz at constant 1% strain at 20°C to study the linear rheological properties of the samples. For non-linear rheological measurements, the pre-stress protocol was used that the sample was held at a rotational pre-stress σ with a small oscillatory stress $d\sigma$ superposed to obtain the corresponding strain $d\gamma$, in order to get $K = d\sigma/d\gamma$. The first rotational pre-stress was 1 Pa, with the followings values 2, 5, 10, 15, 20, 27, 37, 53, 79, 124, 200, 320, 400 and 520 Pa. Each measurement was conducted at 1 Hz for 60s. It is expected that the results measured with a pre-stress protocol should be the same as the results carried out with a strain amplitude sweep protocol, as long as no relaxation takes place.

The gels were also imaged with confocal microscopy and subjected to small angle X ray scattering measurements. The freeze dried samples were characterized with swelling ratio assays and DSC.

Small angle X ray scattering (SAXS)

The SAXS patterns for collagen solution, the conventional collagen gel control and the ZnO-PVP induced collagen gel were recorded on the SAXS beamline at the Australian Synchrotron. The samples were held in 2 mm path-length cells sealed with Kapton tapes and irradiated with 12 KeV radiation. Scattered radiation was collected using a Pilatus 1M detector located at a camera length of 1.6 m.

Investigating the mechanism of ZnO-induced collagen gelation

Due to the different response of ZnO interacting with collagen solution to that of the TiO_2 NP, additional tests were done in order to understand the effect of ZnO.

A. Spatially resolved optical density measurements

   The changes in the optical densities of the collagen solution during the gelation process were recorded with a laser light scattering setup as shown in Figure 2.3. A speckle pattern was generated when a polarized laser light was scattered by the sample, which was then recorded by a multi-pixel camera using a pinhole to spatially filter the light, so different parts of the CCD recorded scattering from different parts of the sample. Figure 2.3(c) is an example of a scattering pattern of a collagen solution. In order to study the spatially and time-resolved gelation process, the scattering pattern of the optically accessible part of the collagen sample (Figure 2.3(b)) was recorded at one frame per second for 10h. The brightness of the speckle reflects the scattering intensity of the sample. Samples

with larger fibril sizes and higher concentrations will scatter more strongly giving brighter speckles in the images.

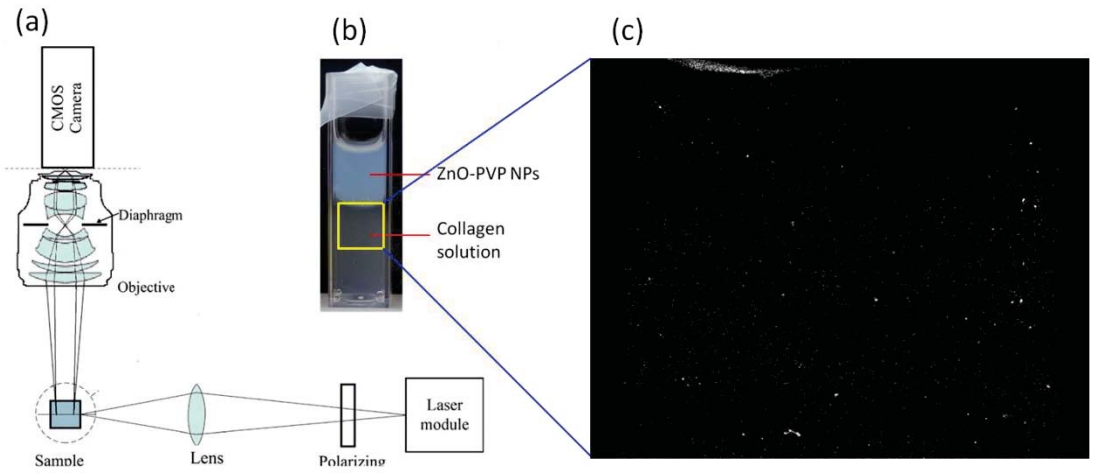

Figure 2.3 (a) A basic setup for a laser light scattering experiment, (b) Scheme of the cuvette used for gelation with optical accessible region marked with a yellow frame, (c) An example of the speckle pattern of collagen scattered by laser light.

A collagen solution (2 mL) was added to a 4 mL plastic cuvette and placed in the laser light scattering setup. The gelation process was started by gently adding ZnO-PVP suspension to the cuvette carefully, avoiding the mixing of the collagen-ZnO interface. As controls, experiments with H_2O, mixture of PBS and NaOH, and bulk ZnO added on the top of the collagen were also conducted.

B. The collagen solution (5 mg/mL, 5 mL) was treated with solutions of zinc acetate or zinc chloride (2.5 mg/mL, 5 mL) in the same way as that with ZnO NPs, in order to examine whether the observed gelation was due to Zn^{2+} or acetate.

C. PVP solution (1.4 mg/mL, equal to the amount of PVP capping on ZnO-PVP, 5 mL) was added to the top of the collagen solution and incubated overnight to examine whether PVP is capable of causing collagen gelation.

D. Five mL collagen solution was enclosed in a dialysis tubing which was immersed in a suspension of ZnO-PVP for three days. Collagen gel was formed inside the dialysis tubing. After that, the gel was cut into three pieces, and they were immersed in water, EDTA solution and acetic acid solution respectively, to see whether the collagen gel formed was soluble in these media.

E. In order to know how the pH of the collagen solution was changed after ZnO-PVP suspension was introduced on top, collagen solution was mixed with pH indicators bromocresol purple (BP), bromothymol blue (BB) and phenol red (PR). Experiments were conducted in 4 mL plastic cuvettes as the laser light scattering experiments were. ZnO-PVP suspension was added to the surface of the pH indicator containing collagen solutions (2 mL) and the colour changes were observed.

2.5. Statistics

All rheological measurements and denaturation temperature measurements were done in duplicate and results were presented as mean ± error, error = (max-min)/2. Swelling ratios were presented as mean ± standard deviation (n=5).

3. TiO_2-collagen nanocomposite hydrogels

In this chapter, surface functionalized TiO_2 NPs were introduced into collagen in order to prepare a new class of collagen based nanocomposites. The TiO_2 NPs were functionalized with chitosan or PAA and characterized by TEM, TGA and FTIR before being introduced to collagen solutions. The properties of the TiO_2-collagen nanocomposites were studied, with a focus on how the linear and non-linear rheological properties changed when varying the collagen concentration, the concentrations of TiO_2 and their surface capping agents. Other techniques including FTIR and microscopy were also used in order to have a better understanding of the system.

3.1. Characterization of surface functionalized TiO_2 NPs

The reaction between $TiCl_4$ and benzyl alcohol is a well known nonhydrolytic sol-gel route to synthesize TiO_2 NP. Benzyl alcohol serves as an oxygen donor, substituting chlorine to form benzyloxy titanium complexes, which then condense to form Ti-O-Ti linkages.[53] The size and morphology of the as-synthesized TiO_2 NPs were characterized by TEM. It can be seen from Figure 3.1 that the product synthesized by this method is composed of irregularly shaped clusters with sizes of 64 (±14) nm in length. The nanoparticles were crystalline as shown by the selected area electron diffraction (SAED) pattern and can be assigned to the anatase crystal phases (JCP DS00-021-1272) (Figure 3.1 insert).

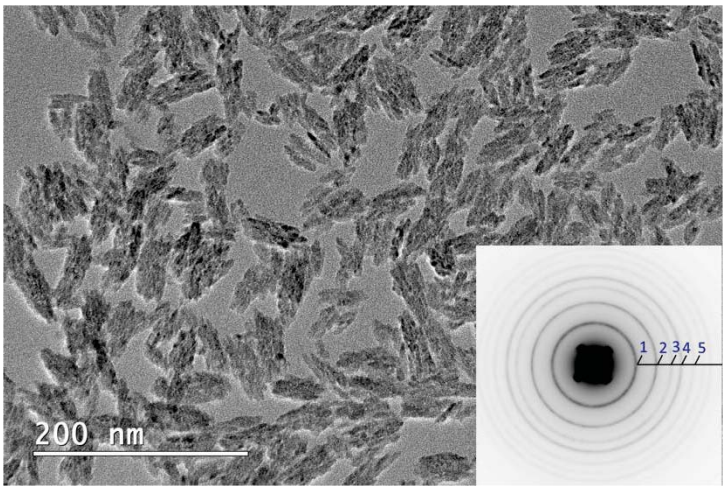

Figure 3.1 Representative TEM image of the TiO_2 NPs. Insert: SAED pattern of the TiO_2 NPs with diffraction rings which correspond to anatase crystal phase.

The TiO_2 NPs were coated with either PAA or chitosan at the post-synthesis stage, so the size, shape and morphology of the particles should be consistent with the un-modified particles. Having a polymer coating on the particle surface can improve the dispersibility of the nanoparticles in a solvent.[24] FTIR is a very useful technique to detect the surface chemistry of particles. The FTIR spectra of the un-modified TiO_2 NP (TiO_2-UM), PAA capped TiO_2 NP (TiO_2-PAA) and chitosan coated TiO_2 NP (TiO_2-CS) are displayed in Figure 3.2. Though the un-modified particles had been dried at 102°C for 48h prior to measurement, the peak at around 3172 cm^{-1} still remained, suggesting that there were a large number of titanol groups, rather than free water molecules attaching on the particle surface.[53] There are also some weak bands between 1600 cm^{-1} and 1400 cm^{-1} which indicate the presence of benzyloxy groups.[53] In the spectrum of TiO_2-PAA nanoparticles (Figure 3.2(a)), the band at 1712 cm^{-1} is from free carboxylic acid groups of PAA. The band at 1634 cm^{-1}, absent in the pure PAA, is due to H-bonding between TiO_2 and PAA.[54] The band at 1276 cm^{-1} is attributed to the symmetrical stretching vibration of COO^- as a monodentate to chelate with TiO_2.[55]

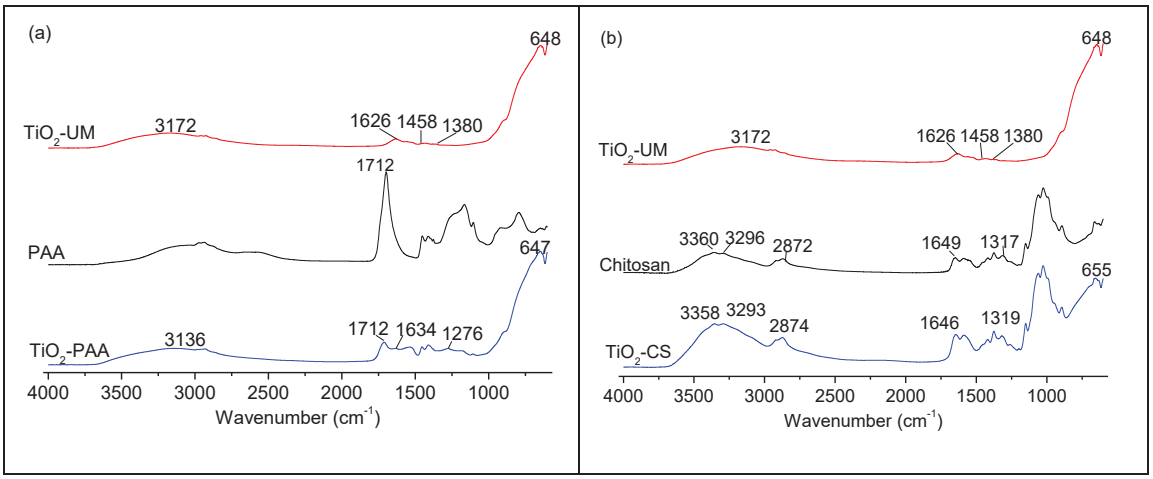

Figure 3.2 FTIR spectra of TiO_2 NPs before and after surface functionalization.

The FTIR spectrum of the TiO_2-CS NP (Figure 3.2(b)) is very similar to that of chitosan alone. The broad band at 3360 cm^{-1} in chitosan has moved to 3358 cm^{-1} after it interacts with TiO_2, while the N-H stretching vibration band at 3296 cm^{-1} is down shifted to 3293 cm^{-1}. The band at 1649 cm^{-1}, which corresponds to the C=O in chitosan, has been shifted to 1646 cm^{-1} in TiO_2-CS NPs, while the band at 1317 cm^{-1}, rising from C-H vibration in the chitosan rings, has been shifted to 1319 cm^{-1}.[56] The FTIR spectrum of TiO_2-CS provides evidence that there is a chitosan coating on the TiO_2 NPs. However, the shifts of the peaks relative to chitosan are not significant enough to say there are bonding interactions between chitosan and the TiO_2 NPs.

Thermogravimetric analysis (TGA) is used to measure the degree of surface functionalization on the nanoparticles. By heating up the sample with a constant heating rate, the unstable and volatile components in the sample will be lost in a stepwise manner. Figure 3.3 presents the TGA plots of the TiO_2 NPs before and after surface functionalization. About 8% weight loss occurs as the TiO_2-UM sample is heated up to 100°C, suggesting that the amount of adsorbed water on the TiO_2-UM NPs is roughly 8% of the total weight of the sample. A further 11% weight loss occurs as the sample is continuously heated up to 600°C. This part of the weight loss is considered to be the

decomposition of organic residues and the condensation of titanols.[53] TiO_2-PAA NPs degrade from about 215°C to 500°C with the fastest weight loss at 300°C. About 75% of the weight remains by the end of the measurement for TiO_2-PAA sample. Compared with that of the TiO_2-UM NPs, it can be estimated that the PAA capping on the particles is about 6% of the total weight of the sample. While chitosan coated NPs have a significant decomposition at temperatures of around 275°C, about 49% of the total weight remains after the heating process. Therefore, the coating of chitosan on the sample is relatively thick, contributing to approximately 32% of the sample (51% total weight loss is observed including 8% water and 11% organic residues and condensation of titanols).

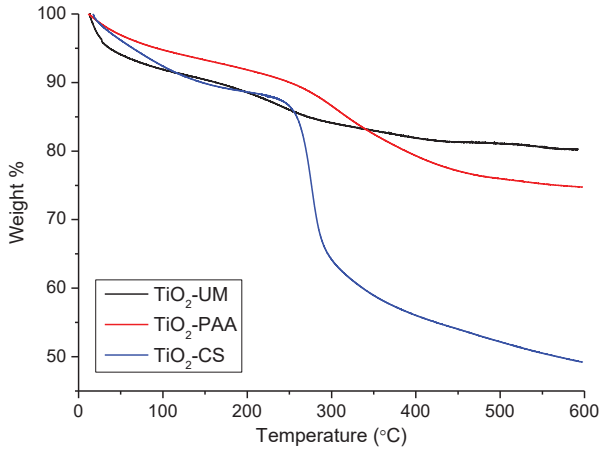

Figure 3.3 Thermogravimetric curves (5°C/min) of TiO_2 NPs.

3.2. Preparation of TiO_2-collagen nanocomposites

The TiO_2-collagen nanocomposite hydrogels were prepared by mixing collagen and TiO_2 suspensions then neutralizing with PBS and NaOH solution to induce the fibrillogenesis. Neutralized mixtures were treated at 30°C to increase the rate of fibrillogenesis and hence to accelerate the gel formation. Mechanical mixing was used in order to try to achieve a homogeneous dispersion of TiO_2 in the collagen matrix before the gelation process. However, this did not work well when introducing TiO_2-

UM NPs into collagen solution. Phase separation still occurred and TiO_2-UM NPs aggregated into large lumps (>100 μm). This could be due to residual hydrophobic organic groups (benzyl groups) from the precursor still attached to the nanoparticles. Phase separation has previously been observed in other inorganic additive polymer matrix systems.[22] On the other hand, having chitosan or PAA coating on the surface of TiO_2 NPs improved the miscibility of collagen and TiO_2, so that the TiO_2 NPs were able to disperse uniformly in the collagen matrix. Collagen gelation was still observed with the presence of the TiO_2 NPs.

3.2.1. Fourier transform infrared spectroscopy

The FTIR spectra of the collagen before and after the fibrillogenesis process and the TiO_2-collagen nanocomposites were presented in Figure 3.4. By comparing the FTIR spectra of the collagen monomer solution and the collagen gel, it can be seen that there is no significant shift in the peak positions after the fibrillogenesis, however, the amide I peak has been broadened and its intensity has decreased. This has been reported by Jakobsen *et al*. for the collagen fibrillogenesis.[57] Jackson and Mantsch suggested these changes should reflect the formation of intermolecular H bonds via the C=O group of the amide to H atoms in the neighbouring protein molecules.[58] In samples with different surface functionalized TiO_2 NPs, the peak positions of the main amide peaks remained the same as the collagen gel, indicating the incorporation of TiO_2 NPs does not interrupt the triple helical structure of the collagen (Figure 3.4). The intensity of the amide I band has been lowered and broadened in all cases, suggesting the fibrillogenesis process is not forbidden completely by TiO_2 NPs. The spectra of TiO_2-UM-collagen and TiO_2-PAA-collagen are almost the same as that of collagen gel because the signals from the TiO_2 NPs are hidden under the signals from collagen. The extra bands at 1075, 1030 and 2921cm^{-1} in the TiO_2-CS-collagen are from chitosan.

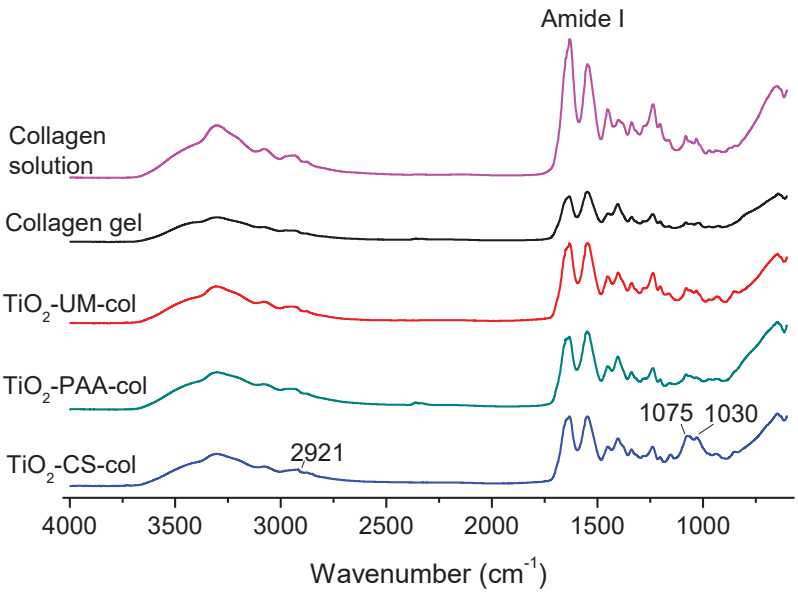

Figure 3.4 FTIR spectra of collagen and TiO_2-collagen nanocomposite hydrogels.

3.3. Rheology

3.3.1. The effects of TiO_2 NPs on collagen gelation kinetics

In order to know whether the introduction of TiO_2 NPs affected the kinetics of the collagen fibrillogenesis, the gelation process was monitored by rheology with G' and G" measured every 20s for 30min at a small oscillatory strain amplitude while the sample started to gel. All samples have a collagen concentration of 4 mg/mL and the mass ratio of collagen to TiO_2 1:0.5. The 4 mg/mL collagen monomer solution had G' slightly greater than G" to start with (data not shown), indicating the weak gel behaviour of the 'solution', due to the entanglement of the collagen molecules.[59] The temperature of the system was ramped up very quickly and stabilized at 30°C about 1min after the experiment was started. The viscoelasticities of the collagen solution, TiO_2-UM-collagen or TiO_2-PAA-collagen mixtures started to increase in about 2min, indicating the fibrillogenesis had entered the growth phase (Figure 3.5). TiO_2-CS-collagen had an extra long lag phase, suggesting the TiO_2-CS NP retarded the nucleation process. In the growth phase, the rates at which the G' changed (K_{growth}) in collagen, TiO_2-UM-

collagen and TiO_2-PAA-collagen are similar (Table 3.1), and the G values reached plateaus in about 9min after the measurements were started. However, the fibrillogenesis was slower for the TiO_2-CS-collagen sample, which took about 15min for the G' to reach a plateau.

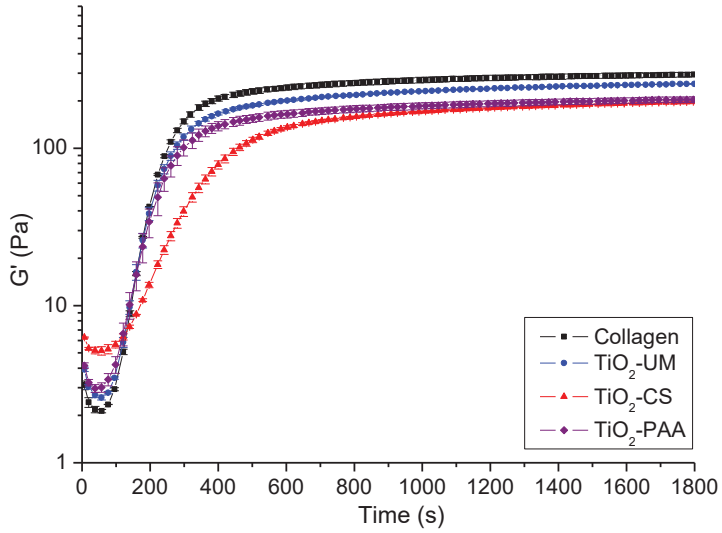

Figure 3.5 G's of the collagen and TiO_2-collagen nanocomposites (4 mg/mL) as a function of time during gelation at 1 Hz, 1% strain and 30°C.

Table 3.1 The rate constants (K_{growth})* of collagen and TiO_2-collagen nanocomposites in the growth phase of gelation (unit: Pa/s).

	Collagen	TiO_2-UM-col	TiO_2-CS-col	TiO_2-PAA-col
1mg/mL	$(2.65\pm0.05)\times10^{-3}$	--	$(1.55\pm0.05)\times10^{-3}$	$(3.15\pm0.15)\times10^{-3}$
4mg/mL	$(3.35\pm0.05)\times10^{-3}$	$(2.90\pm0.1)\times10^{-3}$	$(1.85\pm0.05)\times10^{-3}$	$(3.05\pm0.05)\times10^{-3}$

*K_{growth} is the gradient of the linear increase part of G' when the gel is forming. The average of two measurements is presented and the quoted error is the absolute difference between two measurements divided by 2.

When the same measurements were carried out for 1 mg/mL collagen samples, it was found that the TiO_2-CS NP still slowed down the rate of gelation while TiO_2-PAA NP accelerated the polymerization process (Table 3.1).

Chitosan (deacetylated) is a polysaccharide carrying amino groups.[60] There are two possible types of interactions between collagen and chitosan: electrostatic interactions forming a polycation/polyanion complex and H bonding.[61] TiO_2-CS NPs were introduced to the collagen solutions at a pH of around 4. At that pH, the amino groups of the chitosan molecule were protonated to be NH_3^+ and most of the COOH groups of collagen were also protonated, so that there could only be a limited degree of electrostatic complexation.[61] After the collagen and TiO_2-CS mixture was neutralized, the collagen fibrillogenesis process occurred, involving electrostatic interactions between COO^- and NH_3^+ of the collagen monomers. This process may compete with the polycation/polyanion complexation between NH_3^+ of the chitosan and COO^- of the collagen.[61-62] This is one of the hypotheses to explain why the nucleation process of the collagen sample with TiO_2-CS NPs was observed to be slower than in collagen on its own. Only the COO^- groups of collagen which do not complex with the chitosan are involved in collagen polymerization. The other hypothesis is chitosan forming H bonds with neighbouring collagen molecules and replacing the bridging water molecule which is also crucial for fibrillogenesis.[62] As a result of each of these processes it would be expected that the collagen polymerization process would indeed be retarded with the introduction of TiO_2-CS NPs as observed.

When PAA is the capping agent for TiO_2 NP, it introduces carboxyl groups on the TiO_2 surface. TiO_2-PAA NPs are not stable at acidic pH when the carboxylic groups are protonated, but are well-dispersed in water when the carboxylic groups are deprotonated

at neutral or high pH. Because of that, they were introduced after the collagen has been neutralized at 4°C before the fibrillogenesis occurred. The COO^- of PAA on TiO_2 may also complex with the NH_3^+ of collagen forming complexes in a similar manner to that described for the TiO_2-CS-collagen. However, this reaction is considered to be weak because both collagen and TiO_2-PAA carry net negative charges at neutral pH.[63] In contrast to chitosan, TiO_2-PAA NPs accelerated or did not affect the rate of collagen fibrillogenesis in our study. In the literature, PAA coated Au nanorods were found to influence collagen assembly by promoting collagen nucleation.[29] Wood introduced natural polyanions to collagen and also observed that they accelerated the nucleation process.[64] These studies suggest that TiO_2-PAA NPs facilitate collagen gelation in our study by promoting nucleation in some of the samples, and in that respect these particles provide an interesting contrast to those coated with chitosan.

3.3.2. The effects of collagen concentrations

Linear rheology

In order to investigate the role of collagen concentration on the rheological behaviours of the TiO_2-collagen nanocomposite hydrogels, hydrogels with final collagen concentrations to be 1 mg/ml, 2 mg/ml and 4 mg/ml were prepared, with the constant collagen to TiO_2 NPs mass ratio of 1:0.5. The G' and G" values of the collagen and TiO_2-collagen nanocomposites were determined from measurements made at 1% strain and 1 Hz after the hydrogels were formed on the rheometer. The G' values of the collagen control gels are found to scale with collagen concentration $G' \sim c^{(2.01 \pm 0.05)}$ as shown in Figure 3.6 (black solid line), close to a previously reported literature value $G' \sim c^{2.1}$ for the collagen gels formed at 37°C and can be explained with the model for semi-flexible biopolymers.[65]

The G' values for the TiO_2-collagen nanocomposites do not fall on the power law scaling curve for collagen, but they still increase as the concentrations of collagen increase. The 1 mg/mL and 2 mg/mL TiO_2-PAA-collagen composites have higher G's than the control samples of the same concentrations, while TiO_2-CS NP nanocomposites have slightly lower G's at these two concentrations. However, both the 4 mg/mL TiO_2-CS and TiO_2-PAA collagen nanocomposites have lower G's than the collagen control. As inert fillers for polymers, nanoparticles have been used to increase the moduli of polymer solutions.[66] However, while this should be the case for additives that do not affect the polymerization process, both TiO_2-CS and TiO_2-PAA NPs will have interactions with collagen.[24] At high TiO_2 concentrations, the TiO_2-collagen interactions may reduce collagen-collagen interactions, resulting in hydrogels with lower viscoelasticities. It has been reported in the literature that the composite of collagen and chitosan is weaker than the collagen gel itself.[67] With limited data points available, the TiO_2-CS-collagen hydrogels are fitted with function $G' \sim c^{(1.88\pm0.08)}$ (Figure 3.6 red dash line), with the scaling power similar to that of the collagen controls. The TiO_2-PAA-collagen hydrogels are fitted with $G' \sim c^{(1.47\pm0.08)}$ (Figure 3.6 blue dash dot line), with the scaling power lower than the other two systems. The observed lower dependence of elastic modulus on concentrations could indicate a decrease in the number of long-lived crosslinks, or that the fibrils are contributing lower entropic and larger enthalpic to the restoring force.[65b] Conclusion should not be made in this case as only three data points are available for the fitting.

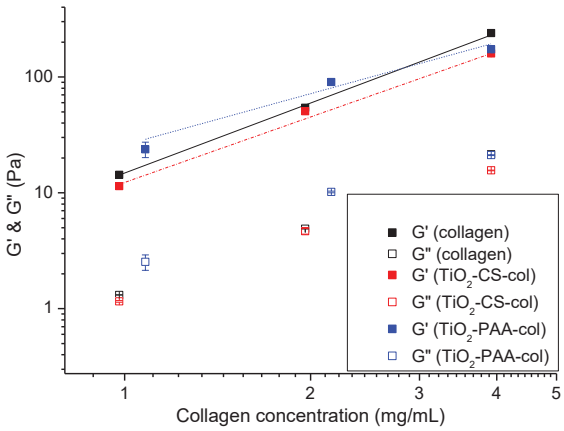

Fitting function: G'~c^p	
	p
G' (collagen)	2.01±0.05
G'(TiO_2-CS-col)	1.88±0.08
G'(TiO_2-PAA-col)	1.47±0.08

Figure 3.6 Left: viscoelasticites of collagen and TiO_2-collagen nanocomposites as functions of collagen concentrations; right: power law scaling for elasticities of collagen and TiO_2-collagen nanocomposites as functions of collagen concentrations.

Non-linear rheology

As a biopolymer, collagen is well known to exhibit strain stiffening behaviour which means that the elasticity of the material becomes larger as it is deformed.[36] The non-linear rheological properties of the samples were measured by a strain amplitude sweep protocol. The critical strain (γ_c), which is the strain at which the material starts to stiffen, remains the same as the collagen controls in spite of the addition of TiO_2-CS NPs (Figure 3.7). Higher concentrations of collagen in both control and TiO_2-CS incubated samples resulted in earlier strain stiffening behaviour. This has also been observed for the acid-solubilised collagen gel formed at 24°C.[40] However, Licup *et al* suggested γ_c should not be affected by the network concentration, because the geometry of the collagen network is fractal.[68] On the other hand, for the TiO_2-PAA incubated samples, the higher the collagen concentration the later the stiffening of the hydrogel occurs (Figure 3.7). The yield strain (γ_y) is the maximum deformation tolerated by the network before irreversible network rearrangements or breakage.[40] There is a linear decrease in yield strains as the collagen concentration increases in TiO_2-PAA-collagen samples (Figure 3.7). The TiO_2-CS NPs raise the yield strains in 1 mg/mL and 4 mg/mL

collagen nanocomposites but not in the 2 mg/mL one, when compared with the yield strains of the collagen controls. The modulus ratio, which is the ratio of the maximum G' in the non-linear measurement to the linear state G'_o, reflects the degree of strain stiffening. Figure 3.8 shows that there is a trend in all the collagen and TiO_2-collagen nanocomposite hydrogels that the higher the collagen concentration, the lower the degree of strain stiffening, which matches with what has been reported previously by Motte.[40] TiO_2-CS NPs increase the degree of strain stiffening while TiO_2-PAA NPs lower the degree of strain stiffening in all the composites with different collagen concentrations.

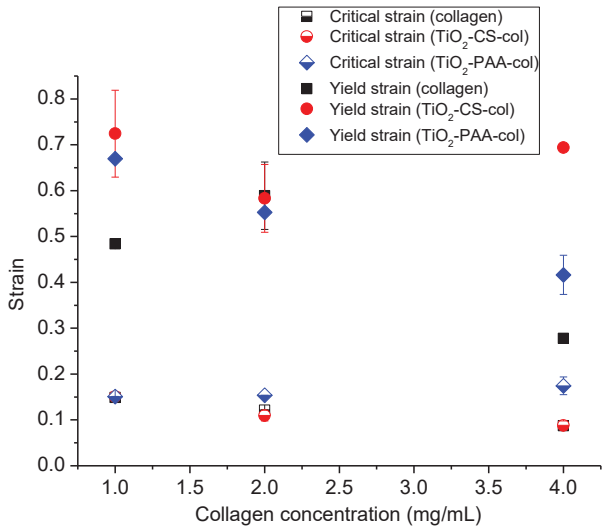

Figure 3.7 Critical strains and yield strains of collagen and TiO_2-collagen nanocomposites as functions of collagen concentration.

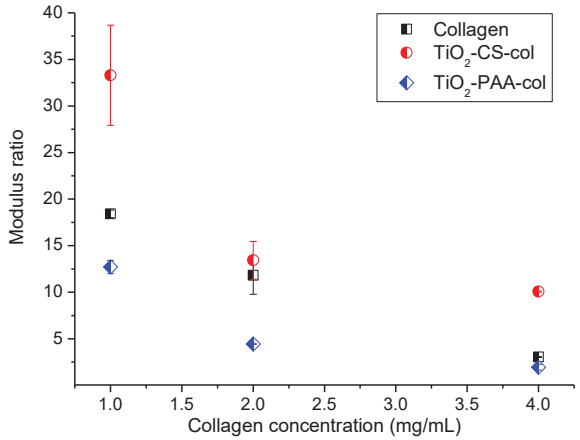

Figure 3.8 Modulus ratios (G'_{max}/G'_o) of collagen and TiO_2-collagen nanocomposites as functions of collagen concentration.

The strain stiffening responses of the collagen and TiO_2-collagen nanocomposites are plotted as differential shear modulus K ($K = \partial\sigma/\partial\gamma$) as a function of the corresponding stress σ (Figure 3.9). Figure 3.9(a) is the plot for collagen at different concentrations. Similar to the plot of G' versus strain (Figure 1.5), the collagen controls have constant K in low stress regime (where $K = G'_o$) and linearly increasing K in the high stress regime. However, it is surprising to see that the linearly increasing parts of the K curves measured at different collagen concentrations collapse to a master line. This can be interpreted as the meaning that the stiffness of the collagen network, reflected by the differential shear modulus K, does not depend on the collagen concentration, as suggested recently by Licup *et al.*[68] Another way to understand is, although the low concentration sample has a lower viscoelasticity in the unstrained state, it can reach similar stiffness to the high concentration sample when they are under the same applied stress. The lower the collagen concentration, the earlier the K curve merges to the master line. The gradient of the master line, given by the stiffening index m ($K = \sigma^m$), is close to 1, which is again in agreement with recent prediction.[68]

TiO_2-CS NPs weaken the collagen nanocomposites in the linear viscoelastic regime and increase the yield strain and the maximum degree of strain stiffening in the non-linear regime as described before. However, the K versus stress curves of TiO_2-CS-collagen nanocomposites in different collagen concentrations also collapse together (Figure 3.9(b)), as is observed for the collagen control samples. They have stiffness indices m close to 1 when the stress is close to the point which starts stiffening, but m decreases towards 1/2 as the stress gets stronger, i. e. the hydrogels become less responsive under high stress. On the other hand, the curves for TiO_2-PAA-collagen samples with different collagen concentrations also merge together. Again, m is about 1 at low stress and low collagen concentrations, but it starts to diverge from 1 at a lower stress than the TiO_2-CS-collagen samples.

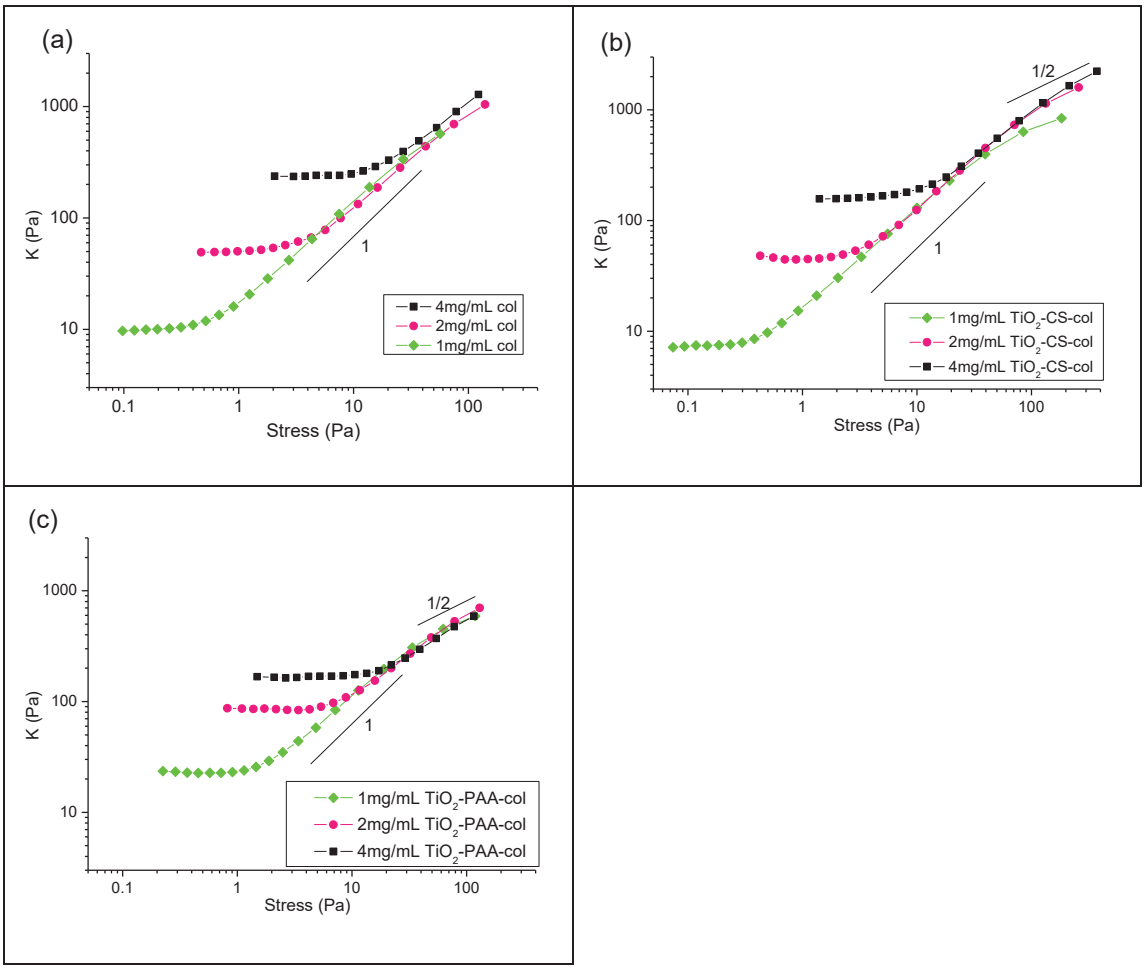

Figure 3.9 Differential shear modulus (K) versus stress curves for collagen (a), TiO_2-CS-collagen nanocomposites (b) and TiO_2-PAA-collagen nanocomposites (c) in different collagen concentrations.

Most of the older literature suggests that the stiffening index m should be 3/2 or has a tendency to go towards 3/2 in polymer systems.[41] We do not observe this in our samples. Instead, the stiffness index m has decreased slightly at high stress in both TiO_2-CS and TiO_2-PAA incorporated hydrogels (Figure 3.9). More recent literature by Licup *et al* finds the index m close to 1 as we do in this study.[68] Based on the nonaffine re-orientation of network model of the strain stiffening response, the strain stiffening is due to bending and stretching of the filaments in the network.[39] Licup *et al* suggested that the indices m would merge to about 1/2 when the stiffening response is finally stretch-dominated.[68] We observe m does appear to approach to 1/2 in hydrogels with TiO_2 NPs, but not quite in the collagen controls. The possible explanation may be the

TiO_2-collagen networks can survive to the strains that the filaments are stretched-dominated, while in collagen control the network ruptures before the stretched dominated stiffening. At high collagen concentration samples (4 mg/mL), m turns to 1/2 at a lower stress for TiO_2-PAA-collagen hydrogels than the TiO_2-CS-collagen hydrogels (Figure 3.9), suggesting that the TiO_2-PAA-collagen turns to the stretch-dominated stiffening earlier than the TiO_2-CS-collagen hydrogel.

3.3.3. The effects of TiO_2 NP concentrations

Linear rheology

Nanocomposites with varied concentrations of TiO_2 NPs were prepared, while the final concentration of collagen in the composites was constant to be 4 mg/ml. Figure 3.10 shows that there is a trend in the data from TiO_2-PAA-collagen nanocomposites that the higher the loading of the nanoparticles, the lower the viscoelasticities of the hydrogel in the un-strained state. For a low TiO_2-PAA loading (collagen:TiO_2-PAA mass ratio 1:0.1), the nanocomposite has a greater G' value than the collagen control. However, when the loading of TiO_2 NP is greater than 50% of the weight of the collagen in both TiO_2-PAA and TiO_2-CS samples, the viscoelasticities of the nanocomposites are reduced. This is presumably owing to the competition of nanoparticles in the fibrillogenesis at high concentration weakens the collagen network.

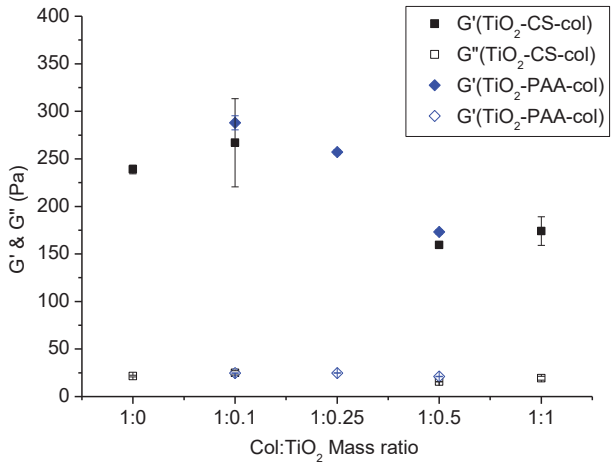

Figure 3.10 Viscoelasticities of TiO_2-collagen nanocomposites as functions of collagen to TiO_2 NP mass ratios. '1:0' refers to the collagen control sample.

Non-linear rheology

The addition of TiO_2-PAA delays the onset of strain stiffening (critical strain) when the loading of TiO_2-PAA is greater than 25% of the mass of the collagen (Figure 3.11). All TiO_2-PAA NP incubated hydrogels have higher resistance to yield compared with the collagen control, although this effect does not correlate to the concentrations of the TiO_2-PAA NPs. The degrees of strain stiffening are not changed in low TiO_2-PAA concentration samples, but are lowered in high TiO_2-PAA concentration systems (Figure 3.12). On the other hand, TiO_2-CS NPs increase the yield resistances and moduli ratios of the nanocomposites when compared with that of the collagen control. Again, the improvements of yield resistances in the nanocomposites are independent of TiO_2 concentrations.

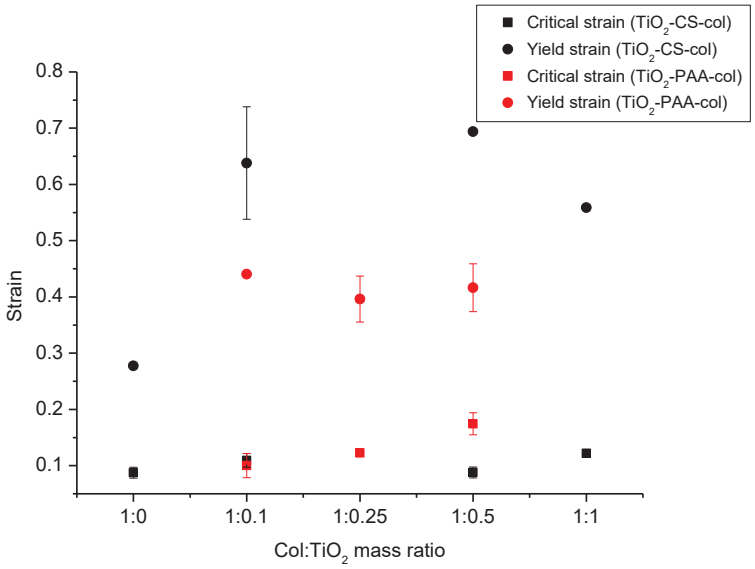

Figure 3.11 Critical strains and yield strains of TiO_2-collagen nanocomposites with different collagen to TiO_2 NP mass ratios. '1:0' refers to the collagen control sample.

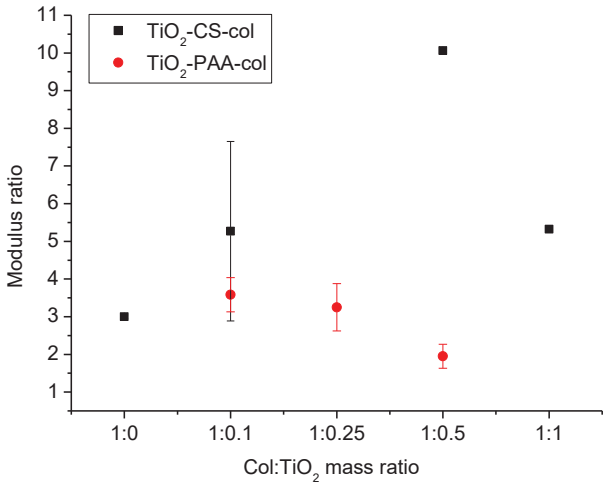

Figure 3.12 Modulus ratios of TiO_2-collagen nanocomposites as a function of collagen to TiO_2 NP mass ratio. '1:0' refers to collagen control sample without any nanoparticles.

The K versus stress curves for the collagen nanocomposites with the addition of different amounts of TiO_2-CS NPs are almost overlapping with that of the collagen gel control in the stiffening regime, with the stiffening indices m close to 1 (Figure 3.13a). Varying the loading of TiO_2-CS NPs from 1:0.1 to 1:1 (collagen:TiO_2-CS mass ratio) does not alter the strain-stress response of the sample. Similarly, the incorporation of TiO_2-PAA NPs does not modify the stiffening index (m) of the nanocomposites when

the concentrations of TiO_2-PAA NPs are low (Figure 3.13(b)). However, the sample with the ratio of 1:0.5 (collagen:TiO_2-PAA) has K lower than other samples in the whole measurement, and m is also lower than other samples (Figure 3.13b).

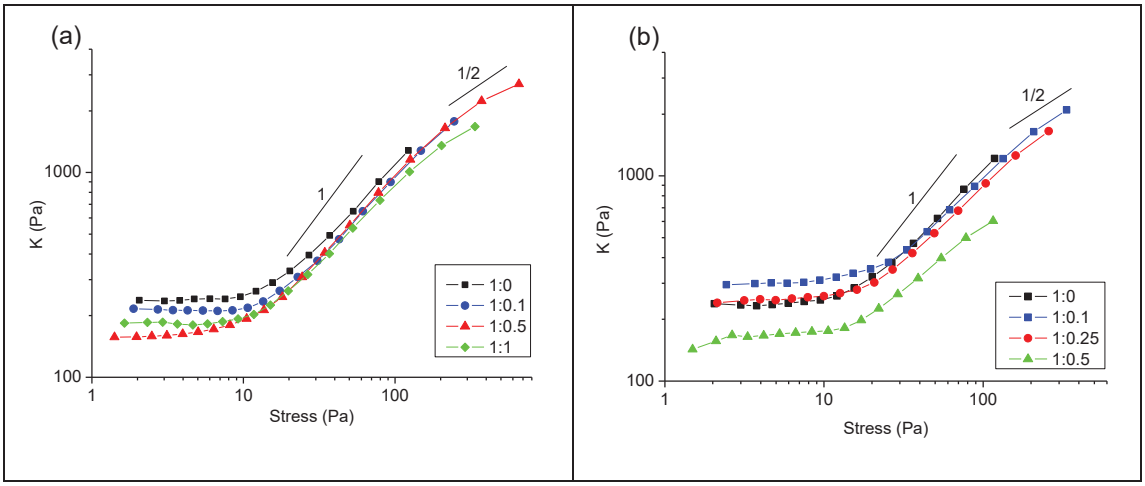

Figure 3.13 K versus stress curves for TiO_2-CS-collagen (a) and TiO_2-PAA-collagen (b) with different mass ratios of collagen to TiO_2 NPs. The collagen concentrations are 4 mg/mL in all hydrogels. '1:0' refers to collagen gel control without any nanoparticle.

3.3.4. The effects of surface functionalizations of TiO_2 NPs

Linear rheology

As experimental controls, collagen hydrogels (final collagen concentration 4 mg/mL) with TiO_2-UM NP or just the capping agents chitosan and PAA alone were prepared and subjected to the same rheological measurement protocol, in order to see whether the changes in the rheological properties of the TiO_2 collagen hydrogels were the results of the surface capping agents only. The TiO_2-UM sample has G' and G" close to the collagen control (Figure 3.14), which may be because without surface modification, the TiO_2-UM NP could not well blend with the collagen solution and the aggregated TiO_2 could not really affect the collagen polymerization at molecular level. Figure 3.14 shows that both the chitosan and PAA lower the storage moduli (G') of the collagen hydrogels slightly. However, the hydrogels prepared with TiO_2-CS and TiO_2-PAA NPs

do have even lower G' and G", suggesting TiO_2 NPs also play some role in affecting the network rheological properties indirectly. We hypothesize that the effects are more obvious than the TiO_2-UM NPs, because the collagen nanoparticle interactions have been maximized when the surface functionalized TiO_2 NPs are well dispersed in the collagen matrix.

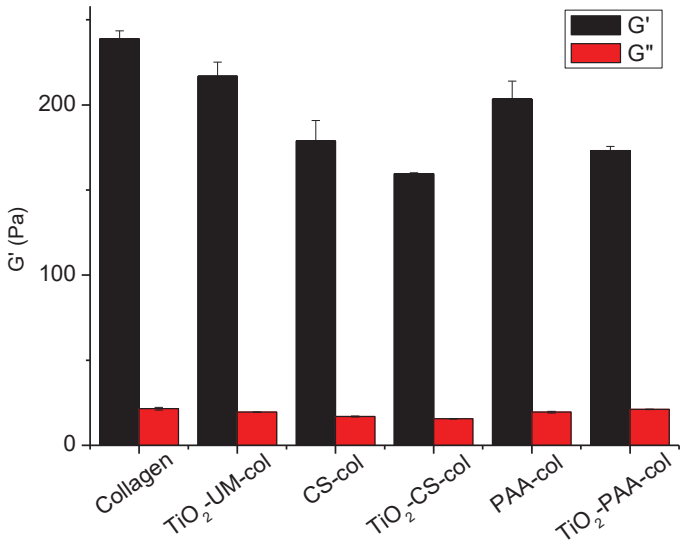

Figure 3.14 Viscoelasticities of collagen, capping agent-collagen composites and TiO_2-collagen nanocomposites hydrogels.

Non-linear rheology

Collagen, TiO_2 incorporating collagen and capping agent-collagen gels all have strain stiffening responses. With TiO_2-UM NP added to collagen, the yield strain as well as the modulus ratio have been improved very mildly, which means it is able to tolerate a greater strain before the network breaks than the collagen control (Figure 3.15). By introducing TiO_2-CS NP into collagen, the hydrogel retains a similar critical strain, but it has the greatest resistance to break in all samples. Its modulus ratio is about 10, which means the G' can reach 10 times the value of the linear viscoelastic regime (reaching 1600 Pa) when the gel is deformed. The TiO_2-PAA-collagen hydrogel does not exhibit as large a stiffening response as the TiO_2-CS-collagen samples in the strain sweep

(Figure 3.15(b)). The control samples confirm that the capping agents introduce variations in the TiO_2 incorporating hydrogels. The collagen-chitosan hydrogel shows improvements in the yield strain and modulus ratio, while the modulus ratio of the collagen-PAA hydrogel is lower than that of the collagen control. These three groups of comparisons suggest that both TiO_2 and its surface cappings can be used to tune the strain stiffening effect in the composite hydrogels. It is hypothesized that the TiO_2 NPs introducing 'microcracks' and 'debonding' upon straining can dissipate some energy, improving the yield strain of the nanocomposites.

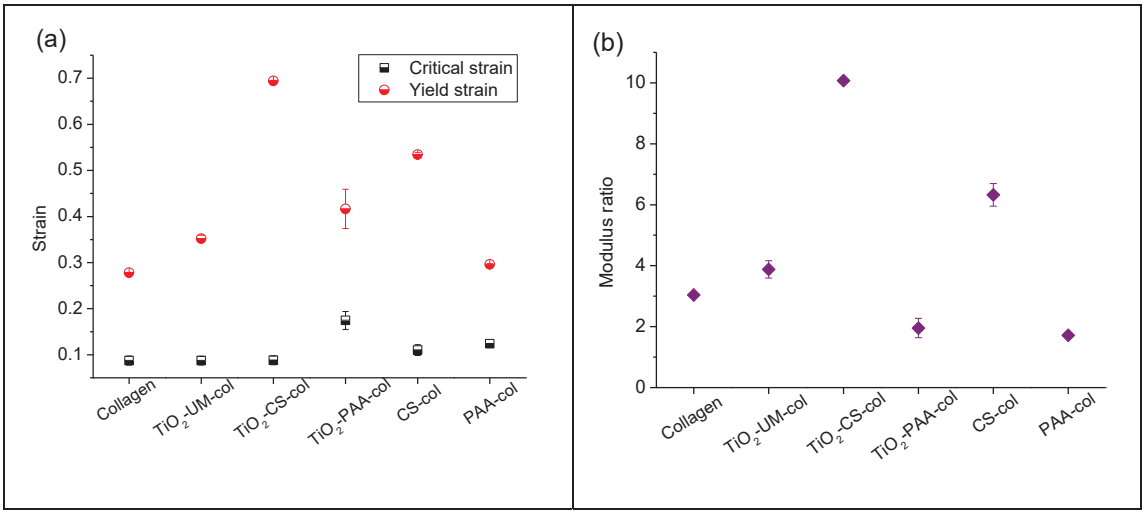

Figure 3.15 Critical strains and yield strains (a) and modulus ratios (b) of TiO_2-collagen and capping agent-collagen hydrogels.

3.3.5. Reversibility of the strain stiffening behaviour

In order to investigate the reversibility of the strain stiffening properties of the collagen and collagen nanocomposites, they were subjected to several strain loading and unloading cycles. Strain was increased from 0.1% to 30% for collagen control, to 40% for TiO_2-CS-collagen and to 35% for TiO_2-PAA-collagen. This upper limit of the strain value used in the strain ramp is about two times the critical strain, but lower than the yield strain of each sample measured in the previous experiments, so as not to cause irreversible damage. The curves plotted in Figure 3.16(a)-(c) are only the successive

upward strain ramping measurements and the intermediate strain decreasing runs between each strain ramp are not included. It can be seen for all the hydrogels including the collagen control and TiO_2 containing nanocomposites that the G' curves of the second strain ramps remain the same shape as the first run but there are small drops in values. The G' versus strain curves of the third and fourth strain ramps are more or less the same as the second run and there are also no big deviations in G_o's. Therefore, the strain stiffening behaviours of the collagen and TiO_2-collagen hydrogels are largely reversible, as long as the strain deformation is lower than the yield strain of the sample. The drop in G' is considered as the process of breaking the irreversible connections in the network.[40] Figure 3.16(d) compares the changes of G_o's after the first strain sweep in three hydrogel samples. There is roughly a 25% drop in G_o' after the first strain sweep in the collagen control, while the drops are more significant in TiO_2-CS and TiO_2-PAA collagen nanocomposites, which means TiO_2-CS and TiO_2-PAA introduce more irreversible crosslinks to the hydrogels structure (Figure 3.16(d)). The extra parts of the irreversible crosslinks may be from the irreversible interactions between collagen and the capping agents CS/ PAA. However, once the samples are deformed to strains which are greater than the yield strain γ_y of the samples, the strain stiffening behaviour is no longer reversible, even if the sample is incubated at the gelation temperature for a long time (data not shown).

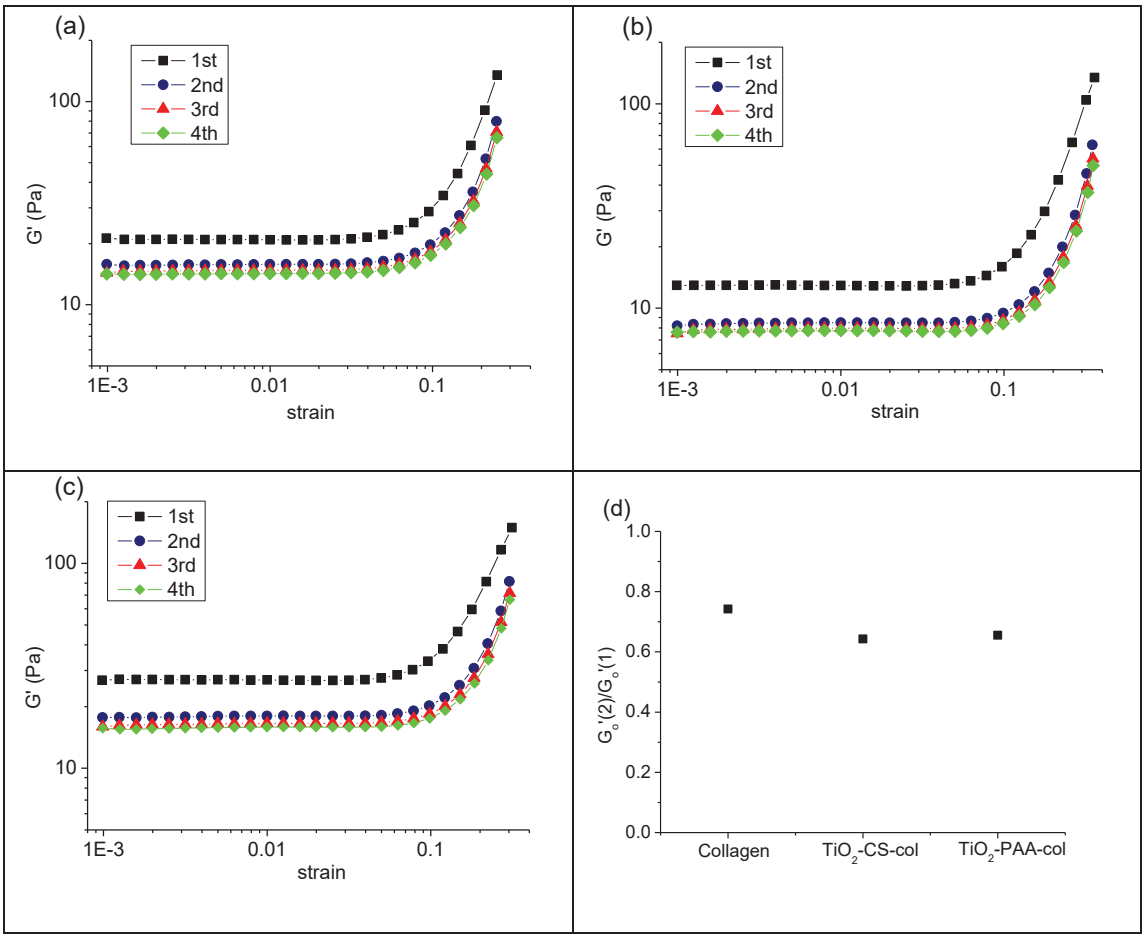

Figure 3.16 Four consecutive strain ramps for (a) collagen, (b) TiO_2-CS-collagen hydrogels and (c) TiO_2-PAA-collagen hydrogels, (d) initial G's of the second strain ramps relative to the first one in hydrogel samples.

3.4. Collagen network morphology

The morphologies of the collagen and TiO_2 NP-collagen nanocomposites were examined using confocal fluorescence microscopy. All the collagen samples were found to have three dimensional fibrillar network structures as expected. Figure 3.17(a) and (b) are images for collagen gels in two different concentrations. Both of them are relatively homogenous and show the presence of protein fibril bundles. The 4 mg/mL sample (Figure 3.17(a)) has a much denser fibrous structure than the 1 mg/mL sample as expected (Figure 3.17(b)). The 1 mg/mL sample is more suitable for structural analysis, owing to the increased potential of analysis in sparser systems. In contrast, the collagen network organization has been distorted significantly in the TiO_2-CS-collagen sample

(Figure 3.17(c)). It has less inter-strand crosslinking points, and becomes very heterogeneous with large pores and thick bundles present, which is very similar to the morphology of a collagen-chitosan composite previously reported.[62] The bright dots on the filaments are considered to be the TiO_2-CS complexing with collagen.[62] On the other hand, the TiO_2-PAA-collagen sample has sharper and thinner fibrils and more inter-strand crosslinking points than the collagen control of the same concentration (Figure 3.17(d)). In contrast to the TiO_2-CS NPs, TiO_2-PAA NPs do not show up, as they carry negative charges that do not attract the dye molecules. It should be noticed that (b), (c) and (d) have the same collagen concentration. The thinner the fibrils, the greater the number of fibrils and the smaller the resulting pore size, explaining why (d) looks much denser than (c). Polymers in (c) on the other hand are gathered into bigger bundles, which do not fill the space as efficiently.

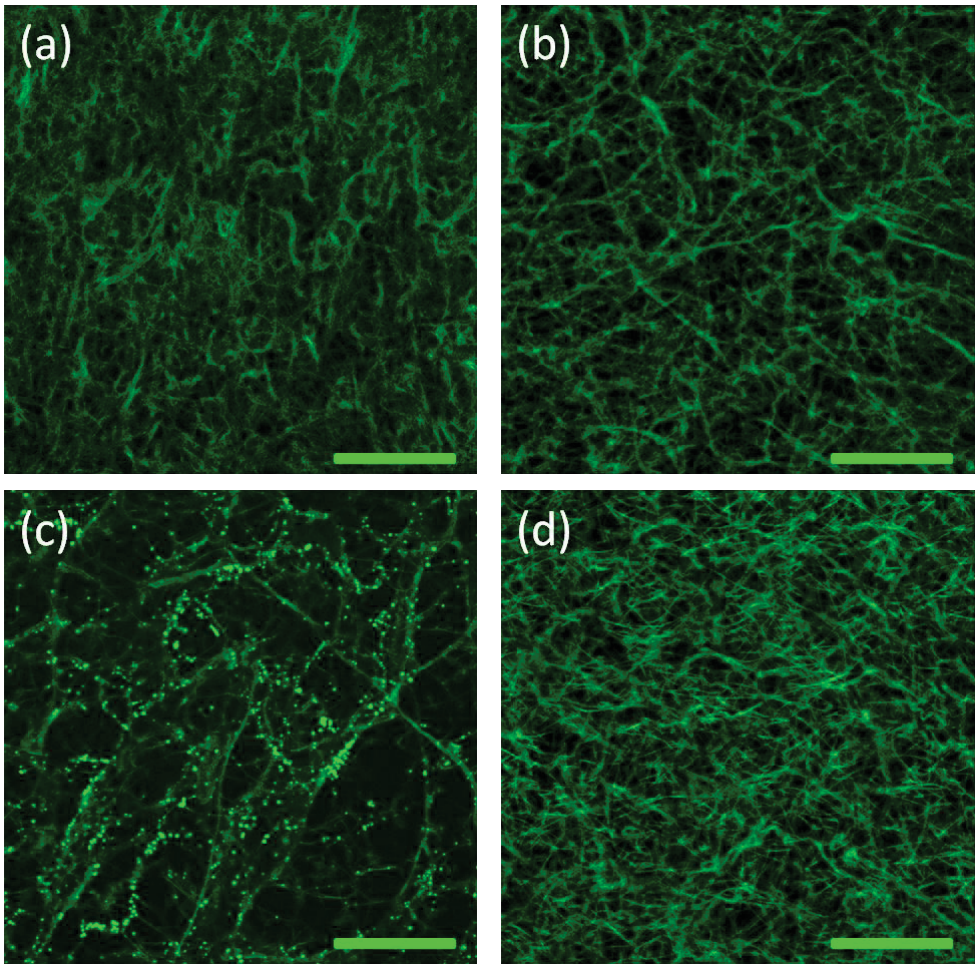

Figure 3.17 Confocal fluorescence images of (a) collagen 4 mg/mL, (b) collagen 1 mg/mL, (c) TiO_2-CS-collagen nanocomposite (1 mg/mL) and (d) TiO_2-PAA-collagen nanocomposite (1 mg/mL). Scale bars are 20 μm.

The fibril diameter is considered to be determined in the nucleation stage of the collagen fibrillogenesis.[69] Based on previous experiments (Table 3.1), the interactions between TiO_2-PAA NPs and collagen monomers indeed accelerate collagen nuclei formation so the nucleation is fast.[29, 64] The nuclei compete with each other for the remaining collagen monomers in the growth stage, so very thin fibrils are formed, as illustrated in Figure 3.18(a).[64, 69] On the contrary, TiO_2-CS retards the collagen nucleation so less nuclei are formed (Table 3.1) and in the growth stage the collagen monomers tend to increase the width of the fibrils (Figure 3.18 (b)).[70]

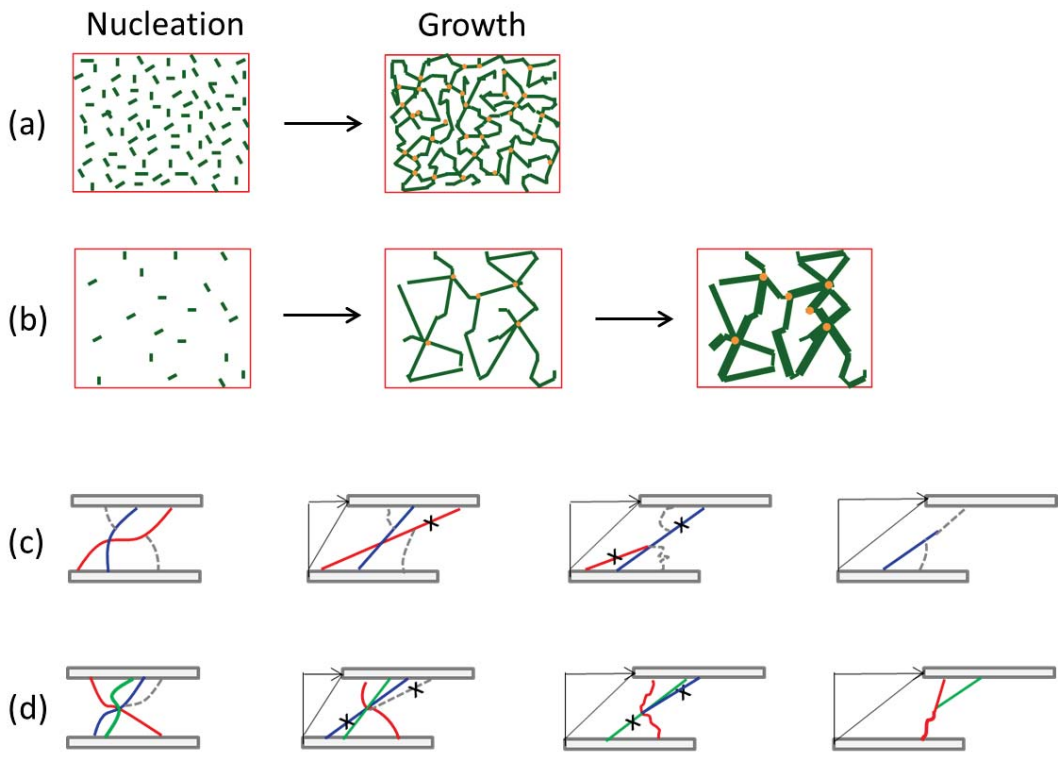

Figure 3.18 Structural network developments of TiO_2-collagen nanocomposites in fibrillogenesis and large amplitude deformations. (a) & (b) the effects of TiO_2-PAA and TiO_2-CS NPs on the structural developments of the collagen networks respectively; (c) & (d) illustrations of fibers under large amplitude deformations in TiO_2-PAA-collagen and TiO_2-CS-collagen composites. (c) TiO_2-PAA-collagen has more crosslinks while (d) TiO_2-CS-collagen has few crosslink but higher connectivity from each crosslink. Both scenarios are resilient to yield by different mechanisms.

The network morphologies of the collagen and collagen nanocomposites help us to understand their rheological behaviours. According to the semi-flexible network model, the strength of the gel is affected by the filament diameter and the mesh size in the network.[65a] Either increasing the filament diameter or reducing the mesh size results in a gel with higher G'. The mesh size is shown to have a more significant effect here. In the 1 mg/mL (collagen concentration) hydrogel samples, the TiO_2-CS-collagen shows a sparse network with increased mesh size while the TiO_2-PAA-collagen hydrogel shows a dense network with reduced mesh size. These correlate quite well with the linear

rheology data that the TiO_2-CS-collagen gel has a lower G' while the TiO_2-PAA-collagen gel has a greater G' than the control sample (at 1 mg/mL collagen concentration).

However, there is no big difference in the non-linear strain-stress response of the collagen with two different types of TiO_2 NPs. They have stiffness indices m close to 1, which is consistent with that of the collagen at the same concentration. This suggests the strain-stress response is not significantly affected by the macroscopic network structure of the hydrogels. In both TiO_2-CS and TiO_2-PAA incorporated gels, the yield strains have been improved which allow the networks to tolerate greater deformations than collagen itself. However, TiO_2-CS and TiO_2-PAA affect the hydrogel structures differently, indicating the nanoparticles make the hydrogels more resilient in two different ways. The yielding point is where the filaments in the network become disconnected. The TiO_2-CS-collagen gel has large fiber bundles and each crosslinking point connects more filaments than the collagen control. Therefore, under deformation, one or few fibrils break from the same crosslinking point will not lead to the network to break down completely, allowing the network to be continued stretching further (Figure 3.18(d)). On the other hand, TiO_2-PAA-collagen hydrogel has more crosslinking points than the control sample, so it can deform further before the structure is ruptured (Figure 3.18(c)).[40]

3.5. Other physical characterizations

Swelling ratio

The swelling ratios of dry films of the collagen and TiO_2-collagen nanocomposites can be used to measure the water uptake capabilities of the samples. It can be seen from Figure 3.19 that the introduction of TiO_2-UM NPs to collagen does not really change

the swelling behaviour of the collagen film. However, the water uptake capability of the collagen nanocomposite with TiO_2-CS NPs has decreased to only about half of that of the collagen gel, while the TiO_2-PAA NP incorporating collagen sample has a slightly increase in swelling ratio. The swelling ratio is usually used as a parameter to reflect the mechanical properties of a polymer system.[71] The lower the swelling ratio of the gel the greater the shear modulus it will be. However, the swelling ratios of the freeze dried TiO_2-CS-collagen and TiO_2-PAA-collagen samples do not match up with the rheological results of these samples. Instead, the swelling ratios may be more dependent on the structure of the samples. The TiO_2-CS-collagen gel contains more rigid network and a smaller surface contact area which do not allow it to swell despite its lower gel strength, while the TiO_2-PAA has thinner filaments and a larger surface contact area so they are able to re-orientate to accommodate a larger volume of solvent.[72]

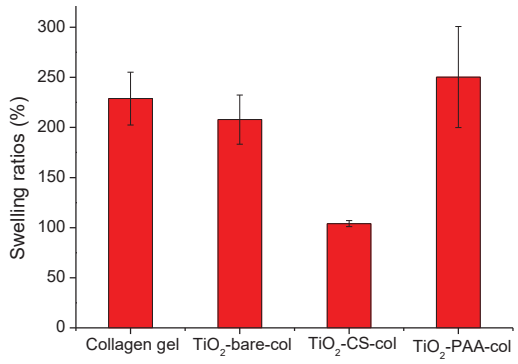

Figure 3.19 Swelling ratios of collagen and TiO_2-collagen nanocomposites.

Denaturation temperature

Denaturation temperatures of the collagen and collagen nanocomposites were measured by DSC and reflect the thermal stabilities of the samples. The fibrillogenesis process polymerizes collagen monomers, forming a gel via electrostatic and H-bonding interactions, stabilizes the collagen, and raises its denaturation temperature by about 18°C as shown in Figure 3.20. The introduction of TiO_2-CS NP has no significant effect

to the thermal stability of the collagen nanocomposite, while both TiO_2-UM and TiO_2-PAA NPs lower the denaturation temperatures slightly when compared with that of the collagen gel. This suggests that TiO_2-UM and TiO_2-PAA NPs affect the collagen fibrillogenesis weakly, but do not inhibit the fibrillogenesis process. On the other hand, the interactions between TiO_2 and collagen are limited to physical interactions, as chemical crosslinking would be expected to produce a dramatic increase in the thermal stability of the collagen.

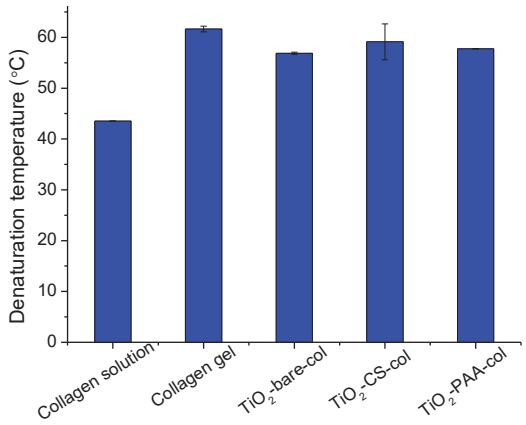

Figure 3.20 Denaturation temperatures of collagen and TiO_2-collagen nanocomposites.

3.6. Chapter summary

In this chapter, PAA and chitosan functionalized TiO_2 NPs have been introduced to collagen to fabricate nanocomposites with varied collagen and nanoparticle concentrations. The linear and non-linear rheological properties, swelling ratios and thermal stabilities of these TiO_2-collagen hydrogels have been studied and summarized in Table 3.2 for comparisons. PAA capped TiO_2 and chitosan coated TiO_2 NPs carry opposite charged functional groups and they affect the fibrillogenesis of collagen in different manners, resulting in gels with different network structures as suggested by the microscopy. The linear and non-linear rheological properties and swelling ratios of the

TiO_2-collagen nanocomposites indeed can be understood from the morphologies of the collagen networks.

Table 3.2 Summarise of the effects of TiO_2 NPs on the structures and properties of the collagen gels.

	TiO_2-PAA NPs	TiO_2-CS NPs
Fibrillogenesis	Accelerate fibrillogenesis in low concentration samples, do not change the rate of fibrillogenesis in high concentration samples	Perturb nucleation, slow down the fibrillogenesis process
Gel structure	Thin and sharp fibrils, homogeneous, dense network, more inter-strand crosslinks	Thick bundles, heterogeneous, large pores, less inter-strand crosslinks
Linear rheology	Low concentration of NPs reinforces the gel slightly, high concentration of NPs weakens the gel slightly	Weaken the gels slightly
Non-linear rheology	Both types of TiO_2 NPs increase the yield strains of the collagen gels. They do not modify the strain-stress response of the gels. The strengths of the gels are governed by the applied stress.	
Swelling ratio	Increased slightly	Decreased
Thermal stability	No change	No change

4. ZnO-induced collagen hydrogel*

In the previous chapter, chitosan and PAA coated TiO_2 NPs were found to modify the network structure of the collagen hydrogels, in a manner dependent on the surface capping agents, giving rise to some interesting linear and non-linear rheological properties. In this chapter, the effect of ZnO NPs on the physical properties of the collagen networks will be investigated. ZnO and TiO_2 NPs share many common properties so they were expected to behave similarly when reacting with collagen solution. However, it was discovered that a collagen hydrogel with enhanced linear rheological properties was obtained when the PVP capped ZnO NPs were introduced to the collagen solution even without the use of a conventional gelation buffer. This chapter will present the preparation, characterization, and the gelation mechanism of this ZnO induced collagen hydrogel system.

4.1. Characterization of PVP capped ZnO NPs

The ZnO NPs used in this study were synthesized by reacting an alcoholic zinc salt solution with a base. The passivating agent PVP was introduced before the hydrolysis to control the growth of ZnO as well as stabilizing the ZnO NPs.[47, 73] The TEM image of the as synthesized PVP capped ZnO (ZnO-PVP) NPs is shown in Figure 4.1 and indicates that the particles are discrete and have regularly spherical shapes with size about 4.3 (±0.5) nm. As an experimental control, ZnO NPs without PVP capping (ZnO-plain) were also synthesized in a similar method except that no PVP was introduced in the preparation process. The size of the ZnO-plain NPs was about 5.2 (±0.5) nm, which

*Portions of this chapter have been previously published as Lian, Jiaxin, et al. ZnO/PVP nanoparticles induce gelation in type I collagen. *European Polymer Journal* **2016**, 75, 399-405.

was bigger than the ZnO-PVP NPs, indicating the role of PVP in size control of the synthesis.[47]

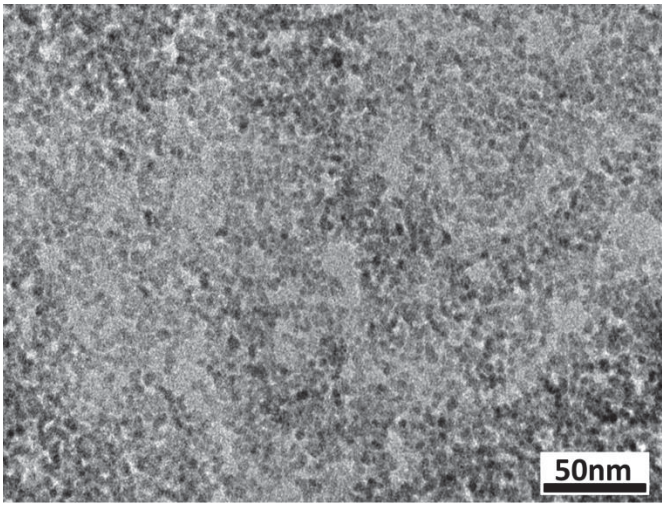

Figure 4.1 TEM image of ZnO-PVP NPs

In order to show that the ZnO NPs were functionalized with PVP, their FTIR spectrum was recorded and compared with that of the ZnO-plain NPs (Figure 4.2). Both types of nanoparticles were purified with hexane. Any excess or unbound PVP is expected to be washed off in the purification process. The ZnO-plain NPs show peaks at 1551, 1402 and 1341 cm^{-1} which can be attributed to C-O stretching of acetate groups arising from the precursor complexing with Zn^{2+}, according to Matsuyama *et al.*[74] The 1402 cm^{-1} peak also presents in the ZnO-PVP spectrum as a shoulder next to the 1421 cm^{-1} peak. The predominant peak in the ZnO-PVP sample at 1651 cm^{-1} is assigned to C=O. The bands at 1288, 1421 and 2925 cm^{-1} correspond to C-N stretching, CH_2 bending and CH_2 stretching vibrations, respectively from PVP (Figure 4.2).[73]

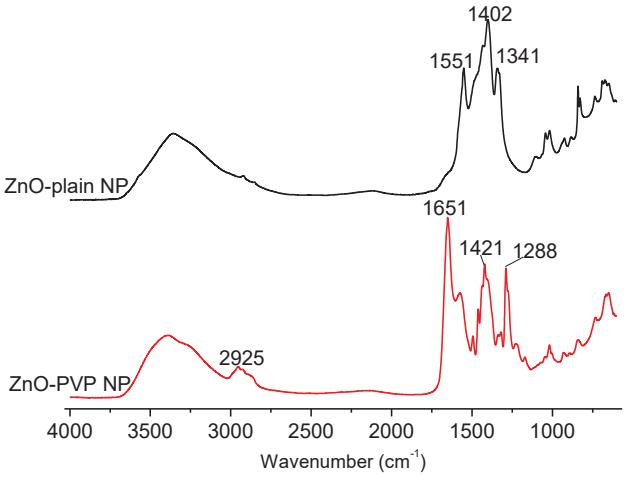

Figure 4.2 FTIR spectra of ZnO NPs prepared without and with PVP capping.

TGA analysis shows that there is about 28% weight loss in the ZnO-plain NPs after it has been heated up to 600°C, due to the loss of the adsorbed moisture and remaining acetate, as shown in Figure 4.3. In contrast, there is roughly 40% weight loss in the ZnO-PVP NPs. This extra 12% weight loss is considered to be the removal of PVP. Therefore, the PVP capping on the ZnO-PVP NPs is about 12% of the weight of the nanoparticles.

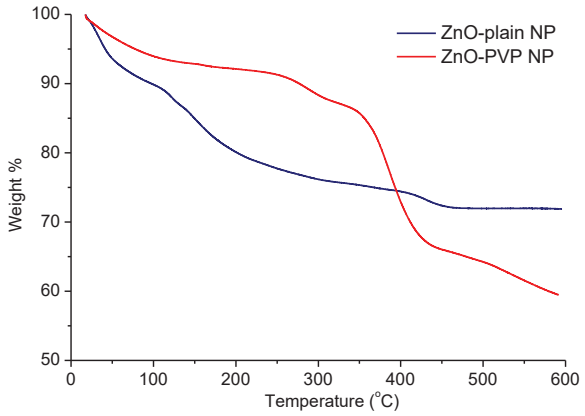

Figure 4.3 Thermogravimetric curves (5°C/min) of ZnO NPs without and with PVP capping.

Both ZnO-plain and ZnO-PVP NPs were stable in alcoholic solvents for more than one month. However, for this study, ethanol was not suitable to be used as the solvent for ZnO NPs as the residual ethanol would affect the structure of collagen when the

nanoparticles were introduced.[75] Therefore, ethanol was removed and the ZnO NPs were re-dispersed in water. This process however, can produce destabilization of the ZnO NPs. As ZnO NPs have an absorption peak at 344 nm in their UV-Vis spectrum and the intensity of the absorption peak is proportional to the concentration of the nanoparticles in the suspension, UV-Vis spectroscopy was used to quantify the concentration of the stable ZnO NPs (Figure 4.4).

Figure 4.4 shows that the concentration of ZnO-plain NPs in the suspension decreases rapidly in the first 5h after they were re-dispersed in water, after which only about 50% of the particles remain, indicating the nanoparticles aggregated and precipitated out from the suspension. The ZnO-PVP NPs are shown however to have much better stability, due to the steric hindrance effect of the PVP coatings reducing aggregation. No particles precipitated out in the first 5h and there were still 80% of the particles well dispersed in the suspension after the ZnO-PVP NPs were re-suspended in water for 28h.

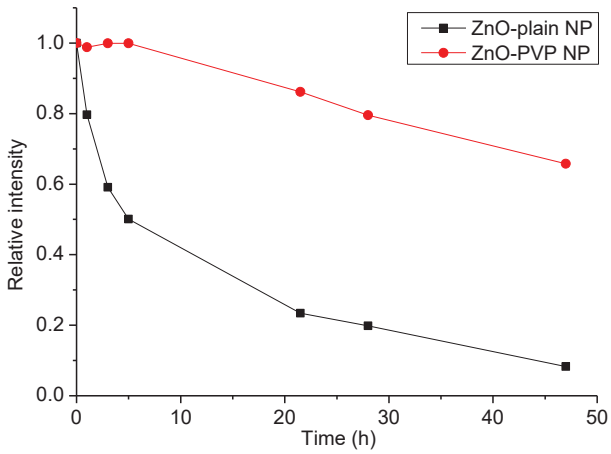

Figure 4.4 The relative intensities of absorbance at 344 nm for purified ZnO-plain and ZnO-PVP NPs in water as a function of time.

4.2. Preparation of ZnO-PVP-induced collagen hydrogel

Direct mixing of the ZnO-PVP NPs with collagen resulted in rapid formation of gel fragments, so an alternative method was trialled. A hydrogel was formed by layering the

ZnO-PVP suspension on top of a collagen solution in a petri dish and incubating at room temperature over night without physically mixing the two phases as illustrated in Figure 4.5. In contrast to the collagen hydrogel prepared with the conventional method, no buffer nor basic solution was required to neutralize the collagen and promote fibrillogenesis. Moreover, the collagen gel prepared using ZnO-PVP NPs (ZnO-PVP-collagen) showed a higher transparency than the collagen gel prepared with the conventional method. A series of ZnO-PVP NP-induced collagen hydrogels were prepared by incubating different concentrations of ZnO-PVP suspensions on top of a collagen layer. The gels formed were then removed and characterized by rheology, DSC and swelling ratio measurements. As an experimental control, a conventional collagen gel was also prepared by overlaying PBS buffer and NaOH solution on top of a collagen solution for comparative study.

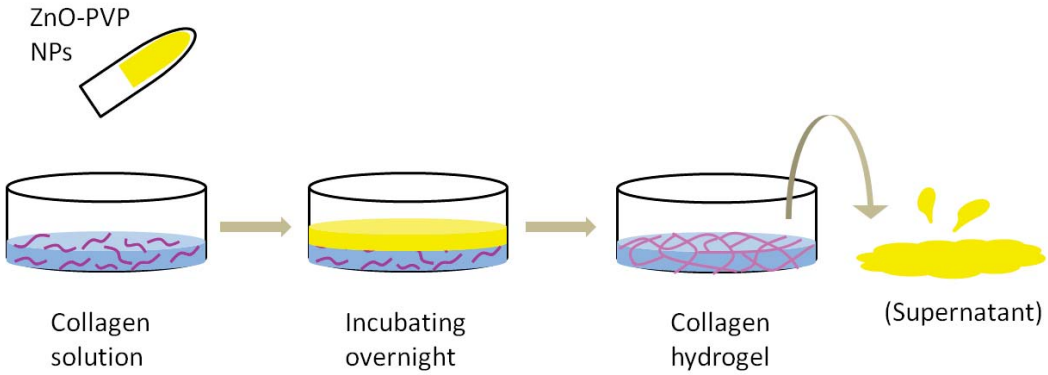

Figure 4.5 Schematic illustration of the fabrication procedure for ZnO-PVP induced collagen hydrogel.

4.3. Rheology of the collagen gels

4.3.1. Linear rheology

The mechanical properties of the ZnO-PVP-induced collagen hydrogels were measured by rheology. The hydrogels were prepared in petri dishes as illustrated in Figure 4.5 before being removed and loaded onto the rheometer for measurements. The linear

rheological behaviour of the samples was determined from measurements carried out at 1 Hz and 1% strain amplitude. Prior to incubation with ZnO-PVP NPs, the collagen solution (5 mg/ml) has very low G' and G" values (Figure 4.6). The conventional collagen gel prepared with PBS buffer and NaOH is relatively strong, with a G' of about 300 Pa. However, once formed, the ZnO-PVP-induced gel has a G' of about 900 Pa, which is about three times as strong as the conventional gel of the same collagen concentration. When varying the concentrations of the ZnO-PVP NPs added on the top of the collagen, it was observed that 5% ZnO-PVP (to the weight of collagen) was not sufficient to induce gelation. However, once the ZnO-PVP solution had a concentration greater than 10% (to the weight of collagen), hydrogels were formed, and their mechanical strengths were not affected by the loading concentration of the ZnO-PVP NPs, as shown in Figure 4.6.

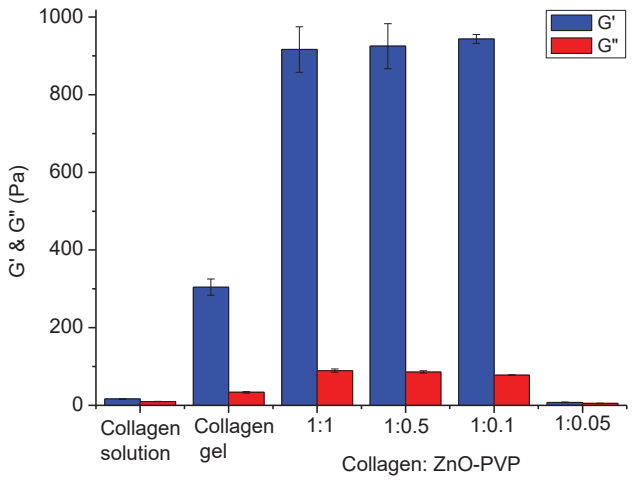

Figure 4.6 The viscoelasticities of conventional collagen gel (control) and the ZnO-PVP induced collagen gels with different collagen to ZnO-PVP mass ratios. All the samples have collagen concentration 5 mg/mL.

A series of hydrogels were also prepared by varying the collagen concentrations from 4 mg/mL to 10 mg/mL while keeping the mass ratio of collagen to ZnO constant (1 to 0.5). No intact gel could be formed when the collagen concentration was lower than 2

mg/mL. As expected, the elasticities of the collagen hydrogels increase as the collagen concentrations increase (Figure 4.7). The power scaling factor of G' as a function of collagen concentration in these ZnO-PVP-induced gels is 1.20 (± 0.14), which is lower than the scaling factor for the conventional collagen gels measured in Chapter 3, but closer to the result from the TiO_2-PAA collagen system. As discussed in the last chapter, the scaling factor for conventional type I collagen gels formed by fibrillogenesis is usually in the range between 2.1 to 2.8, depending on the fibrillogenesis conditions and can be explained with the semi-flexible network model.[40, 76] However, in the case of ZnO-induced collagen gel, it has been realized that the applicability of the semi-flexible model is not so obvious as a different architecture is present in the collagen gel as shown by the confocal microscopy later in this chapter.

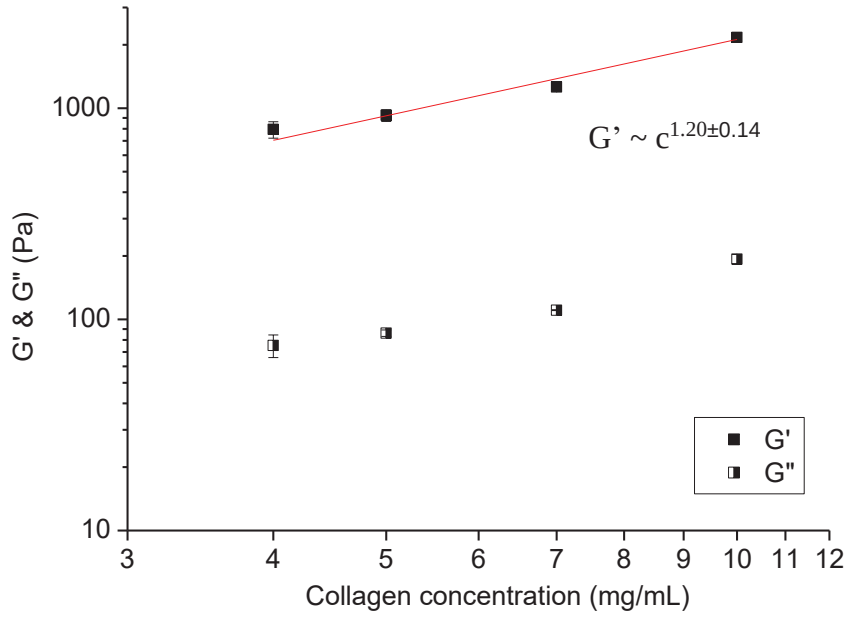

Figure 4.7 The viscoelasticities of ZnO-PVP NPs-induced collagen gels as a function of collagen concentration. The mass ratio of collagen to ZnO is 1:0.5.

4.3.2. Non-linear rheology

The non-linear rheological behaviours of the hydrogels prepared with ZnO-PVP NPs were studied using a pre-stress protocol. The samples were subjected to a constant pre-stress while a very small oscillatory stress was superposed to measure the modulus (details in 2.4.2). Figure 4.8 shows that the conventional collagen gel (control sample) has stiffening index m about 1, which is close to what was observed for a 4 mg/mL collagen gel in the last chapter measured with a strain amplitude ramp protocol and previously reported in the literature.[68] The ZnO-PVP-induced gels have a much higher linear state G'_o as discussed above, and they start to stiffen at a higher stress than the conventional collagen sample. Only a small degree of stiffening behaviour could be recorded for the ZnO-PVP-induced samples, due to the gels slipping between the two plates during the measurements, though the protocol used already minimized this compared with the strain amplitude ramp protocol previously discussed. Interestingly, the non-linear parts of the differential modulus (K) versus stress plots also show the tendency to go towards a stiffening index of 1, which means the ZnO-PVP-induced gels have similar strain-stress responses to the conventional collagen gels.

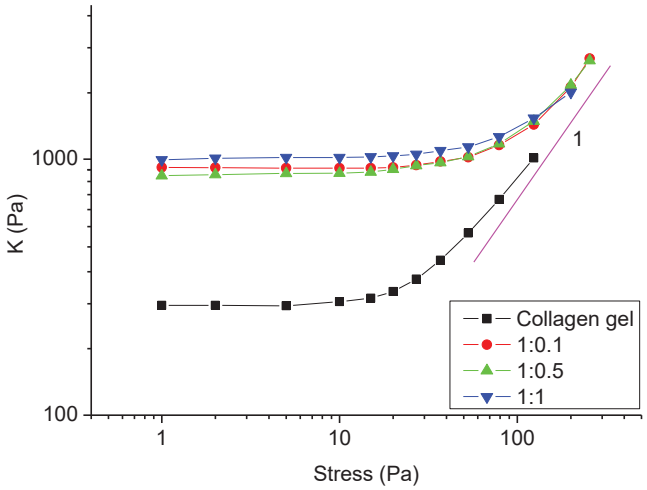

Figure 4.8 Differential shear modulus (K) versus stress curves for conventional collagen (control) and ZnO-PVP-induced collagen gels in different collagen to ZnO-PVP mass ratios. The collagen concentrations are 5 mg/mL in all the samples.

Figure 4.9 is the differential shear moduli of the ZnO-PVP-induced collagen gels at different collagen concentrations measured as a function of stress. They have the same features as the conventional collagen gels and the TiO_2-collagen composites presented in Chapter 3, that the collagen gels with lower concentrations start to stiffen at lower stress. Also, the non-linear part of all the different concentration samples coalesces to a single line. As discussed before, in the non-linear stage, gels with low collagen concentrations can reach the same strength as the high concentration gels under the same stress, even though they are weaker in the linear rheology.

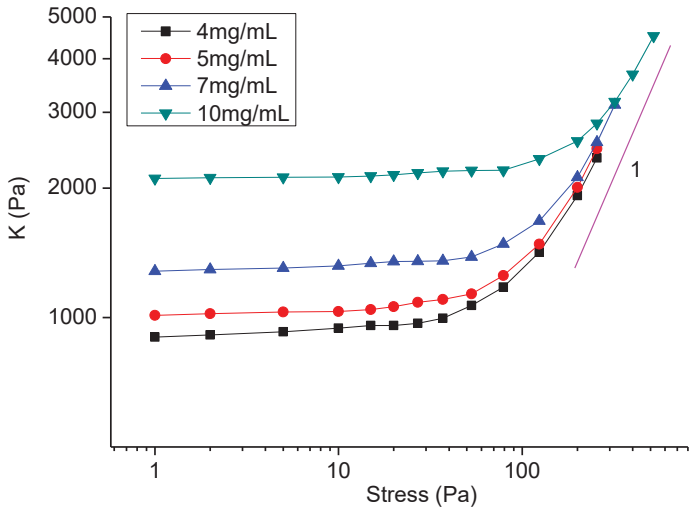

Figure 4.9 Differential shear modulus (K) versus stress curves for ZnO-PVP-induced collagen gels in different collagen concentrations. The mass ratio of collagen to ZnO-PVP is 1: 0.5.

4.4. Hydrogel network morphology

In order to know whether there were any structural differences between the ZnO-PVP-induced collagen gels and the conventional collagen gels, they were visualized using confocal fluorescence microscope. As shown in Figure 4.10, they present completely different network structures. The collagen hydrogel formed with the conventional gelling buffer solution has a structured semi-flexible network and each individual filament can be distinguished clearly. In contrast, the ZnO-PVP-induced gel shows very heterogeneous network structures. Clusters and large pores are present in some regions. Most of the individual filaments can not be clearly defined. The network components are thick and highly associated which may explain why it has a much higher viscoelasticity than the conventional collagen gel of the same collagen concentration. The complete differences in the network structures of the two gelling systems may suggest collagen molecules have different assembly states.

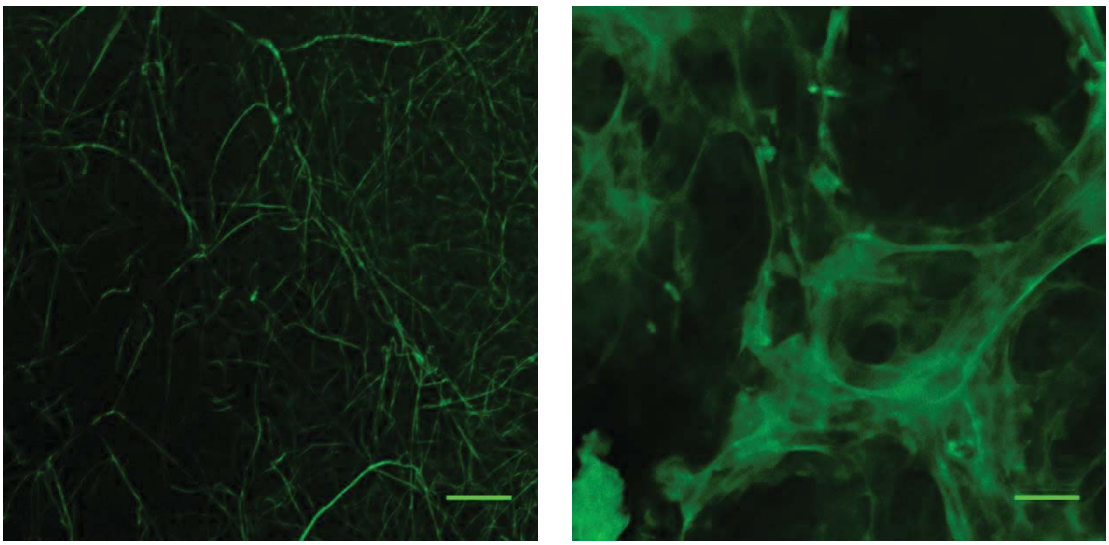

Figure 4.10 Confocal fluorescence images of conventional collagen gel (left) and ZnO-PVP NP-induced collagen gel (right) with collagen concentration 5 mg/mL. Scale bar is 10 μm.

4.5. Small angle X ray scattering (SAXS)

A collagen solution, a ZnO-PVP NP-induced collagen gel and a conventional collagen gel were subjected to SAXS measurements. The scattering intensities of these samples were corrected by subtracting the scattering from the aqueous solvent and the kapton films making up the holders, and plotted as functions of the scattering vector q. It can be seen that at low q the collagen solution has a fractal dimension of -1, suggesting the presence of rod shaped objectives in the collagen solution which are likely to be the oligomers of few collagen molecules.[77] Oligomers are likely to present when the pH of the collagen solution is greater than 4 as is the case here.[78] Both the conventional fibrous collagen gel and the ZnO-PVP-induced collagen gel have higher fractal dimensions in the low q regions, suggesting larger molecular components were produced in the gelation process. The conventional fibrous collagen gel has a fractal dimension of -1 in the high q region and -4 in the low q region, which can be explained with the well known hierarchical structure: smaller rod-shaped microfibrils assembling into the larger fiber structures. The fractal dimension of -4 indicates the scattering is

from well defined entities with smooth surfaces, so very large structural components are present, which is consistent with the microscopy of this sample.[77] On the other hand, the ZnO-PVP NP-induced collagen gel does not have the high fractal dimension as the conventional fibrous gel, which coincides with the information suggested by the confocal image that the structural components in the ZnO-PVP-induced gel are less well defined. On the whole the data is consistent with a picture where in the conventional gel well ordered fibrils are generated from solution. On the other hand the ZnO-induced gels appear to retard this process displaying something that has partially ordered but trapped in a more solution style arrangement.

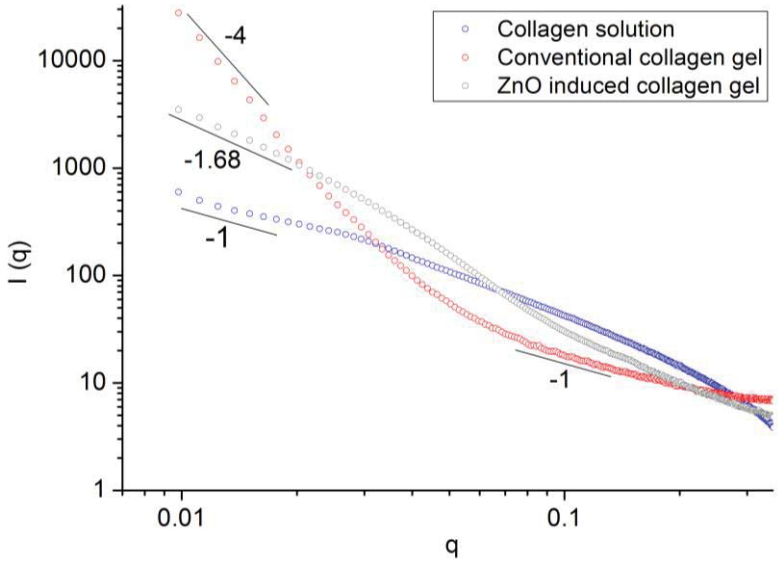

Figure 4. 11 SAXS profiles, I(q) versus q(Å^{-1}) for collagen solution, conventional fibrous collagen gel and ZnO-PVP NP-induced collagen gel.

4.6. Investigating the mechanism of gel formation

The effects of PVP and particle sizes

The first hypothesis that was proposed to explain the phenomena of collagen gel formation by the addition of ZnO-PVP NPs without mechanically mixing (Figure 4.5) was that the ZnO-PVP NPs penetrated through the collagen solution from the interface

by diffusion and subsequently the capping agent PVP crosslinked the collagen molecules. Indeed, it has been reported that PVP molecules are able to crosslink collagen via H-bonding.[48] However, in an experimental control, it was found that collagen solution with just PVP solution added could not form a gel (data not shown). For comparison studies, conventional collagen gels containing PVP were prepared which showed a similar viscoelasticity to the collagen gel without PVP (Figure 4.12), indicating PVP itself does not modify the rheological properties of the collagen gels. In addition, ZnO-plain NPs and even bulk ZnO particles (purchased commercially, unknown size) were also incubated on top of a collagen solution using the same protocol as illustrated in Figure 4.5 and it was found that they were also able to trigger collagen gelation, although it is highly unlikely that they penetrated into the collagen solution owing to their size. The linear rheological properties of these samples had G' and G" similar to the ZnO-PVP NP-treated gels (Figure 4.12). Hence, this group of studies suggested that PVP was not the crucial factor in collagen gelation, and crucially that it is not necessary for ZnO NPs to penetrate into the collagen solution for gelation to occur.

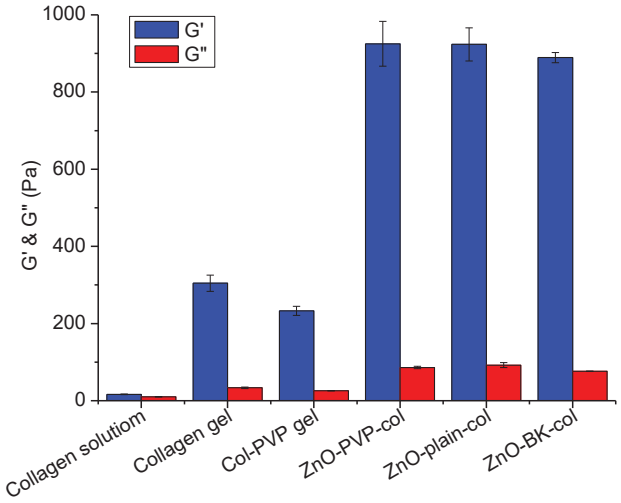

Figure 4.12 The viscoelasticities of PVP containing conventional collagen gel and gels formed with different ZnO. ZnO-plain-col: ZnO-plain NP-induced collagen hydrogel; ZnO-BK-col: bulk ZnO-induced collagen hydrogel.

Spatially resolved optical density measurements

Speckle patterns formed by scattered laser light transmitted through samples during the gelation processes were recorded using a light scattering setup as described in 2.4.2. During the gelation process, the intensity of light scattered by the samples increases and the speckles recorded become brighter as the fibrils in the samples develop. From a series of images, it was found that the increasing intensity of the scattered light developed from the interface between the ZnO and collagen solutions along the z direction (Figure 4.13). This indicated the fibrillogenesis process started from the collagen-ZnO or collagen-buffer interface, rather than isotropically inside the collagen solution. For the ease of analysis, the intensity of each scattering image was averaged across the horizontal direction of the cuvette as it is expected that the scattering intensity is only changing along the z direction over time (Figure 4.13). Z-resolved average scattering intensities of each scattering image in the first 10h of the gelation process were combined in this manner to give the time versus spatially resolved optical density plots (Figure 4.14(a)-(d)). For ease of visualization, the intensity is quantified with

different colours changing from blue to dark red, as shown in scale bar on the right of each plot (note the different scales in different plots).

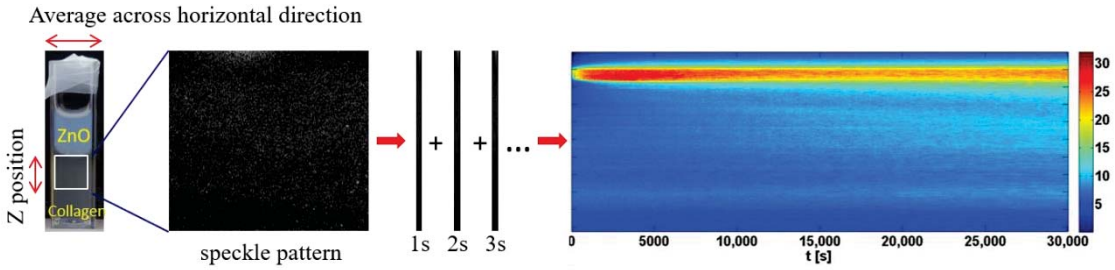

Figure 4.13 From the individual scattering patterns to obtain the time and spatial resolved optical density plot.

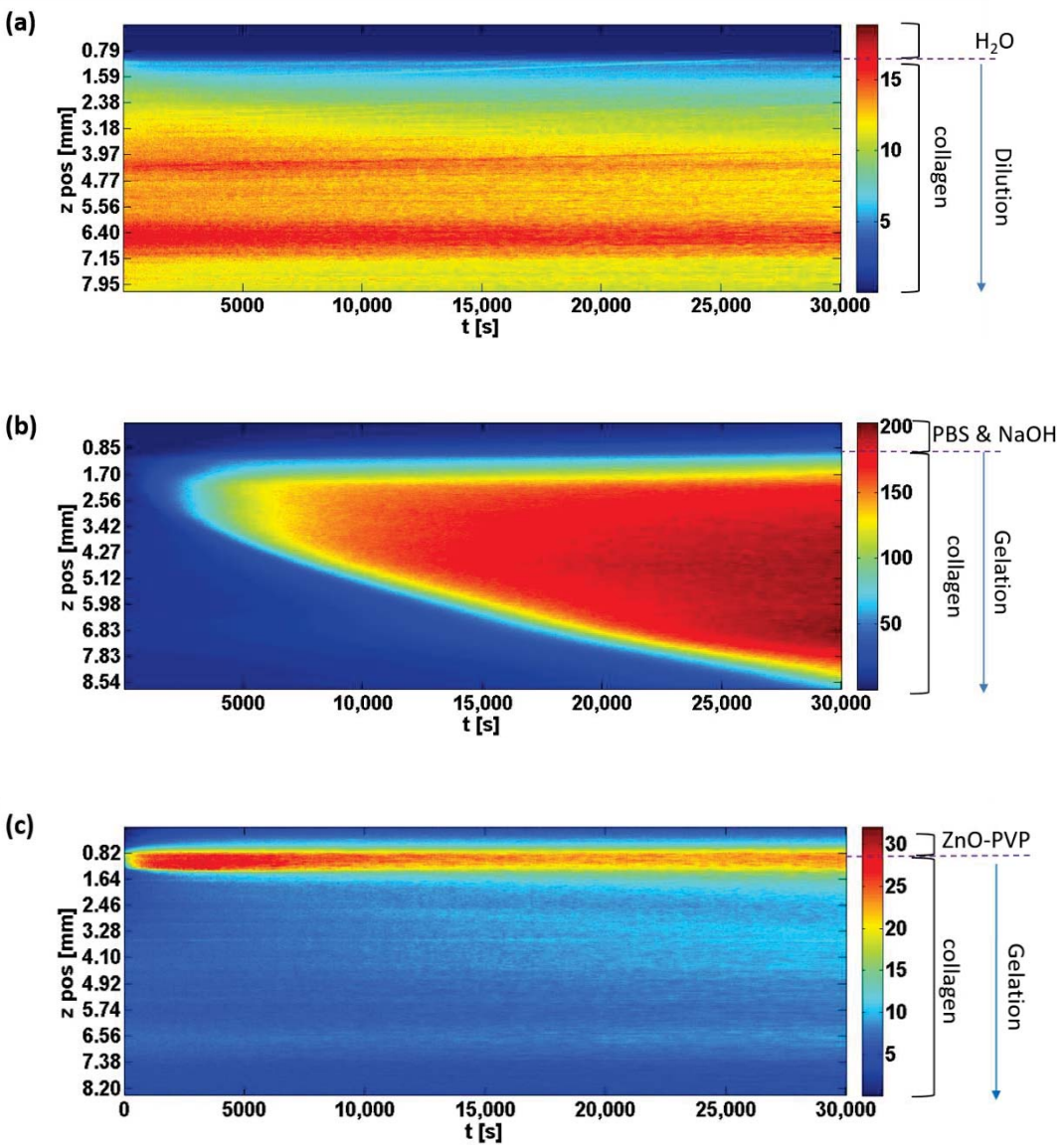

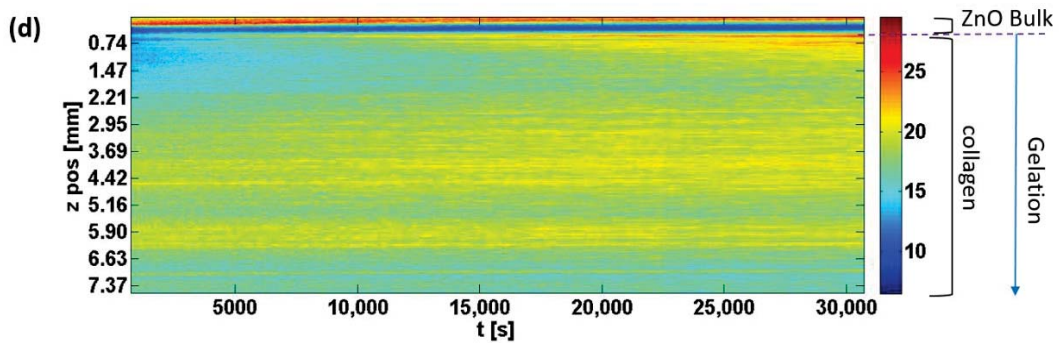

Figure 4.14 The spatially resolved optical density plots recorded over 10h in collagen solutions with the layering of the followings on top (a) water (as control), (b) conventional gelation buffer, (c) ZnO-PVP NPs, (d) bulk ZnO.

In a control sample with just H_2O added (Figure 4.14(a)), the scattering intensity becomes lower gently along z direction over time, which can be explained as the process of water diffusing into the collagen solution and diluting it. The dramatic changes in the scattering intensities of the collagen gelled by the addition of conventional gelation buffer indicate large fibrils in the sample are developing as expected (Figure 4.14(b)). However, the changes in intensities with the ZnO-PVP NPs and bulk ZnO particles on the top are quite weak (Figure 4.14(c) & (d)). This suggests that the gelling processes were slow and the structure components formed may have much smaller refractive index contrast than the ones formed with the conventional buffer. It has been observed by the confocal images that the ZnO induced collagen gel does not have a substantial amount of the large length scale semi-flexible fibrils which scatter the wavelength of visible light. This may explain why its change in scattering intensity in the gelation process was weaker.

After it became clear that gels formed with ZnO did not have a substantial amount of conventional fibrils and furthermore that ZnO particles were not directly involved in the gelation process, several other hypotheses were investigated to explain the gel formation in this case.

The effects of ions and the solubility of ZnO-PVP-induced collagen gel

Ion-induced gelation is well known generally and is one of the gelation mechanisms exploited with pectin and alginate.[79] By considering the fact that there may be some Zn^{2+} or acetate from the precursor present in the ZnO-PVP suspension, zinc acetate and zinc chloride solutions were also introduced to collagen, in order to examine whether the collagen gelled with ZnO-PVP was forming with Zn^{2+} or acetate. However, collagen gels were not obtained in both cases.

In order to further investigate the factors for causing collagen gelation by ZnO-PVP NPs, an experiment was carried out with collagen solution in dialysis tubing which was immersed in a suspension of ZnO-PVP (Figure 4.15). The dialysis tubing had a pore size (<2 nm) too small for ZnO-PVP NPs to penetrate. However, collagen gel was also formed, further suggesting that indeed it was not necessary for ZnO to penetrate through the collagen solution to trigger gel formation. After this gel was formed, it was removed from the dialysis tubing and cut into three pieces, each of which was immersed in a solution of water, EDTA solution (neutral pH) or acetic acid solution respectively, as shown in Figure 4.15. The formed collagen gel was not soluble in water. EDTA solution in neutral pH has a very high affinity to chelate with Zn^{2+}, and it was assumed that the collagen gel would fall apart as the results of Zn^{2+} being removed if the gel was formed by Zn^{2+} crosslinking the collagen monomers.[80] However, this did not occur. Interestingly, the collagen gel was soluble in acetic acid solution, suggesting the gel is pH sensitive and formed by non-covalent interactions.

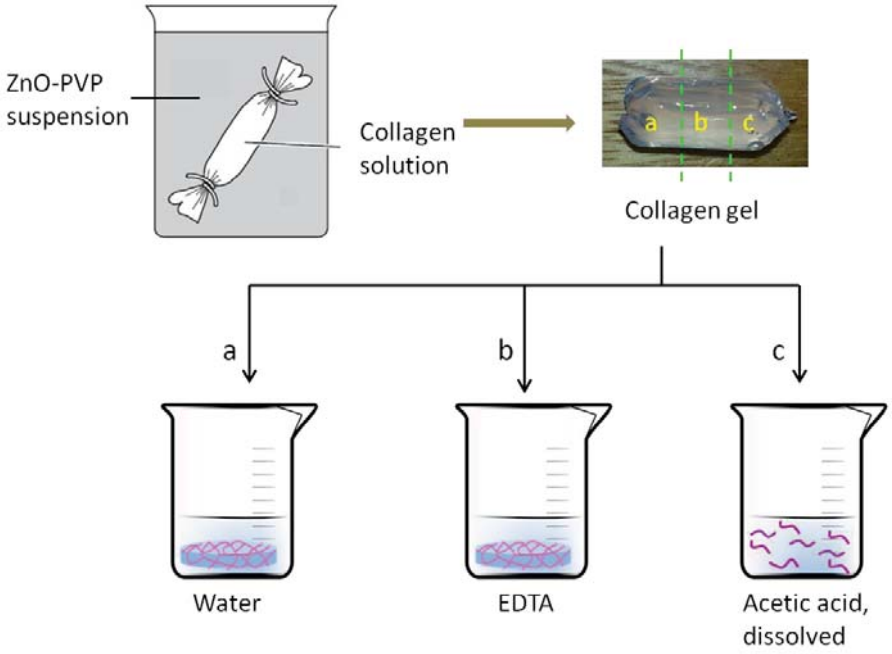

Figure 4.15 Schematic illustration to test the effect of Zn^{2+} and the solubility of the ZnO-PVP-induced gel.

pH measurements during the gelation process

It is known that collagen fibrillogenesis occurs when acidic collagen solution is neutralized and treated at physiological temperature.[6] In this study when ZnO was incubated in contact with collagen solution in acetic acid as a solvent, it would interact with H^+ dissociated from acetic acid to form Zn^{2+}. Therefore, ionic transport across the interface would lead to H^+ cations being consumed, increasing the pH of the system. It was postulated that when the pH of the collagen gets close to its isoelectric point, gelation can occur.[78, 81] In this scenario, the slow pH change caused indirectly by ZnO NPs without a buffer as opposed to the rapid pH changed coupled with the PBS buffer in fibrillogenesis generated a different network assembly and ultimately a distinct gel.

In order to test the hypothesis that the collagen gelation triggered by ZnO is simply caused by increasing the pH of the system, the pH changes of the collagen during the gelation process were monitored by the colour changes of the collagen solution with three different types of pH indicators (Bromocresol purple (BP), Bromothymol blue

(BB) and Phenol red (PR)). A pH meter was initially used but no sensible data was collected in long run experiments, as the electrode could not be calibrated during the experiments. The colours of the pH indicators and the limits of values that yield a colour transition are listed in Table 4.1. The collagen solutions were yellow or amber before the addition of the layer of ZnO-PVP NPs as shown in Figure 4.16, as the pH of the collagen was about 4 (measured by pH meter). The top part of the collagen turned into purple after the ZnO-PVP suspension was added to the BP containing collagen sample for 1h, while there was no obvious colour changes in the other two samples, which means the pH of this part of the collagen had increased to over 5.2 but was still below 6.0, the lowest colour transition pH of BB (Figure 4.16). After 24h, the colour of the BP containing sample changed quite significantly and a colour gradient from the top to the bottom of the collagen in the cuvette was visible. The colour had not yet reached purple (colour of the high pH of BP) which means the pH was between 5.2 and 6.8. The top parts of the BB and PR samples started to change colours so the pH of the top part of the collagen had increased to over 6.4 after one day. The colours were continuously changing slowly and after one week, the BP containing sample had turned to purple uniformly. However, the BB containing sample had a greenish blue colour on the top part and yellowish green at the bottom part of the collagen solution, suggesting pH gradients still exist. It had not turned to the end point (blue) so the pH of the collagen was lower than 7.6 at that time. PR indicator had the most basic transition pH (6.4). The sample had turned into very pale pink from yellow and did not turn into pink. Summarizing above, it is suggested that the pH of the collagen reached the range between 6.4 and 7.6. It has been observed that collagen fibrillogenesis can occur in this pH range, although it should be noted that the confocal images suggest that the ZnO

induced gel does not contain a substantial amount of the conventional fibrils formed by fibrillogenesis.[78]

Table 4.1 The colours of the pH indicators and their transition pHs.

Indicator	Low pH colour	Transition low end	Transition high end	High pH colour
Bromocresol purple (BP)	yellow	5.2	6.8	purple
Bromothymol blue (BB)	yellow	6.0	7.6	blue
Phenol red (PR)	yellow	6.4	8.0	red

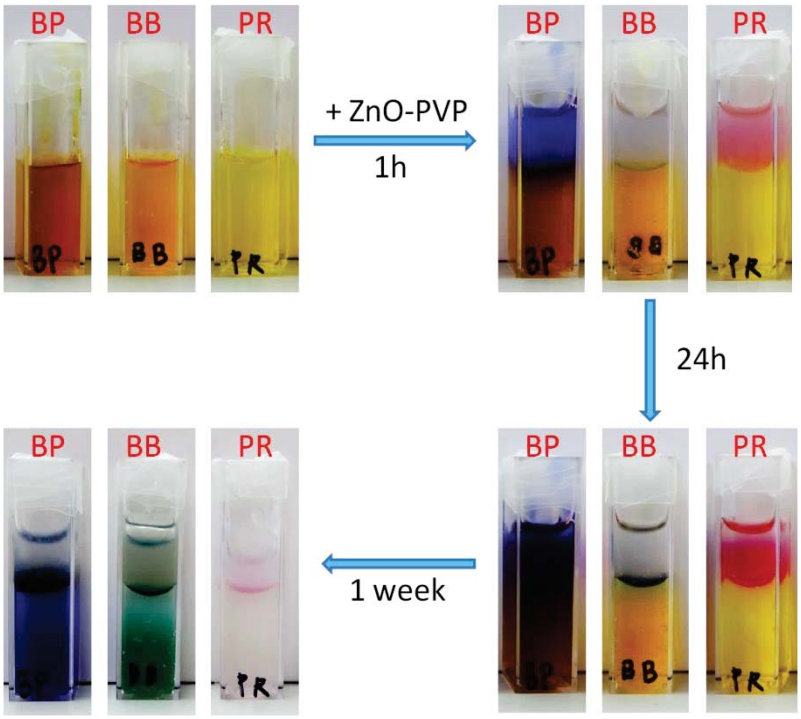

Figure 4.16 Colour changes in the gelation processes of the pH indicator containing collagen, triggered by ZnO-PVP NPs.

The above experiments have demonstrated that the collagen gel induced by ZnO-PVP NPs is not because the ZnO-PVP NPs interact directly with collagen molecules, but

they indirectly neutralize the acidic collagen solution to reduce the charges on the collagen molecules so the collagen molecules aggregate, as illustrated in Figure 4.17.[82] In the conventional collagen sample, PBS buffer is used which has been shown to assist the formation of nuclei.[83] It also has the buffering effect to prevent the aggregation of collagen molecules caused by a sudden pH change and give them the time to self-organize towards an equilibrium state which has a periodic banding fibrillar structure (Figure 4.17). However, no buffer was used for the ZnO-PVP induced collagen gel, so random aggregation between molecules occurs after the local pH of the collagen solution gets close to its isoelectric point. The collagen molecules are kinetically trapped by these associations so they can not orientate to form the thermodynamically favourable fibrillar structure (Figure 4.17).[78]

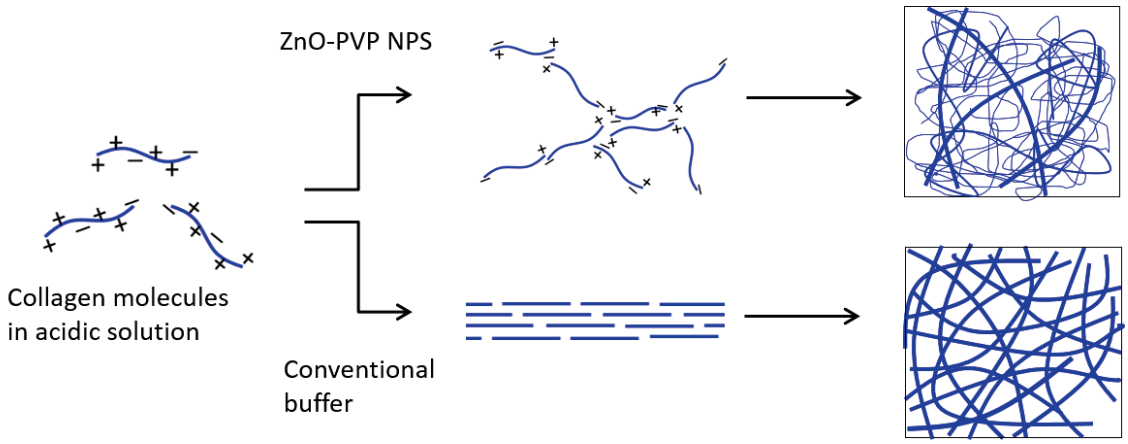

Figure 4.17 Postulated gelation mechanisms and network structures of the ZnO-PVP NPs induced collagen gel and the conventional collagen gel.

4.7. Swelling ratio

Figure 4.18 presents the results of the water uptake capabilities of the lyophilized gels formed with ZnO-PVP NPs. The dry collagen film prepared by direct drying of the collagen solution has as high swelling ratio of 2000 wt% relative to its dry weight. Samples treated with ZnO-PVP NPs have significantly decreased swelling ratios. The

higher the concentration of ZnO-PVP NPs used, the lower the swelling ratio of the dry film, but the differences between each sample are not dramatic. The sample formed with a collagen to ZnO-PVP ratio of 1:0.05 does not have a high enough ZnO-PVP concentration to form a gel, but its swelling ratio has decreased to about 70% of that of the un-treated collagen. However, all the ZnO-PVP-induced samples have higher swelling ratios than the dried conventional collagen gel which is only about 10% of that of the untreated collagen. In general, the lower the swelling ratio, the higher the degree of crosslinking, and the higher the mechanical strength of the polymer hydrogel will be.[71] Here, the dry films of the ZnO-PVP-induced gels have higher swelling ratios than the dry film of the conventional fibrous collagen gel, suggesting the ZnO-PVP-induced gels have lower degrees of crosslinking than the conventional gel, however, their shear elastic moduli (G') are greater. The reason may be that the collagen gel formed by fibrillogenesis creates a very high concentration of intra-strand crosslinks to the gel. But these intra-strand crosslinks do not contribute to the shear modulus. From the structure point of view, the ZnO-PVP-induced gels have more flexible networks, so they are easier to re-orientate to accommodate larger volumes of solvent than the semi-flexible fibrous conventional gel.[72] Also, there are large pores present, in addition to the large biopolymer surface area in the ZnO-PVP-induced gels. As a result, although the ZnO-PVP NP-induced gels are stronger, they have higher swelling ratios than the conventional collagen gel.

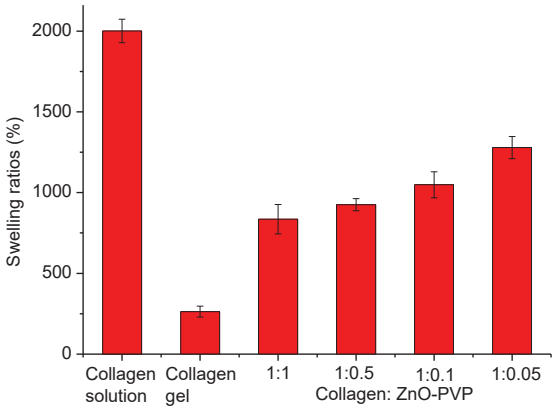

Figure 4.18 The swelling ratios (in %) of the lyophilized films of collagen and ZnO-PVP NP-induced collagen gels.

4.8. Thermal stabilities of the ZnO-PVP-induced collagen hydrogels

In order to know whether making gels using ZnO-PVP NPs had any effect on the thermal stability of the collagen, the denaturation temperatures of the ZnO-PVP-induced collagen hydrogels were measured by DSC. From Figure 4.19, it can be seen that the thermal stabilities of the ZnO-PVP treated collagen samples have increased slightly when compared with the collagen solution which has not been treated with ZnO-PVP NPs. The hydrogel with 1:1 mass ratio (of collagen to ZnO-PVP) has the highest denaturation temperature which is about 53°C. It is approximately 7°C higher than that of the collagen solution. Such a small improvement suggests that there should be only physical interactions, such as H-bonding or/ and electrostatic interactions, or a small number of chemical interaction involved in the gelation process. We already postulated that electrostatic interaction is the driving force for the gelation previously. There is a weak decreasing trend for the denaturation temperatures of the gels with decreasing the concentrations of the ZnO-PVP NPs used in the gel induction. As mentioned before, the use of ZnO-PVP in a 1:0.05 (collagen to ZnO-PVP) mass ratio did not cause the gelation of collagen. Here it shows that correspondingly the thermal stability has not been improved in this sample either. While the ZnO-PVP-induced collagen hydrogels

do have much higher viscoelasticities than the conventional collagen gels, however, their thermal stabilities are the other way round, with the conventional collagen gel showing a higher thermal stability. As discussed before, the fibrillogenesis process is a self-assembly process which is thermodynamically favourable and the system is in its most stable state,[6] while the ZnO-PVP-induced collagen gels exhibit random aggregation which should be in a 'kinetic trap' so the gels are not in the most stable state. Therefore, the ZnO-PVP-induced gels have lower thermal stabilities than the conventional gel.

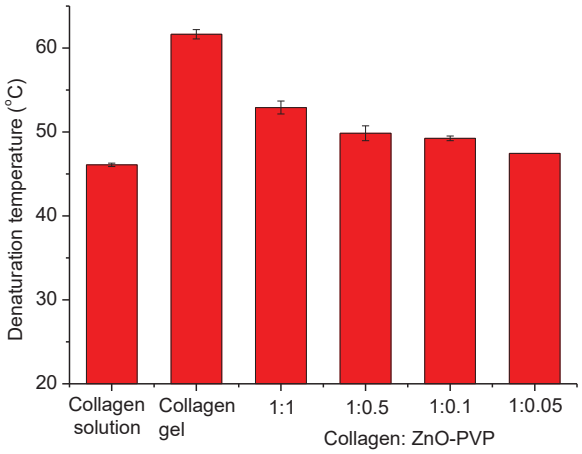

Figure 4.19 The denaturation temperatures of untreated collagen solution, conventional collagen gel and ZnO-PVP induced collagen gels. The collagen concentrations in all samples are 5 mg/mL.

4.9. Chapter summary

Instead of forming ZnO-collagen nanocomposites, the ZnO-PVP NPs acted as a neutralizing agent to induce collagen gelation. This chapter has investigated the structure and some physical properties of this ZnO-PVP NP-induced gel and compared with that of the conventional collagen gel. The details of two distinct gelling systems are summarized in Table 4.2. Similar to the TiO_2-collagen system, their physical

properties observed are consistent with what can be predicted from their morphological structures.

Table 4.2 Comparing the properties and structures of the ZnO-induced collagen gel and the conventional collagen gel.

	ZnO NP-induced collagen gel	Conventional collagen gel
Linear rheology	Higher viscoelasticity	Lower viscoelasticity
Non-linear rheology	Similar stiffening index, stiffening at a higher stress	Similar stiffening index, stiffening at a lower stress
Transparency	Higher	Lower
Swelling ratio	Higher	Lower
Thermal stability	Lower	Higher
Rate of gelation	Slower	Faster
Structure	A substantial amount of non-fibrous structures, highly associated heterogeneous network, clusters present	Semi-flexible fibrous network, large length scale structure components

5. Conclusions and Future work

5.1. Conclusions

In this study, surface functionalized TiO_2 and ZnO NPs have been introduced to collagen solutions. Both TiO_2 and ZnO NPs are metal oxide NPs and they share many similar properties. However, they affect collagen hydrogel formation differently. The mechanical properties of the collagen hydrogels prepared using nanoparticles have been studied with rheology. Their morphological structures have been visualized with confocal fluorescence microscopy. In some cases, light scattering and pH indicators have been used to monitor the assembly process. In addition, techniques including SAXS, DSC, swelling ratio assay and FTIR have also been used to characterize the collagen hydrogels.

TiO_2 NPs functionalized with chitosan or PAA were introduced into collagen solutions and thoroughly mixed prior the fibrillogenesis process to form hydrogels. By varying the surface functionalization of the nanoparticles, the interactions between the surface functional groups and the collagen molecules were observed to affect the fibrillogenesis process, resulting in different network structures. The nanocomposite hydrogels had different structures to the native collagen which predominantly determined their rheological properties.

The interactions between chitosan coated TiO_2 NPs and the collagen molecules were shown to slow down the collagen gelation process. The slow fibrillogenesis results in the formation of thick fibrils. On the other hand, negatively charged PAA functionalized TiO_2 promoted the collagen nucleation and accelerated the fibrillogenesis, so the fibrils formed were thin. Evidence was supplied by confocal images that indeed the TiO_2-CS

introduced gel has thick fibrils, large pores, less inter-strand crosslinks and rigid structure, whilst the TiO_2-PAA incorporated gel has thin and dense fibrils with a concomitant greater number of inter-fibril crosslinks. Correspondingly, TiO_2-PAA gives a collagen gel with a mildly enhanced linear state G', and the TiO_2-CS included collagen has a slightly lower G'. However, both modifications have made the collagen hydrogels more resilient to strain likely. No significant differences were observed in the non-linear strain-stress response when compared with the native collagen hydrogel.

ZnO-PVP NPs were added to the surface of the collagen solution without mixing the two phases. This was because direct mixing of ZnO-PVP with collagen resulted in rapid formation of gel fragments. In contrast to the conventional gelation protocol, no gelation buffer nor NaOH solution for neutralization was used. From several experiments, it was concluded that ZnO-PVP actually acts as a neutralizing agent here. It reacts with the H^+ dissociated from the acidic acid molecules in the collagen solution to raise the pH of the system from 4 to close to the isoelectric point of the collagen. No buffer is used, which explains why the heterogeneous clustered structure of the collagen hydrogel with large pores are formed. Most fibrils are not well defined, instead the highly interconnected network gives the hydrogel three times the elastic modulus of the collagen networks formed with the conventional gelation protocol. The non-linear strain-stress responses of these two types of collagen gel are not significantly different, even though they have completely different network structures.

Both TiO_2 and ZnO NP-collagen systems demonstrate how the direct or indirect molecular interactions between the nanoparticle and the collagen monomer solution affect the macroscopic structures of the hydrogels, which then determine their physical properties. This allows us to use nanoparticles to control the structure of the collagen

hydrogel networks to achieve the suitable properties for certain applications. For example, conventionally the stronger the hydrogel, the weaker the water uptake capability, but the ZnO induced collagen gel has the merits of having high viscoelasticity and high water uptake capability at the same time. It also has a very high transparency which may be a benefit for applications such as corneal transplants. On the other hand, TiO_2 NPs introduce extra functions to collagen to broaden its applications. For example, TiO_2 collagen nanocomposites would have anti-bacterial properties which makes them suitable for wound dressing, but its mechanical strength and thermal stability are not significantly different to collagen itself.

5.2. Future perspectives

The basic gelation mechanism and network morphology of the ZnO-PVP-induced collagen hydrogel have been investigated in this study. However, the detailed information about the molecular arrangements of the collagen molecules is still unknown. The confocal image suggests that it would be definitely different to the molecular assembly in the native collagen gel. SAXS patterns have been recorded for those samples, and the very basic results have been presented in Chapter 4. However, they have not been fitted with models to explore the morphological details which will be studied in the future. In addition, how the morphologies of the collagen network develop in the gelation process should be analysed. The SAXS data will also be analysed for the TiO_2-collagen nanocomposites to study how the functionalized TiO_2 NPs affect the collagen molecules assembly.

Collagen gels induced by bulk ZnO, ZnO-plain NP and ZnO-PVP NP do not show any significant difference in rheological measurements. However, whether they have differences in the rate of gelation has not been investigated in this study. Both the size

and the surface capping of the ZnO are considered to affect the rates of their interactions with acetic acid, hence they may be used to modify the rates of collagen gelation. It would be interesting to further investigate how the network structures of the collagen gels induced by different types of ZnO are varied if they gel at different rates.

TiO_2 is a well known photocatalyst and it has been used as a photo-initiator to photo-crosslink some polymers.[23] Studying the photocrosslinking effect initiated by TiO_2 NPs in the nanocomposites is also an area for potential future experiments. The mechanical properties of the TiO_2-collagen hydrogels before and after UV irradiation would be compared.

A basic drug release study has been carried out using the ZnO-PVP-induced collagen to encapsulate drug molecules by our collaborators. It has been found the sample has a rapid drug release in the first 24h followed by a slow constant release process for more than 14 days. Drug release profiles should be monitored for the TiO_2-collagen nanocomposites with different coatings on TiO_2 NPs, as they have been shown to have different pore sizes and swelling behaviours, both of which affect the rate of drug release.

The applications of the collagen materials are tightly related to their physical properties. With a fundamental understanding of how the physical properties of collagen can be tailored with NPs, designing collagen based materials and composites to achieve the properties required for specific applications can be carried out in the future.

References

1. Li, D.; Yang, W.; Li, G.-Y., Extraction of native collagen from limed bovine split wastes through improved pretreatment methods. *Journal of Chemical Technology and Biotechnology* **2008,** *83* (7), 1041-1048.

2. Zhang, Z. K.; Li, G. Y.; Shi, B., Physicochemical properties of collagen, gelatin and collagen hydrolysate derived from bovine limed split wastes. *Journal of the Society of Leather Technologists and Chemists* **2006,** *90* (1), 23-28.

3. Friess, W., Collagen - biomaterial for drug delivery. *European Journal of Pharmaceutics and Biopharmaceutics* **1998,** *45* (2), 113-136.

4. Bhattacharjee, A.; Bansal, M., Collagen structure: The Madras triple helix and the current scenario. *Iubmb Life* **2005,** *57* (3), 161-172.

5. Shoulders, M. D.; Raines, R. T., Collagen Structure and Stability. In *Annual Review of Biochemistry*, 2009; Vol. 78, pp 929-958.

6. Fratzl, P., *Collagen: Structure and mechanics*. Springer: New York, 2008.

7. Glowacki, J.; Mizuno, S., Collagen scaffolds for tissue engineering. *Biopolymers* **2008,** *89* (5), 338-344.

8. Lee, C. H.; Singla, A.; Lee, Y., Biomedical applications of collagen. *International Journal of Pharmaceutics* **2001,** *221* (1-2), 1-22.

9. Singh, P.; Benjakul, S.; Maqsood, S.; Kishimura, H., Isolation and characterisation of collagen extracted from the skin of striped catfish (Pangasianodon hypophthalmus). *Food Chemistry* **2011,** *124* (1), 97-105.

10. O'Brien, F. J., Biomaterials & scaffolds for tissue engineering. *Materials Today* **2011,** *14* (3), 88-95.

11. Castaneda, L.; Valle, J.; Yang, N.; Pluskat, S.; Slowinska, K., Collagen cross-linking with Au nanoparticles. *Biomacromolecules* **2008,** *9* (12), 3383-3388.

12. Duan, X.; Sheardown, H., Crosslinking of collagen with dendrimers. *Journal of Biomedical Materials Research Part A* **2005,** *75* (3), 510-518.

13. Hornyak, G. L., *Introduction to nanoscience / Gabor L. Hornyak ... [et al.]*. Boca Raton : CRC Press, c2008: 2008.

14. Cargnello, M.; Gordon, T. R.; Murray, C. B., Solution-Phase Synthesis of Titanium Dioxide Nanoparticles and Nanocrystals. *Chemical Reviews* **2014,** *114* (19), 9319-9345.

15. Singh, R.; Lillard, J. W., Jr., Nanoparticle-based targeted drug delivery. *Experimental and Molecular Pathology* **2009,** *86* (3), 215-223.

16. Yin, Z. F.; Wu, L.; Yang, H. G.; Su, Y. H., Recent progress in biomedical applications of titanium dioxide. *Physical Chemistry Chemical Physics* **2013,** *15* (14), 4844-4858.

17. Ludi, B.; Niederberger, M., Zinc oxide nanoparticles: chemical mechanisms and classical and non-classical crystallization. *Dalton Transactions* **2013,** *42* (35), 12554-12568.

18. Kołodziejczak-Radzimska, A.; Jesionowski, T., Zinc Oxide—From Synthesis to Application: A Review. *Materials* **2014,** *7* (4), 2833.

19. Qi, K.; Xin, J. H., Room-Temperature Synthesis of Single-Phase Anatase TiO2 by Aging and its Self-Cleaning Properties. *Acs Applied Materials & Interfaces* **2010,** *2* (12), 3479-3485.

20. Harzallah, O. A.; Dupuis, D., Rheological properties of suspensions of TiO2 particles in polymer solutions. 1. Shear viscosity. *Rheologica Acta* **2003,** *42* (1-2), 10-19.

21. Yang, Y.; Zhang, H.; Wang, P.; Zheng, Q.; Li, J., The influence of nano-sized TiO2 fillers on the morphologies and properties of PSFUF membrane. *Journal of Membrane Science* **2007,** *288* (1-2), 231-238.

22. Nasu, A.; Otsubo, Y., Rheology and UV protection properties of suspensions of fine titanium dioxides in a silicone oil. *Journal of Colloid and Interface Science* **2006,** *296* (2), 558-564.

23. Liao, C.; Wu, Q.; Su, T.; Zhang, D.; Wu, Q.; Wang, Q., Nanocomposite Gels via in Situ Photoinitiation and Disassembly of TiO2-Clay Composites with Polymers Applied as UV Protective Films. *Acs Applied Materials & Interfaces* **2014,** *6* (3), 1356-1360.

24. Aimé, C.; Coradin, T., Nanocomposites from biopolymer hydrogels: Blueprints for white biotechnology and green materials chemistry. *Journal of Polymer Science Part B: Polymer Physics* **2012,** *50* (10), 669-680.

25. Desimone, M. F.; Helary, C.; Quignard, S.; Rietveld, I. B.; Bataille, I.; Copello, G. J.; Mosser, G.; Giraud-Guille, M.-M.; Livage, J.; Meddahi-Pelle, A.; Coradin, T., In vitro Studies and Preliminary In vivo Evaluation of Silicified Concentrated Collagen Hydrogels. *Acs Applied Materials & Interfaces* **2011,** *3* (10), 3831-3838.

26. Desimone, M. F.; Helary, C.; Rietveld, I. B.; Bataille, I.; Mosser, G.; Giraud-Guille, M.-M.; Livage, J.; Coradin, T., Silica-collagen bionanocomposites as three-dimensional scaffolds for fibroblast immobilization. *Acta Biomaterialia* **2010,** *6* (10), 3998-4004.

27. Solange Alvarez, G.; Helary, C.; Mathilde Mebert, A.; Wang, X.; Coradin, T.; Federico Desimone, M., Antibiotic-loaded silica nanoparticle-collagen composite hydrogels with prolonged antimicrobial activity for wound infection prevention. *Journal of Materials Chemistry B* **2014,** *2* (29), 4660-4670.

28. Schuetz, T.; Richmond, N.; Harmon, M. E.; Schuetz, J.; Castaneda, L.; Slowinska, K., The microstructure of collagen type I gel cross-linked with gold nanoparticles. *Colloids and Surfaces B-Biointerfaces* **2013,** *101*, 118-125.

29. Wilson, C. G.; Sisco, P. N.; Gadala-Maria, F. A.; Murphy, C. J.; Goldsmith, E. C., Polyelectrolyte-coated gold nanorods and their interactions with type I Collagen. *Biomaterials* **2009,** *30* (29), 5639-5648.

30. Nidhin, M.; Vedhanayagam, M.; Sangeetha, S.; Kiran, M. S.; Nazeer, S. S.; Jayasree, R. S.; Sreeram, K. J.; Nair, B. U., Fluorescent nanonetworks: A novel bioalley for collagen scaffolds and Tissue Engineering. *Scientific Reports* **2014,** *4*.

31. Sangeetha, S.; Ramamoorthy, U.; Sreeram, K. J.; Nair, B. U., Enhancing collagen stability through nanostructures containing chromium(III) oxide. *Colloids and Surfaces B-Biointerfaces* **2012,** *100*, 36-41.

32. Goodwin, J. W. H., R. W., *Rheology for Chemists An Introduction*. The Royal Society of Chemistry: Cambridge, UK, 2008.

33. Brummer, R., *Rheology essentials of cosmetic and food emulsions*. Springer Berlin Heidelberg: Berlin, Germany, 2006.

34. Oscillatory rheology-measuring the viscoelastic behaviour of soft materials. *G. I. T. Laboratory Journal* **2007,** *3-4*, 68-70.

35. Yan, C.; Pochan, D. J., Rheological properties of peptide-based hydrogels for biomedical and other applications. *Chemical Society Reviews* **2010,** *39* (9), 3528-3540.

36. Storm, C.; Pastore, J. J.; MacKintosh, F. C.; Lubensky, T. C.; Janmey, P. A., Nonlinear elasticity in biological gels. *Nature* **2005,** *435* (7039), 191-194.

37. Erk, K. A.; Henderson, K. J.; Shull, K. R., Strain stiffening in synthetic and biopolymer networks. *Biomacromolecules* **2010,** *11* (5), 1358-1363.

38. Manning, G. S., The persistence length of DNA is reached from the persistence length of its null isomer through an internal electrostatic stretching force. *Biophysical Journal* **2006,** *91* (10), 3607-3616.

39. Wen, Q.; Janmey, P. A., Effects of non-linearity on cell–ECM interactions. *Experimental cell research* **2013,** *319* (16), 2481-2489.

40. Motte, S.; Kaufman, L. J., Strain stiffening in collagen I networks. *Biopolymers* **2013,** *99* (1), 35-46.

41. Jaspers, M.; Dennison, M.; Mabesoone, M. F.; MacKintosh, F. C.; Rowan, A. E.; Kouwer, P. H., Ultra-responsive soft matter from strain-stiffening hydrogels. *Nature communications* **2014,** *5*.

42. Head, D.; Levine, A.; MacKintosh, F., Distinct regimes of elastic response and deformation modes of cross-linked cytoskeletal and semiflexible polymer networks. *arXiv preprint cond-mat/0308275* **2003**.

43. (a) López-Cruz, A.; Barrera, C.; Calero-DdelC, V. L.; Rinaldi, C., Water dispersible iron oxide nanoparticles coated with covalently linked chitosan. *Journal of Materials Chemistry* **2009,** *19* (37), 6870-6876; (b) Belessi, V.; Zboril, R.; Tucek, J.; Mashlan, M.; Tzitzios, V.; Petridis, D., Ferrofluids from Magnetic− Chitosan Hybrids. *Chemistry of Materials* **2008,** *20* (10), 3298-3305.

44. (a) Ma, L.; Gao, C.; Mao, Z.; Zhou, J.; Shen, J.; Hu, X.; Han, C., Collagen/chitosan porous scaffolds with improved biostability for skin tissue engineering. *Biomaterials* **2003,** *24* (26), 4833-4841; (b) Agnihotri, S. A.; Mallikarjuna, N. N.; Aminabhavi, T. M., Recent advances on chitosan-based micro-and nanoparticles in drug delivery. *Journal of Controlled Release* **2004,** *100* (1), 5-28.

45. Liufu, S.; Xiao, H.; Li, Y., Adsorption of poly (acrylic acid) onto the surface of titanium dioxide and the colloidal stability of aqueous suspension. *Journal of Colloid and Interface Science* **2005,** *281* (1), 155-163.

46. Barbani, N.; Lazzeri, L.; Cristallini, C.; Cascone, M. G.; Polacco, G.; Pizzirani, G., Bioartificial materials based on blends of collagen and poly (acrylic acid). *Journal of Applied Polymer Science* **1999,** *72* (7), 971-976.

47. Guo, L.; Yang, S. H.; Yang, C. L.; Yu, P.; Wang, J. N.; Ge, W. K.; Wong, G. K. L., Highly monodisperse polymer-capped ZnO nanoparticles: Preparation and optical properties. *Applied Physics Letters* **2000,** *76* (20), 2901-2903.

48. Sionkowska, A., Interaction of collagen and poly (vinyl pyrrolidone) in blends. *European Polymer Journal* **2003,** *39* (11), 2135-2140.

49. Niederberger, M.; Bartl, M. H.; Stucky, G. D., Benzyl alcohol and titanium tetrachloride - A versatile reaction system for the nonaqueous and low-temperature preparation of crystalline and luminescent titania nanoparticles. *Chemistry of Materials* **2002,** *14* (10), 4364-4370.

50. Rabotyagova, E. S.; Cebe, P.; Kaplan, D. L., Collagen structural hierarchy and susceptibility to degradation by ultraviolet radiation. *Materials Science & Engineering C-Biomimetic and Supramolecular Systems* **2008,** *28* (8), 1420-1429.

51. Guzzi Plepis, A. M. D.; Goissis, G.; Das - Gupta, D. K., Dielectric and pyroelectric characterization of anionic and native collagen. *Polymer Engineering & Science* **1996,** *36* (24), 2932-2938.

52. Laemmli, U. K., Journal of the American Chemical SocietyCleavage of structural proteins during assembly of head of bacteriophage-T4. *Nature* **1970,** *227* (5259), 680-&.

53. Kotsokechagia, T.; Cellesi, F.; Thomas, A.; Niederberger, M.; Tirelli, N., Preparation of ligand-free TiO2 (anatase) nanoparticles through a nonaqueous process and their surface functionalization. *Langmuir* **2008,** *24* (13), 6988-6997.

54. Hu, Y.; Ge, J.; Sun, Y.; Zhang, T.; Yin, Y., A self-templated approach to TiO2 microcapsules. *Nano Letters* **2007,** *7* (6), 1832-1836.

55. Chen, H.-J.; Jian, P.-C.; Chen, J.-H.; Wang, L.; Chiu, W.-Y., Nanosized-hybrid colloids of poly(acrylic acid)/titania prepared via in situ sol-gel reaction. *Ceramics International* **2007,** *33* (4), 643-653.

56. Pawlak, A.; Mucha, M., Thermogravimetric and FTIR studies of chitosan blends (vol 396, pg 153, 2003). *Thermochimica Acta* **2004,** *409* (1), 95-97.

57. Jakobsen, R.; Brown, L.; Hutson, T.; Fink, D.; Veis, A., Intermolecular interactions in collagen self-assembly as revealed by Fourier transform infrared spectroscopy. *Science* **1983,** *220* (4603), 1288-1290.

58. Jackson, M.; Mantsch, H. H., The use and misuse of FTIR spectroscopy in the determination of protein structure. *Critical reviews in biochemistry and molecular biology* **1995,** *30* (2), 95-120.

59. Lai, G.; Li, Y.; Li, G., Effect of concentration and temperature on the rheological behavior of collagen solution. *International Journal of Biological Macromolecules* **2008,** *42* (3), 285-291.

60. Wang, X.; Li, D.; Wang, W.; Feng, Q.; Cui, F.; Xu, Y.; Song, X.; van der Werf, M., Crosslinked collagen/chitosan matrix for artificial livers. *Biomaterials* **2003,** *24* (19), 3213-3220.

61. Taravel, M. N.; Domard, A., Collagen and its interaction with chitosan. 2. Influence of the physicochemical characterisatics of collagen. *Biomaterials* **1995,** *16* (11), 865-871.

62. Wang, X.; Sang, L.; Luo, D.; Li, X., From collagen–chitosan blends to three-dimensional scaffolds: the influences of chitosan on collagen nanofibrillar structure and mechanical property. *Colloids and Surfaces B: Biointerfaces* **2011,** *82* (1), 233-240.

63. Nezu, T.; Winnik, F. M., Interaction of water-soluble collagen with poly (acrylic acid). *Biomaterials* **2000,** *21* (4), 415-419.

64. Wood, G., The formation of fibrils from collagen solutions. 3. Effect of chondroitin sulphate and some other naturally occurring polyanions on the rate of formation. *Biochemical Journal* **1960,** *75* (3), 605.

65. (a) Yang, Y.-l.; Leone, L. M.; Kaufman, L. J., Elastic Moduli of Collagen Gels Can Be Predicted from Two-Dimensional Confocal Microscopy. *Biophysical Journal* **2009,** *97* (7), 2051-2060; (b) MacKintosh, F.; Käs, J.; Janmey, P., Elasticity of semiflexible biopolymer networks. *Physical Review Letters* **1995,** *75* (24), 4425.

66. (a) Jordan, J.; Jacob, K. I.; Tannenbaum, R.; Sharaf, M. A.; Jasiuk, I., Experimental trends in polymer nanocomposites—a review. *Materials science and engineering: A* **2005,** *393* (1), 1-11; (b) Pryamitsyn, V.; Ganesan, V., Origins of linear viscoelastic behavior of polymer-nanoparticle composites. *Macromolecules* **2006,** *39* (2), 844-856.

67. Taravel, M. N.; Domard, A., Collagen and its interactions with chitosan. 3. Some biological and mechanical properties. *Biomaterials* **1996,** *17* (4), 451-455.

68. Licup, A. J.; Münster, S.; Sharma, A.; Sheinman, M.; Jawerth, L. M.; Fabry, B.; Weitz, D. A.; MacKintosh, F. C., Stress controls the mechanics of collagen networks. **2015**.

69. Yang, Y.-l.; Kaufman, L. J., Rheology and Confocal Reflectance Microscopy as Probes of Mechanical Properties and Structure during Collagen and Collagen/Hyaluronan Self-Assembly. *Biophysical Journal* **2009,** *96* (4), 1566-1585.

70. Tsai, S. W.; Liu, R. L.; Hsu, F. Y.; Chen, C. C., A study of the influence of polysaccharides on collagen self‐assembly: Nanostructure and kinetics. *Biopolymers* **2006,** *83* (4), 381-388.

71. Norihiro, K.; Stevin, H. G., Rate-Limiting Steps in Volume Change Kinetics of Fast Responsive Microporous Gels. In *Reflexive Polymers and Hydrogels*, CRC Press: 2004.

72. Koshimizu, N.; Bessho, M.; Suzuki, S.; Yuguchi, Y.; Kitamura, S.; Hara, M., Gamma-crosslinked collagen gel without fibrils: analysis of structure and heat stability. *Bioscience, biotechnology, and biochemistry* **2009,** *73* (9), 1915-1921.

73. Sui, X.; Liu, Y.; Shao, C.; Liu, Y.; Xu, C., Structural and photoluminescent properties of ZnO hexagonal nanoprisms synthesized by microemulsion with polyvinyl pyrrolidone served as surfactant and passivant. *Chemical Physics Letters* **2006,** *424* (4), 340-344.

74. Matsuyama, K.; Ihsan, N.; Irie, K.; Mishima, K.; Okuyama, T.; Muto, H., Bioimaging application of highly luminescent silica-coated ZnO-nanoparticle quantum dots with biotin. *Journal of Colloid and Interface Science* **2013,** *399*, 19-25.

75. Russell, A. E.; Cooper, D. R., Structural and functional factors in the hydrogen bonding of polar organic solvents to acid-soluble collagen. Effect on renaturation kinetics and thermal stability. *Biochemistry* **1969,** *8* (10), 3980-3990.

76. Piechocka, I. K.; van Oosten, A. S.; Breuls, R. G.; Koenderink, G. H., Rheology of heterotypic collagen networks. *Biomacromolecules* **2011,** *12* (7), 2797-2805.

77. Mansel, B. W.; Chu, C.-Y.; Leis, A.; Hemar, Y.; Chen, H.-L.; Lundin, L.; Williams, M. A. K., Zooming in: Structural Investigations of Rheologically Characterized Hydrogen-Bonded Low-Methoxyl Pectin Networks. *Biomacromolecules* **2015,** *16* (10), 3209-3216.

78. Harris, J. R.; Soliakov, A.; Lewis, R. J., In vitro fibrillogenesis of collagen type I in varying ionic and pH conditions. *Micron* **2013,** *49*, 60-68.

79. Lee, K. Y.; Rowley, J. A.; Eiselt, P.; Moy, E. M.; Bouhadir, K. H.; Mooney, D. J., Controlling mechanical and swelling properties of alginate hydrogels independently by cross-linker type and cross-linking density. *Macromolecules* **2000,** *33* (11), 4291-4294.

80. Pires, M. M.; Przybyla, D. E.; Chmielewski, J., A Metal‐Collagen Peptide Framework for Three‐Dimensional Cell Culture. *Angewandte Chemie International Edition* **2009,** *48* (42), 7813-7817.

81. Li, Y.; Asadi, A.; Monroe, M. R.; Douglas, E. P., pH effects on collagen fibrillogenesis in vitro: Electrostatic interactions and phosphate binding. *Materials Science and Engineering: C* **2009,** *29* (5), 1643-1649.

82. Nalinanon, S.; Benjakul, S.; Visessanguan, W.; Kishimura, H., Use of pepsin for collagen extraction from the skin of bigeye snapper (Priacanthus tayenus). *Food Chemistry* **2007,** *104* (2), 593-601.

83. Silver, F. H., Type I collagen fibrillogenesis in vitro. Additional evidence for the assembly mechanism. *Journal of Biological Chemistry* **1981,** *256* (10), 4973-4977.